ACCSCIENCE PUBLISHING

Volume 2 · Issue 4
December 2023

Advanced Neurology

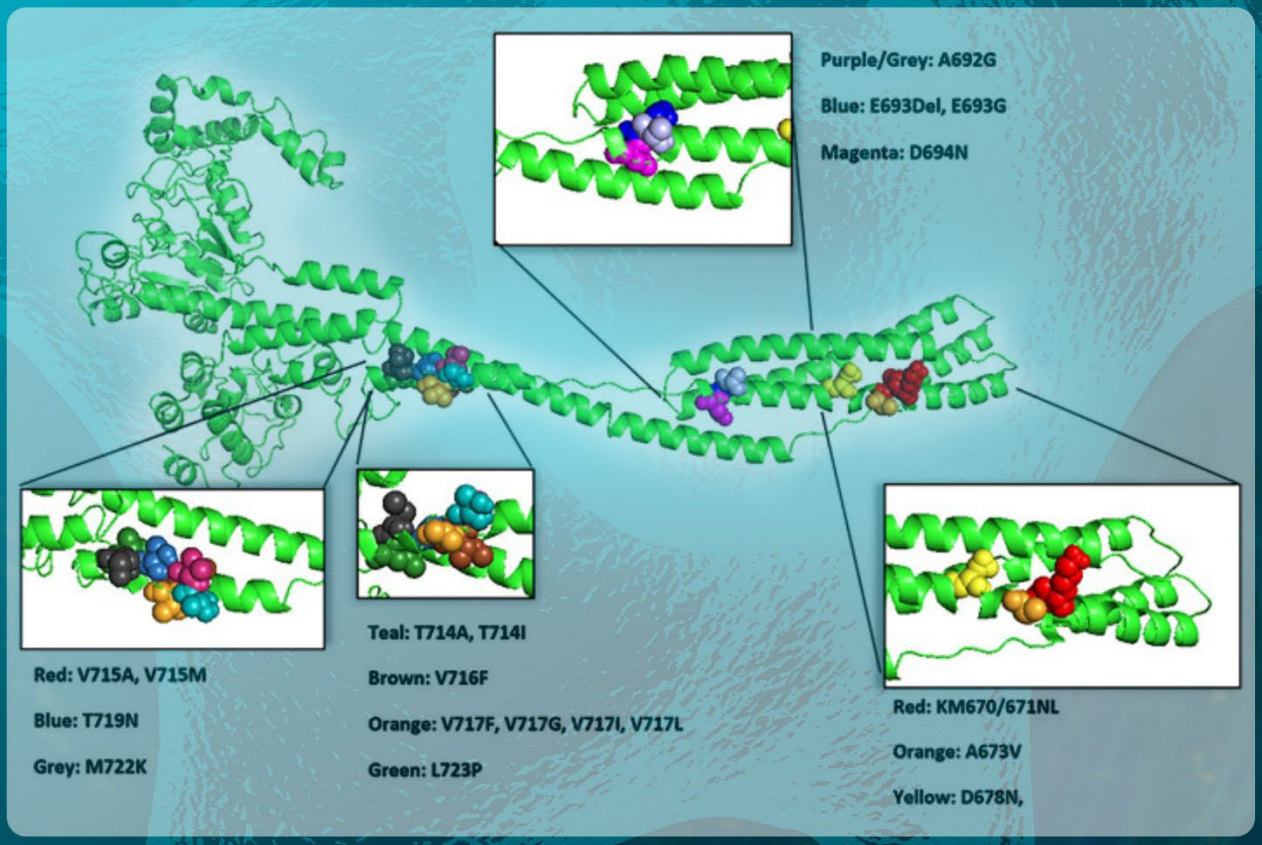

Ethnogenetic-specific mutations in Alzheimer's disease: A marker of clinical outcomes

ISSN: 3060-8589 (Print)
ISSN: 2810-9619 (Online)

ACCSCIENCE PUBLISHING

Advanced Neurology

Print ISSN: 3060-8589
Online ISSN: 2810-9619

Advanced Neurology is a peer-reviewed and open-access journal that aims to publish and disseminate novel research on basic, clinical, and translational medicine related to neurological diseases. The journal's mission is to advance our understanding of the diseases related to the nervous system and to provide a platform to showcase the latest findings in fundamental research and clinical research as well as present new ideas that might contribute to the improvement of neurological clinical practice. The target audience of Advanced Neurology includes physicians, epidemiologists, and neuroscientists working in the disciplines of neurology, neurosurgery, neuroimaging, neurointervention, neuropsychology, and so on.

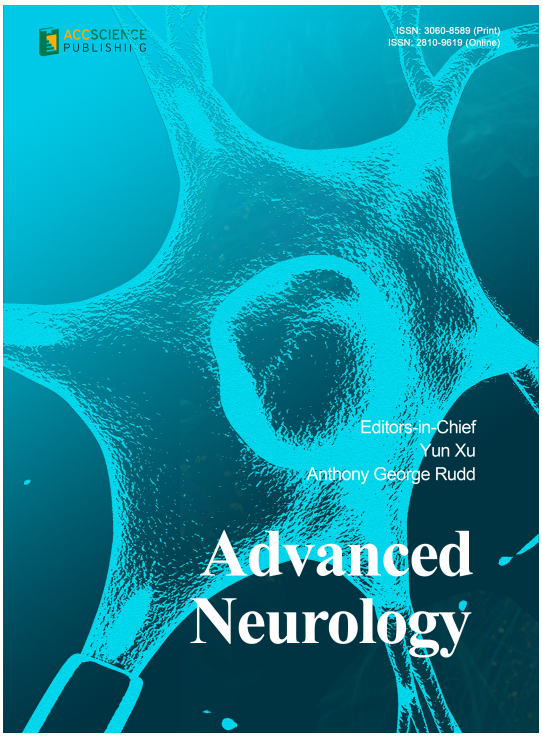

About the Publisher

AccScience Publishing is a publishing company based in Singapore. We publish a range of high-quality, open-access, peer-reviewed journals and books from a broad spectrum of disciplines.

Contact Us

Managing Editor
an.office@accscience.sg

AccScience Publishing
8 Burn Road, #15-03 Trivex, Singapore 369977.

Volume 2 • Issue 4 • December 2023
ISSN 3060-8589 (print) ISSN 2810-9619 (online)

ADVANCED NEUROLOGY

ACCSCIENCE PUBLISHING

Access Science Without Barriers

ADVANCED NEUROLOGY

ISSN: 3060-8589 (print)
ISSN: 2810-9619 (online)

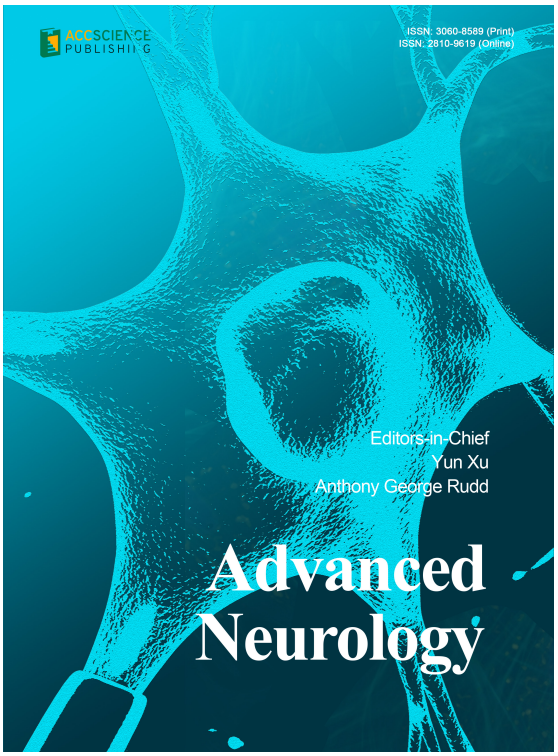

Editorial and Production Credits

Publisher: AccScience Publishing
Managing Editor: Zoe Zhang
Production Editor: Sharmila Velapasamy
Special Issue Commissioning Editor: Zoe Zhang
Article Layout and Typeset: Sinjore Technologies (India)
Cover Design: ProPub (China)

For all advertising queries, contact an.office@accscience.sg.

Supplementary file

Supplementary files of articles can be obtained at https://accscience.com/journal/AN/2/4.

Disclaimer

AccScience Publishing is not liable to the statements, perspectives, and opinions contained in the publications. The appearance of advertisements in the journal shall not be construed as a warranty, endorsement, or approval of the products or services advertised and/or the safety thereof. AccScience Publishing disclaims responsibility for any injury to persons or property resulting from any ideas or products referred to in the publications or advertisements. AccScience Publishing remains neutral with regard to jurisdictional claims in published maps and institutional affiliations.

Advanced Neurology

Editorial Board

ACCSCIENCE PUBLISHING

Volume 2 | Issue 4 | December 2023 |

Advanced Neurology

https://accscience.com/journal/AN

CONTENTS

ACCSCIENCE PUBLISHING

Advanced Neurology

REVIEW ARTICLE

Worsening of cerebral palsy following neonatal encephalopathy: A meta-analysis

Meng Yang[1], Sarah Eide[1], Emily W.Y. Tam[2], Vann Chau[2], S.R. Wayne Chen[3], Steven P. Miller[4], Hong-Shuo Sun[1,5], and Zhong-Ping Feng[1]*

[1]Department of Physiology, Temerty Faculty of Medicine, University of Toronto, Toronto, Ontario, Canada

[2]Department of Pediatrics, The Hospital for Sick Children, Toronto, Ontario, Canada

[3]Department of Physiology and Pharmacology, Cumming School of Medicine, University of Calgary, Calgary, Alberta, Canada

[4]Department of Pediatrics, Faculty of Medicine, University of British Columbia and BC Children's Hospital, Vancouver, British Columbia, Canada

[5]Department of Surgery, Temerty Faculty of Medicine, University of Toronto, Toronto, Ontario, Canada

Abstract

Cerebral palsy (CP), the most common motor disorder in early childhood, arises from neonatal brain injury. The potential role of neonatal encephalopathy (NE) as a risk factor for cerebral palsy has been postulated, yet a systematic examination of its clinical impact on cerebral palsy patients remains absent. This meta-analysis aims to delineate the incidence of commonly reported complications associated with cerebral palsy following NE compared to those without a history of NE. A systematic search of PubMed and Google Scholar yielded 424 studies, with 7 meeting the inclusion criteria. These studies reported at least one comparison of cerebral palsy symptoms between patients with or without NE and provided the corresponding case numbers for each group. Utilizing RevMan 5.4, we analyzed the data and assessed potential publication bias. Among the 7 studies included, we compared the characteristics of 117 patients with cerebral palsy with preceding NE to 287 without such antecedents. Significantly, the incidence of the spastic quadriplegic subtype of cerebral palsy was higher in patients with NE (odds ratio [OR]: 4.34, 95% confidence interval [CI]: 2.69 – 7.00, $P < 0.00001$). CP patients following NE exhibited a significantly increased incidence of severe communication difficulties (OR: 2.33, 95% CI: 1.32 – 4.10, $P = 0.003$), difficulty swallowing (OR: 2.50, 95% CI: 1.31 – 4.77, $P = 0.005$), and cognitive impairment (OR: 2.73, 95% CI: 1.45 – 5.13, $P = 0.002$). Children with cerebral palsy born following NE were more predisposed to the most severe spastic quadriplegic subtype and encountered significant comorbidities. It is essential to acknowledge the limitations of this study, primarily the small number of studies that separately reported cerebral palsy cases with or without NE. Nevertheless, these findings contribute valuable insights for a more accurate clinical prognosis and the prospective development of targeted treatments for specific complications associated with cerebral palsy in patients with NE.

Keywords: Neonatal encephalopathy; Cerebral palsy; Hypoxic-ischemic brain injury; Patients

***Corresponding author:**
Zhong-Ping Feng
(zp.feng@utoronto.ca)

Citation: Yang M, Eide S, Tam EWY, *et al.*, 2023, Worsening of cerebral palsy following neonatal encephalopathy: A meta-analysis. *Adv Neuro,* 2(4): 1719. https://doi.org/10.36922/an.1719

Received: August 30, 2023

Accepted: November 28, 2023

Published Online: December 15, 2023

1. Introduction

Cerebral palsy (CP) stands as the most prevalent movement disorder emerging in early childhood attributed to brain damage during development[1,2]. Globally, CP impacts approximately 2 in every 1000 live births[3]. Despite medical advancements, the prevalence of CP has not exhibited a decline in recent decades, potentially attributable to the increased survival rate of pre-term infants who face a heightened risk of CP[4,5]. The manifestations of CP vary among individuals and may develop over time[6]. The common symptoms include impaired motor function, such as challenges in maintaining balance and posture and deficient muscle coordination[6]. In certain cases, the patients develop seizures and/or cognitive comorbidities[7]. Classification of CP hinges on the distributional pattern of affected limbs and the prevailing neuromotor abnormality[8]. Pertinent subtypes for the present analysis include (i) Spasticity affecting all four limbs (quadriplegia), (ii) spasticity affecting both lower extremities without upper limb involvement (diplegia), (iii) spasticity manifesting on one side of the body (hemiplegia), and (iv) dyskinetic.

It is evident that CP results from a series of events that combine to cause injury to the brain during the developmental period of the fetus or infant[9]. While risk factors for the development of CP may occur at any stage of development – from prenatal to postnatal – (Figure 1), it is reported that perinatal events contribute to 30.5% of CP cases[10]. A number of risk factors may cause damage to the central nervous system at the early stage of its development. Neonatal encephalopathy (NE) results from various conditions, including infections (e.g., neonatal sepsis)[11], perinatal vascular accidents (e.g., arterial ischemic stroke and intracranial hemorrhage)[12,13], metabolic disturbances (e.g., hypoglycemia and electrolyte abnormalities)[14,15], seizures or epilepsies[16], genetic or congenital factors[17,18], and exposure to prenatal medications that cause toxicity[19,20]. Hypoxic-ischemic encephalopathy (HIE), which is the direct result of a perinatal hypoxic, ischemic, and/or asphyxial event, is the most common cause of NE. HIE affects up to 8/1000 infants in developed countries and 26/1000 infants in underdeveloped countries[21], responsible for up to 1 million neonatal deaths each year globally[22].

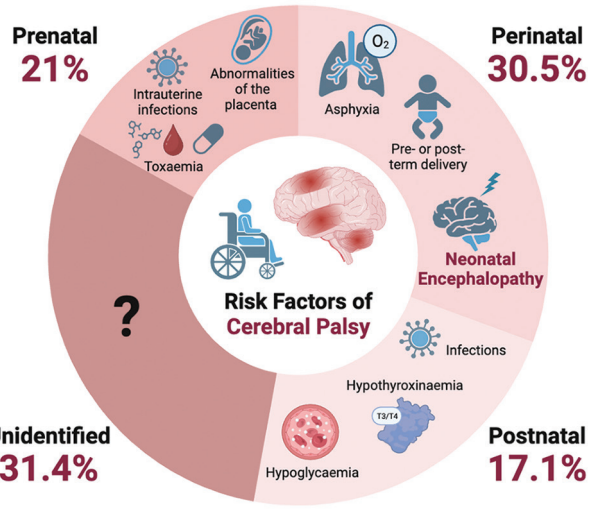

Figure 1. Predominant events and risk factors leading to cerebral palsy[9,48]. Examples of risk factors are listed under each category, with a specific emphasis on the perinatal NE event. The image was created using BioRender.com.

Significantly, NE may result in brain damage, which in the context of HIE is due to inadequate levels of oxygen and blood to the brain[23,24]. As a result of brain injury, patients may suffer from periods of apnea, seizures, cardiorespiratory failure, and even death[24,25]. Currently, hypothermia therapy stands as the sole acute treatment for neonates following HIE, offering some degree of neuroprotection[26,27]. However, its efficacy is limited by the short time window of delivery. Recent studies have reported that TRPM7 channel blockers[28,29] or ryanodine receptor inhibitor[30] can effectively mitigate brain damage and improve neurobehavior outcomes in mouse models of HIE. Nevertheless, as of now, there is no pharmacological solution available for clinical NE patients that would permit early prevention of the development of severe complications[25]. Following the current standard of care, survivors living with NE can develop long-term behavioral impairments, including motor disability[21,24,31].

Previous studies have identified NE as a significant risk factor for CP. One study has reported a significant increase in the incidence of CP in neonates experiencing asphyxia or hypoxic conditions at birth[5]. Children with birth defect, such as NE, were found to be three times more likely to develop CP[32]. Among those children with CP following NE, 1 in every 5 succumbed to death before the age of 5[33]. For those who survived, NE was linked to a poor clinical prognosis in individuals with CP due to irreversible HIE brain damage, contributing to more debilitating CP features compared to non-NE patients[4,32-34]. Furthermore, approximately one-quarter of CP cases in term-born infants had preceding moderate or severe NE, and CP following NE was more likely to manifest as the spastic quadriplegic and spastic dyskinetic subtypes[33].

While studies have found that standard physical therapy, treadmill training, and functional gait training are safe, feasible, and effective interventions to improve walking ability in patients with CP[35,36], CP remains a permanent disability in children. Additionally, beyond motor disability, children with CP also suffer from other complications that

affect their activities of daily living, challenges that are not fully addressed by current treatment. At present, the optimal training intensity and delivery for CP patients remain unknown. Therefore, clinicians encounter challenges in clinical judgment, both prognostically and during therapy. These challenges may be further complicated in patients with a history of NE.

The present analysis aims to compare and characterize features of CP with and without preceding NE conditions in patients. Characterizing features of CP following NE may provide a more accurate clinical prognosis and, in turn, contribute to the development of more effective, personalized treatment plans for CP patients with NE conditions.

2. Methods

2.1. Publication search

Two electronic databases, PubMed (https://pubmed.ncbi.nlm.nih.gov/) and Google Scholar (https://scholar.google.com/), were used for publication searches. The search terms employed in both databases were as follows: (i) Cerebral Palsy AND Hypoxia, (ii) Cerebral Palsy AND HIE, (iii) Cerebral Palsy AND NE, (iv) Cerebral Palsy AND Neonatal Brain Injury, (v) Cerebral Palsy Risk Factors, (vi) Cerebral Palsy Clinical Cases, and (vii) Cerebral Palsy Cohort. These searches encompassed publications up to September 2021 and were limited to publications in the English language.

2.2. Publication selection

Studies relevant to the present analysis and meeting the inclusion criteria were initially identified through title and abstract screening, followed by a comprehensive review of full texts. The inclusion criteria comprised: (i) the study must report cases of CP in human neonates or children, (ii) The study must separately report CP cases with and without preceding NE, (iii) The study must measure and characterize at least one parameter or characteristic of CP in both groups, such as subtype of CP, sex of the patient, and subsequent complications, with and without NE conditions, (iv) The study must report original data regarding CP; reviews and meta-analyses were excluded.

Through the screening of included studies, clinical characteristics of CP in patients with preceding NE and those without preceding NE conditions were gathered. Two reviewers (MY and SE) worked independently to ensure the extracted data met the criteria for inclusion in the present analysis. The data extracted from the studies fell into 4 parameter categories: (i) the number of CP cases with and without NE, (ii) the incidence of CP cases across sex, (iii) the number of patients with and without NE across CP subtypes, and (iv) the incidence of CP-related complications, including difficulties or impairments in communication, hearing, vision, swallowing, and cognitive function in each patient group, as well as the occurrence of seizures. Subsequent to data extraction, analyses were carried out for each parameter accordingly.

2.3. Data analysis

RevMan 5.4 software was used to conduct a random-effects model meta-analysis, aiming to identify differences in the incidence of CP and each clinical characteristic of CP between individuals with or without preceding NE conditions. The parameters considered in the present analysis were reported as dichotomous variables. The number of cases for each parameter and the total number of cases in each group were utilized to calculate odd ratios (OR).

For each comparison of the incidence of CP or the CP-related complication in those with or without preceding NE, case numbers in each category across all included studies were pooled together to calculate an overall estimate of effect size, reported as an OR, using the random-effects model with inverse variance methods. Statistical significance was determined by a two-tailed $P < 0.05$ between CP patients with or without preceding NE conditions. For each OR, the 95% confidence interval (CI) was calculated using RevMan5.4. Particularly, to determine the sex-specific difference in the incidence of CP patients with or without preceding NE conditions, the number of cases in each sex was tallied within each condition and analyzed using OR and a two-tailed significance test.

The statistical algorithms utilized by RevMan 5 have been previously described[37]. To assess publication bias for each parameter, funnel plots were generated in RevMan 5.4, plotting OR against the standard error of log(OR) for the included studies.

3. Results

3.1. Selected studies

A total of 424 studies were collected after conducting publication searches using the two electronic databases, of which 355 were identified as duplicates either within or across databases, leaving 69 studies for full-text review (Figure 2). Among these, 57 studies were excluded as they did not report the number of cases of CP with preceding HIE or NE, and 1 study was excluded due to inaccessibility. A full-text review was then conducted on the remaining 11 studies. Following the full-text reviews, 4 additional articles were excluded as they did not provide a comparison between CP patients with or without NE[32,38-40]. Therefore, 7 studies met the inclusion criteria and were included in the present meta-analysis[4,33,41-45]. Of the 7 included studies,

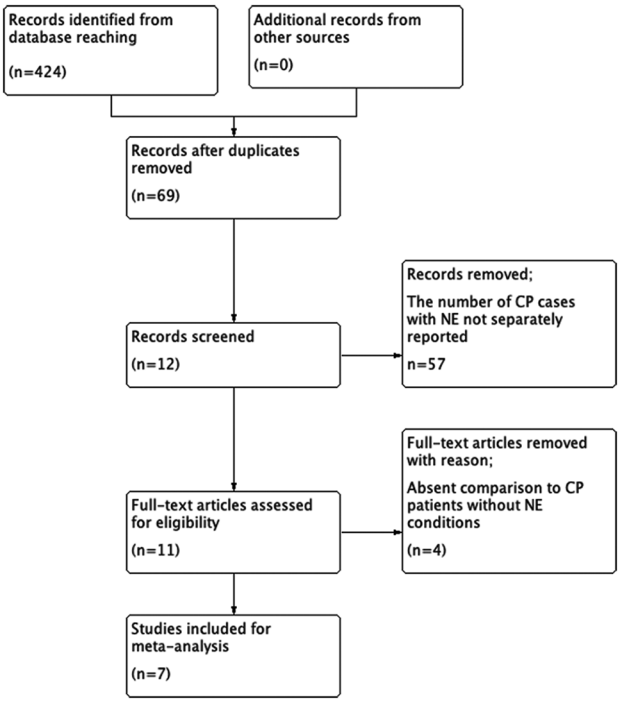

Figure 2. Flow diagram of publication selection. A total of 424 studies were collected from the two electronic databases, with 355 identified as duplicates either within or across databases. After removing duplicates, 69 studies were selected. Out of these, 58 were excluded – 57 due to a lack of reported cases of cerebral palsy with preceding hypoxic-ischemic encephalopathy or NE and 1 due to inaccessibility. Subsequently, a full-text review was conducted on 11 studies. After the full-text review, an additional 5 articles were excluded because they lacked a comparison between CP patients with or without NE conditions. Ultimately, the present analysis is based on 7 studies.
Abbreviations: CP: Cerebral palsy; NE: Neonatal encephalopathy.

all were used to analyze the incidence of NE in CP patients, 3 were used to analyze the subtype and comorbidities of CP with and without preceding NE studies[33,41,42], and 2 studies were used to assess NE incidence in CP patients across sex[33,42].

3.2. Study participants

In total, data from 1657 CP patients were available (Table 1) for analyzing the incidence of CP with or without preceding NE conditions. Among these, 504 CP cases were associated with preceding NE, while 1153 were not. The sex of patients was specified in 263 cases, comprising 146 male and 117 female patients. It is noteworthy that all cases included in the subtype and comorbidities analyses were neonates born at term and were followed up for a duration of 5 years.

3.3. Incidence of NE in cerebral palsy patients

To assess the incidence of preceding NE in CP patients, the numbers of CP cases with or without an NE history were collected and analyzed (Figure 3). A small cohort of patients with an NE history was identified among the total CP patients, with an OR of 0.18 (95% CI: 0.10 – 0.32, $P < 0.00001$).

Table 1. Characteristics of CP patients included in the present analysis

Characteristic	Number of cases
Total patients	1657
With NE	413
With HIE	91
Without NE/HIE	1153
Total patients with gender specified in the included studies	263
Male	146
Female	117

Abbreviations: CP: Cerebral palsy; HIE: Hypoxic-ischemic encephalopathy; NE: Neonatal encephalopathy.

To investigate potential sex-specific differences in the incidence of CP patients with an NE history, a separate analysis of NE incidence in male and female CP patients was conducted using data from two studies categorizing CP cases by biological sex (Figure 4). The total number of cases with or without preceding NE conditions was pooled together across the two studies, and the number of cases for each sex was counted within each group. In both patient groups, male CP patients exhibited a marginally increased incidence compared to female CP patients (with NE conditions: OR: 0.4, 95% CI: 0.06 – 2.54, $P = 0.33$; without NE conditions: OR: 0.73, 95% CI: 0.48 – 1.09, $P = 0.12$). However, this difference was not statistically significant at the $p<0.05$ level. Further clinical studies comparing male and female cases are warranted to determine whether the incidence of NE in CP patients is significantly affected by biological sex.

3.4. Severity of cerebral palsy complications in patients with and without preceding NE

To determine if CP subtypes exhibit variations with and without preceding NE, individuals with CP were divided into 2 major categories of CP subtypes: (i) the most severe spastic quadriplegic subtype and (ii) spastic diplegia, hemiplegia, dyskinesia, and other subtypes. Analysis was performed to identify the incidence of these subtypes in those who experienced preceding NE conditions and those who did not (Figure 5). The incidence of spastic quadriplegic subtype was found to be significantly higher in those with CP that had experienced NE compared to CP patients that did not have prior reports of NE with OR: 4.34 (95% CI: 2.69 – 7.00, $P < 0.00001$).

To further explore whether CP patients with preceding NE conditions manifest different symptoms associated

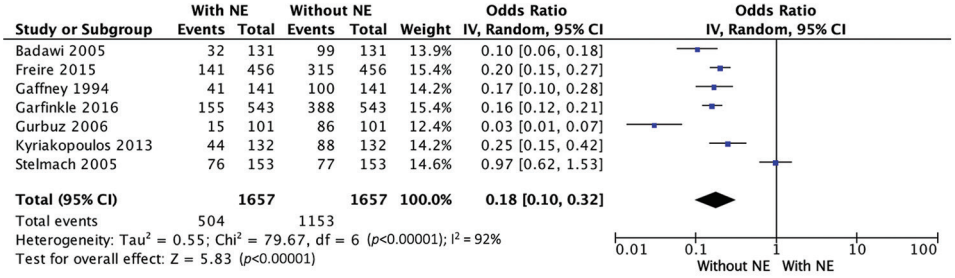

Figure 3. The number of CP cases, with or without NE. The forest plot compares the number of CP cases with preceding NE conditions to the number of CP cases without NE. Patients with NE conditions constituted a smaller proportion of the total recorded CP cases, with an odds ratio of 0.18 (95% CI: 0.10 – 0.32, $P < 0.00001$).
Abbreviations: CI: Confidence interval; CP: Cerebral palsy; NE: Neonatal encephalopathy.

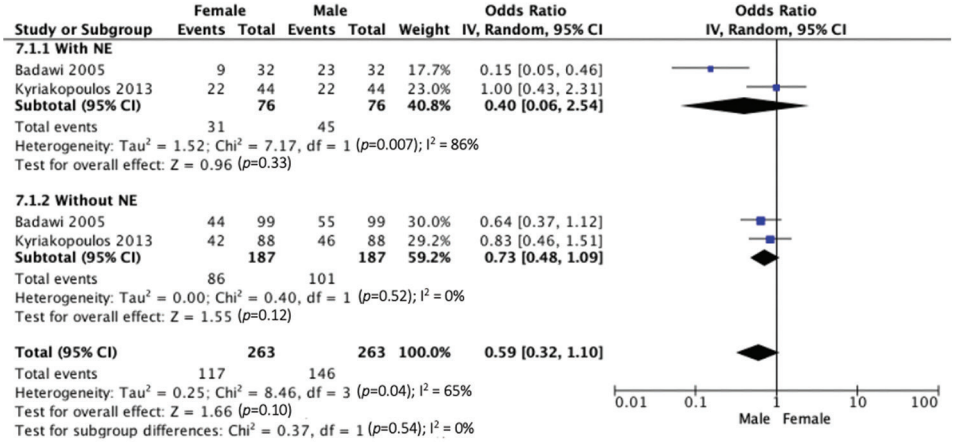

Figure 4. The number of CP cases in each sex, with or without NE. The forest plot compares the number of male or female CP cases with preceding NE conditions to the number of cases without preceding NE conditions. NE demonstrated no significant effect on the sex of CP patients. However, CP in males had slightly higher incidence than females, regardless of a history of NE, with an odds ratio of 0.59 (95% CI: 0.32 – 1.10, $P = 0.1$).
Abbreviations: CI: Confidence interval; CP: Cerebral palsy; NE: Neonatal encephalopathy.

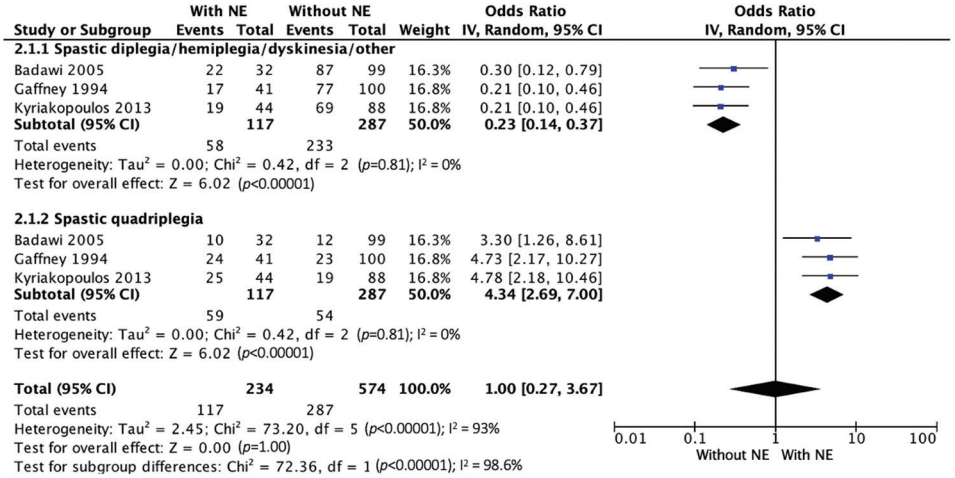

Figure 5. The number of cases with or without NE in different subtypes of CP. The forest plot compares the number of CP cases with preceding NE conditions in patients belonging to 2 major categories of CP against the number of cases without preceding NE conditions. The incidence of spastic quadriplegic subtype showed a significant positive correlation with preceding NE conditions in patients compared to those without NE, with an odds ratio of 4.34 (95% CI: 2.69 – 7.00, $P < 0.00001$).
Abbreviations: CI: Confidence interval; CP: Cerebral palsy; NE: Neonatal encephalopathy.

with CP compared to patients with no history of NE, the incidence of six commonly reported comorbidities was analyzed. The incidence of severe communication difficulties, severe auditory impairment, cortical blindness, severe visual impairment, seizures, difficulty swallowing, and cognitive impairment was compared in CP patients with and without prior NE (Figure 6). The results from the analysis (Table 2) indicate that CP patients with preceding NE conditions had a significantly higher incidence of severe communication difficulties (OR: 2.33, 95% CI: 1.32 – 4.10, P = 0.003), difficulty swallowing (OR = 2.50, 95% CI: 1.31 – 4.77, P = 0.005), and cognitive impairment (OR = 2.73, 95% CI: 1.45 – 5.13, P = 0.002). The incidence of severe auditory impairment (OR = 1.62, 95% CI: 0.34 – 7.59, P = 0.54) and severe visual impairment (OR = 1.61, 95% CI: 0.81 – 3.20, P = 0.17) also showed a positive correlation with preceding NE conditions but did not reach statistical significance. The incidence of epilepsy was not observed to be affected by preceding NE in CP patients (OR = 1.03, 95% CI: 0.47 – 2.24, P = 0.94).

3.5. Publication bias

Publication bias did not emerge as a concern in the present analysis (Figures 7-10). All generated funnel plots demonstrated a symmetric scattering of the included published data on either side of the calculated OR for each analysis.

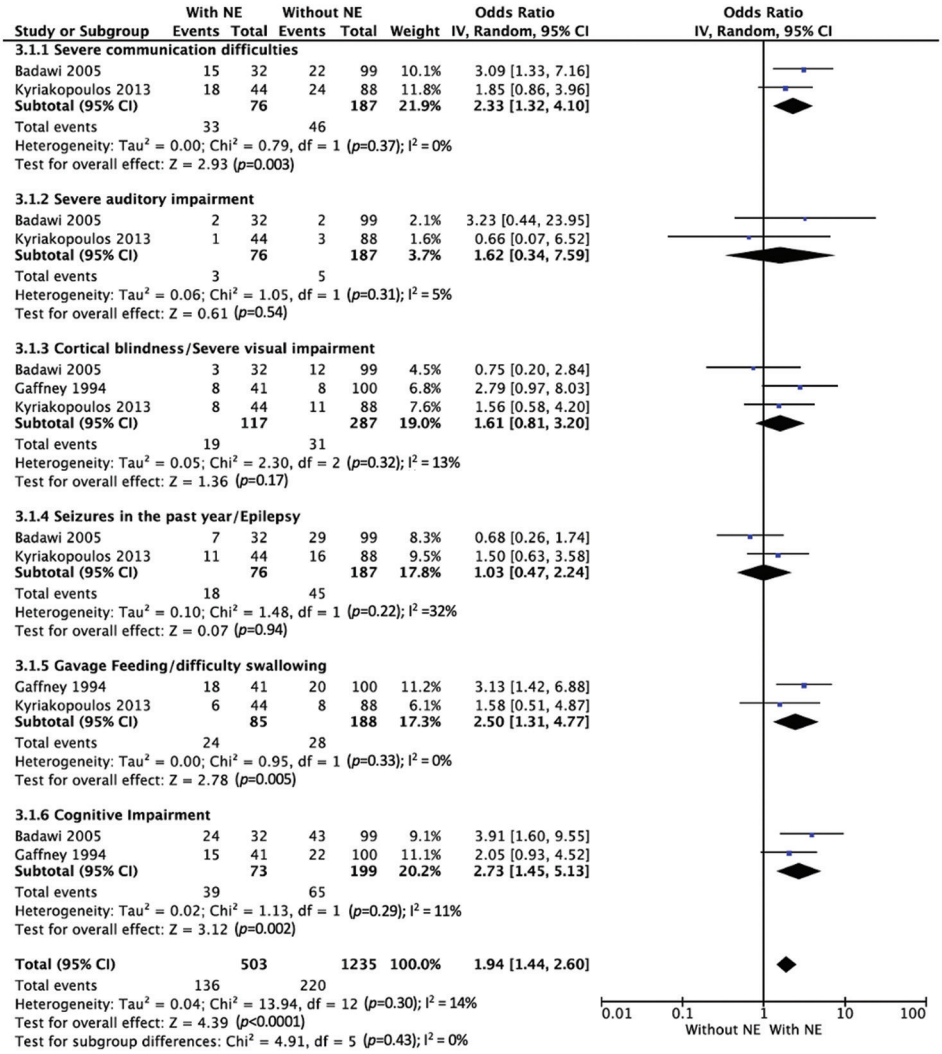

Figure 6. The number of CP cases with different comorbidities, with or without NE. The forest plot compares the number of cases with preceding NE conditions in CP patients to the number of cases without preceding NE conditions across 6 common comorbidities. CP patients with preceding NE conditions exhibited a significantly higher incidence of severe communication difficulties (OR: 2.33, 95% CI: 1.32 – 4.10, P = 0.003), difficulty swallowing (OR: 2.50, 95% CI: 1.31 – 4.77, P = 0.005), and cognitive impairment (OR: 2.73, 95% CI: 1.45 – 5.13, P = 0.002). However, there was no significant increase in severe auditory impairment, severe visual impairment, and epilepsy (OR: 1.03, 95% CI: 0.47 – 2.24, P = 0.94) in patients with preceding NE.
Abbreviations: CI: Confidence interval; CP: Cerebral palsy; NE: Neonatal encephalopathy.

4. Discussion

Our meta-analysis was conducted on the pooled data from 1657 CP patients across 7 independent studies in the existing literature, revealing that NE conditions exacerbate the severity of clinical manifestations in CP patients. Specifically, CP patients with a history of NE exhibited a higher incidence of spastic quadriplegia, consistent with previous reports[33]. Our work also highlighted the increased incidence of difficulties or impairments in communication, swallowing, and cognitive function in these patients. It is essential to acknowledge that the interpretation of our findings may be constrained by the limited number of clinical studies that separately report on CP cases with or without NE conditions at birth. Furthermore, NE has diverse etiologies beyond HIE[46,47], introducing challenges and limitations to clinical diagnosis, where only severe events may be identifiable. This may contribute to underestimation in patients with

Table 2. Summary of OR across defined types of comorbidities

Comorbidities	OR	95% CI	*P*-value
Severe communication difficulties	2.33	1.32 – 4.10	0.003*
Severe auditory impairment	1.62	0.34 – 7.59	0.54
Severe visual impairment	1.61	0.81 – 3.20	0.17
Epilepsy	1.03	0.47 – 2.24	0.94
Difficulty swallowing	2.50	1.31 – 4.77	0.005*
Cognitive impairment	2.73	1.45 – 5.13	0.002*

Note: *P<0.05. Abbreviations: 95% CI: 95% confidence intervals; OR: Odd ratio.

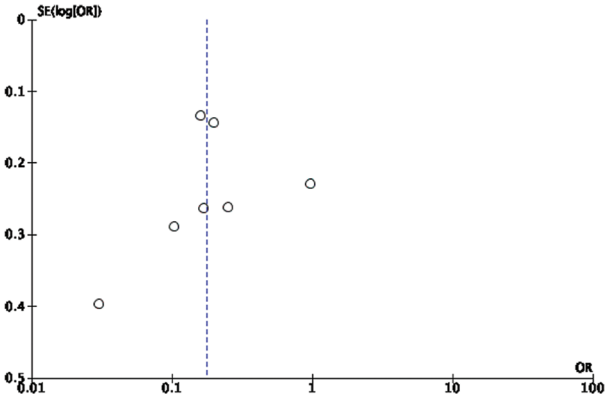

Figure 7. Funnel plot of OR for all CP cases included in the present analysis. Relatively symmetric scattering of published data is observed on both sides of the overall OR (OR: 0.18).
Abbreviations: CP: Cerebral palsy; OR: Odds ratio.

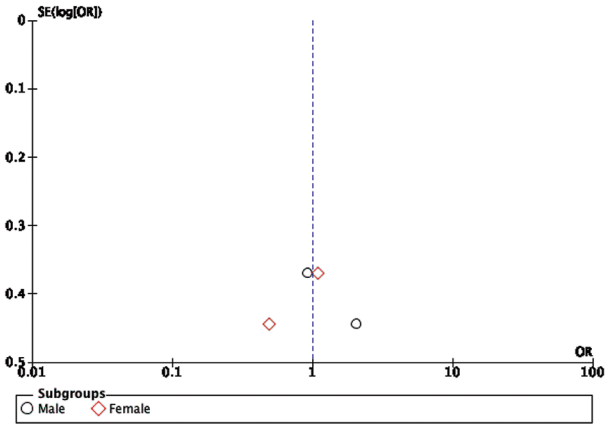

Figure 8. Funnel plot for the sex factor in the CP cases included in the present analysis. Symmetric scattering of published data is observed on both sides of the overall OR (OR: 1.00).
Abbreviations: CP: Cerebral palsy; OR: Odds ratio.

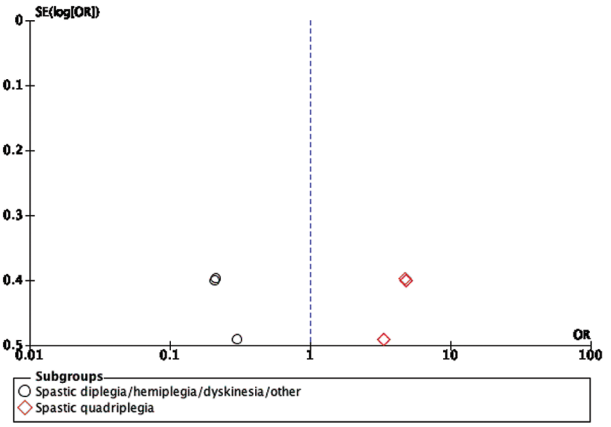

Figure 9. Funnel plot for different subtypes of CP cases included in the present analysis. Symmetric scattering of published data is observed on both sides of the overall OR (OR: 1.00).
Abbreviations: CP: Cerebral palsy; OR: Odds ratio.

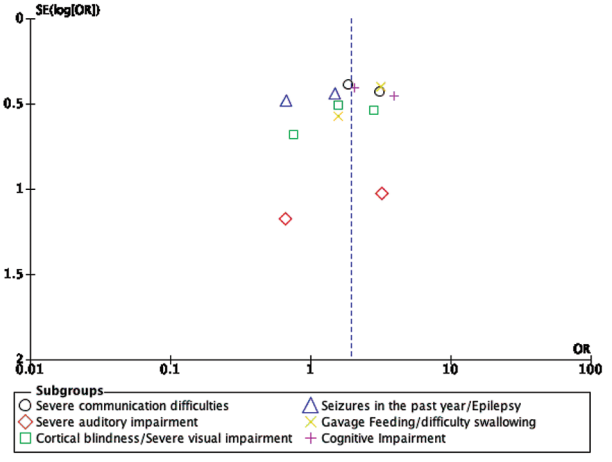

Figure 10. Funnel plot for comorbidities in CP cases included in the present analysis. Symmetric scattering of published data is observed on both sides of the overall OR (OR: 1.94).
Abbreviations: CP: Cerebral palsy; OR: Odds ratio.

NE and overestimation in patients without NE, potentially explaining our finding of a smaller portion of CP patients with a history of NE. It is crucial to recognize that, beyond NE, numerous preconceptional, prenatal, perinatal, and postnatal factors contribute to CP development[9].

While our study primarily focused on establishing the independent correlation between NE to CP, it is equally important to investigate the cumulative causes contributing to CP development. Perinatal pathology resulting in brain injury, such as birth asphyxia[9,48], plays a pivotal role in CP development, accounting for approximately 30.5% of reported CP cases; prenatal factors also contribute significantly, representing 21% of CP cases[10] (Figure 1). Prematurity and being underweight are considered the most significant contributing prenatal risk factors for CP[9,48]. A previous study using a database encompassing over 6000 children with CP demonstrated that CP incidences were 70 times higher among premature infants weighing less than 1500 grams at birth compared to those with a birth weight exceeding 2500 g[49]. Furthermore, research has revealed that the incidence of CP increased to 146 cases/1000 live births in premature infants born before the 28th week of pregnancy[50]. Moreover, recent genetic studies have provided novel insights into CP etiology, identifying cases devoid of prenatal, natal, or postnatal explanations. Investigating these areas holds the potential for uncovering correlations between multiple conditions and CP, thereby improving strategies for the prevention and management of clinical CP patients.

Although the subset of patients with a history of NE represents a small portion of the total CP patient population, this specific cohort is disproportionately affected by a higher incidence of severe CP-associated complications than CP patients without a history of NE. Previous studies have suggested that the increased incidence of CP in neonates who experienced NE-related conditions at birth indicates a heightened vulnerability among neonates afflicted by NE[9,51]. In this analysis, we incorporated considerations for sex differences, utilizing studies that separately reported the number of CP cases for each sex. While our findings do not indicate a statistically significant difference in the incidence of NE-associated CP between male and female patients, it is crucial to acknowledge the limitations of our analysis, which stem from the restricted number of studies reporting CP cases by sex. Notably, earlier studies have reported that male patients tend to suffer from a more severe form of NE and exhibit more pronounced long-term cognitive deficits than their female counterparts[52,53]. A population-based study has also highlighted that CP subsequent to NE is more likely to affect males and manifest with greater severity than in females[33]. To comprehensively discern potential distinctions between male and female CP patients with a history of NE, further investigations are imperative.

The present analysis identified a subset of CP patients with a history of NE. Notably, this subset, though smaller in comparison to the total CP patient population, manifests a heightened incidence of severe complications. This observation is consistent with prior research indicating that children who were encephalopathic and subsequently developed CP faced a more unfavorable prognosis than their non-encephalopathic CP counterparts[33]. A recent meta-analysis focusing on neurodevelopmental outcomes in pre-term infants following intraventricular hemorrhage and white matter injury has highlighted a significantly increased crude risk of moderate to severe CP, as well as visual, hearing, and cognitive impairment[54]. Within the scope of our analysis, 5 of the 6 common complications associated with CP exhibited a positive correlation with a history of NE, and notably, 3 of these correlations reached statistical significance. The discerned pattern of complications in individuals with a history of NE provides valuable insights that can inform and guide future efforts aimed at preventing and mitigating CP-related impairments through early intervention in infants following NE.

CP is commonly diagnosed between the ages of 12 – 24 months; however, advancements in high-income countries now enable the diagnosis of CP before 6 months[51]. The current clinical diagnosis of CP relies on the collective use of clinical presentations, physical assessments, and neuroimaging[9]. Early diagnosis holds significance as it facilitates early intervention during the earliest developmental stages of patients. The present analysis posits a prospective preventive and therapeutic strategy for neonates exposed to NE-related conditions even before reaching 6 months, aiming to reduce the development of CP. There is currently no specific therapy available for CP patients who have experienced NE. For instance, in the cases of CP children with NE suffering from pronounced communication difficulties, existing clinical strategies to support communication skills are limited to supplementing or replacing functional oral communication rather than actively assisting patients in developing functional oral communication skills. Augmentative and alternative communication (AAC)[55,56], a commonly employed clinical intervention for patients with severe communication disabilities, enhances patients' interaction with others through the use of manual signs, gestures, pointing, pictures, boards, books, and speech-generating devices[56,57]. However, AAC's efficacy is highly dependent on auditory, visual, cognitive, and upper limb function[56,58], all of which were identified, in the present analysis, to be exacerbated in CP patients with preceding NE conditions. This observation suggests that the potential

of AAC may be insufficient for CP children with a history of NE. Concurrently, these patients also exhibit a heightened incidence of swallowing difficulties. Current clinical therapies primarily focus on physical training, which proves inadequate for supporting improvements in oral feeding[59]. Previous randomized controlled trials of oral feeding interventions for children with CP demonstrated potential for improvement in oral motor function. However, these interventions did not yield significant enhancements in feeding efficiency or weight gain[60-62], indicating the necessity for further development in this domain. Moreover, our analysis revealed a notably higher rate of cognitive impairment in CP patients with an NE history. Assessments of cognitive abilities in these children often rely on assumptions rather than providing an accurate evaluation of intellectual ability. This reliance on assumptions may result in potential erroneous determinations of intellectual disability[63], consequently limiting their opportunities for treatment[64], intellectual growth, and mainstream schooling[65,66]. Taken together, our findings suggest the pressing need for the development of new therapeutic strategies specifically targeted at CP patients with an NE history. Future research should prioritize addressing complications exacerbated by NE.

The present analysis also furnishes evidence indicating a significantly higher incidence of the spastic quadriplegic subtype of CP in cases where the patient has a history of NE. A recent review highlighted that CP spastic quadriplegic children often develop atypical movement patterns leading to multisystem consequences, aggravating the condition and diminishing their quality of life[67]. Given that physical disability is a shared characteristic across all CP cases, established therapies such as standard physical therapy, treadmill training, and functional gait training have proven effective interventions clinically employed to improve walking ability in patients with CP[35,36]. However, an individual case report involving a non-ambulatory young adult with spastic quadriplegic CP revealed a 9.4% decrease in the distance covered in a walking endurance test after 6 weeks of gait training. This case report suggests that while physical therapies have demonstrated efficacy in improving movement ability in CP patients overall, a combination of interventions or novel approaches may be necessary to effectively support the physical health of patients with the spastic quadriplegic subtype of CP, which was observed to be a predominant subtype following NE.

Therapeutic hypothermia is the currently recognized standard of care for NE and has demonstrated efficacy in improving the survival rate and neurological outcomes in affected neonates[68,69]. However, despite undergoing this treatment, a substantial number of patients continue to experience long-term neurological disorders, showing limited improvement in abnormalities of functional connectivity in the brain[70]. The efficacy of therapeutic hypothermia in reducing the prevalence of CP remains inconclusive. While several studies have reported a significant reduction in CP incidence with therapeutic hypothermia[71-73], another study found no clear differences in CP rates among children aged six to seven who underwent therapeutic hypothermia compared to those who did not[74]. This inconsistency underscores the imperative need for further research, especially in investigating the impact of therapeutic hypothermia on CP patients with a history of NE. Our recent meta-analysis study has demonstrated that the combination of therapeutic hypothermia with neuroprotective adjuvants not only shows promise in reducing the length of hospital stay for infants diagnosed with NE[75] but also opens avenues for further exploration. Delving into the effects of these combined therapeutic approaches on CP patients with a history of NE may pave the way for a new direction in the management of CP.

In summary, our analysis identifies an increased incidence of specific, commonly reported CP comorbidities in patients with preceding NE conditions, particularly encompassing communication challenges, swallowing difficulties, and cognitive impairment. Thus, therapeutic strategies should extend beyond addressing mobility issues and emphasize the preservation of speech, swallowing, and cognitive functions. For future clinical studies, there should be a strategic focus on monitoring a more comprehensive range of characteristics in CP patients with preceding NE conditions, with a particular emphasis on gender-specific differences. This targeted approach aims to refine the profiling of NE-induced symptoms and characteristics in CP, consequently better informing the customization of new treatment initiatives. Additionally, further research should delve into the mechanisms underlying NE-induced neurological impairments. This exploration holds the potential to contribute to the development of more effective therapies designed not only to alleviate mobility impairments but also to address additional cognitive and motor impairments in CP patients with an NE history. A more favorable clinical prognosis entails early interventions and improved access to rehabilitation resources, potentially aiding in the survival and improving neurological outcomes for children with CP. This, in turn, contributes to a more enriched daily life experience extending from childhood and into the future.

5. Conclusion

Children with CP following NE conditions at birth are more inclined to exhibit the most severe spastic quadriplegic subtype. Those CP patients with an NE history show a significant increase in the incidence of comorbidities,

particularly impairments in speech, swallowing, and cognitive functions, compared to those without such a history.

Acknowledgments

None.

Funding

This work was supported by the Natural Sciences and Engineering Research Council of Canada (NSERC RGPIN-2016-04574), awarded to Hong-Shuo Sun, and the Canadian Institutes of Health Research (CIHR- PJT-153155), awarded to Zhong-Ping Feng. Meng Yang and Sarah Eide were the recipients of the Ontario Graduate Scholarship (Doctoral).

Conflict of interest

The authors declare that they have no competing interests.

Author contributions

Conceptualization: Zhong-Ping Feng
Formal analysis: Meng Yang
Investigation: Meng Yang
Writing – original draft: Meng Yang, Sarah Eide, Zhong-Ping Feng
Writing – review & editing: All authors

All authors have made substantial contributions to this study, and all authors have agreed to publish the findings as meta-analysis.

Ethics approval and consent to participate

Not applicable.

Consent for publication

Not applicable.

Availability of data

Data used in this study can be obtained or downloaded from PubMed: https://pubmed.ncbi.nlm.nih.gov/and/or Google Scholar: https://scholar.google.com

References

1. Walstab JE, Bell RJ, Reddihough DS, *et al*., 2004, Factors identified during the neonatal period associated with risk of cerebral palsy. *Australian and New Zealand Journal of Obstetrics and Gynaecology*, 44: 342–346.

   https://doi.org/10.1111/j.1479-828X.2004.00249.x

2. Wimalasundera N, Stevenson VL, 2016, Cerebral palsy. *BMJ J*, 16: 184–194.

   https://doi.org/10.1136/practneurol-2015-001184

3. Oskoui M, Coutinho F, Dykeman J, *et al*., 2013, An update on the prevalence of cerebral palsy: A systematic review and meta-analysis. *Dev Med Child Neurol*, 55: 509–519.

   https://doi.org/10.1111/dmcn.12080

4. Garfinkle J, Wintermark P, Shevell MI, *et al*., 2016, Cerebral palsy after neonatal encephalopathy: Do neonates with suspected asphyxia have worse outcomes? *Dev Med Child Neurol*, 58: 189–194.

   https://doi.org/10.1111/dmcn.12953

5. Zhang S, Li B, Zhang X, *et al*., 2020, Birth asphyxia is associated with increased risk of cerebral palsy: A meta-analysis. *Front Neurol*, 11: 704.

   https://doi.org/10.3389/fneur.2020.00704

6. Bax M, Goldstein M, Rosenbaum P, *et al*., 2005, Proposed definition and classification of cerebral palsy, April 2005. *Dev Med Child Neurol*, 47: 571–576.

   https://doi.org/10.1017/s001216220500112x

7. Rosenbaum P, Paneth N, Leviton A, *et al*., 2007, A report: The definition and classification of cerebral palsy April 2006. *Dev Med Child Neurol,* Supplement, 109: 8–14.

8. Gorter JW, Rosenbaum PL, Hanna SE, *et al*., 2004, Limb distribution, motor impairment, and functional classification of cerebral palsy. *Dev Med Child Neurol*, 46: 461–467.

   https://doi.org/10.1017/s0012162204000763

9. Paul S, Nahar A, Bhagawati M, *et al*., 2022, A review on recent advances of cerebral palsy. *Oxid Med Cell Longev*, 2022: 2622310.

   https://doi.org/10.1155/2022/2622310

10. Abd Elmagid DS, Magdy H, 2021, Evaluation of risk factors for cerebral palsy. *Egypt J Neurol Psychiat Neurosurg*, 57: 13.

    https://doi.org/10.1186/s41983-020-00265-1

11. Grunt S, Mazenauer L, Buerki SE, *et al*., 2015, Incidence and outcomes of symptomatic neonatal arterial ischemic stroke. *Pediatrics*, 135: e1220–e1228.

    https://doi.org/10.1542/peds.2014-1520

12. Tann CJ, Nakakeeto M, Willey BA, *et al*., 2018, Perinatal risk factors for neonatal encephalopathy: An unmatched case-control study. *Arch Dis Child Fetal Neonatal Ed*, 103: F250–F256.

    https://doi.org/10.1136/archdischild-2017-312744

13. Gupta SN, Kechli AM, Kanamalla US, 2009, Intracranial hemorrhage in term newborns: Management and outcomes. *Pediatr Neurol*, 40: 1–12.

    https://doi.org/10.1016/j.pediatrneurol.2008.09.019

14. Alkalay AL, Sarnat HB, Flores-Sarnat L, *et al*., 2005, Neurologic aspects of neonatal hypoglycemia. *Isr Med Assoc J*, 7: 188–192.

15. Diringer M, 2017, Neurologic manifestations of major electrolyte abnormalities. *Handb Clin Neurol*, 141: 705–713.

https://doi.org/10.1016/B978-0-444-63599-0.00038-7

16. Glass HC, Shellhaas RA, Wusthoff CJ, *et al*., 2016, Contemporary profile of seizures in neonates: A prospective cohort study. *J Pediatr*, 174: 98–103.e1.

https://doi.org/10.1016/j.jpeds.2016.03.0

17. Saudubray JM, Garcia-Cazorla À, 2018, Inborn errors of metabolism overview: Pathophysiology, manifestations, evaluation, and management. *Pediatr Clin North Am*, 65: 179–208.

https://doi.org/10.1016/j.pcl.2017.11.002

18. Felix JF, Badawi N, Kurinczuk JJ, *et al*., 2007, Birth defects in children with newborn encephalopathy. *Dev Med Child Neurol*, 42: 803–808.

19. Ryan KS, Prewitt KC, Hayer S, *et al*., 2023, Opioid use in pregnancy: A review. *Obstet Gynecol Surv*, 78: 35–49.

https://doi.org/10.1097/OGX.0000000000001094

20. Badawi N, Pemberton PJ, Kurinczuk JJ, *et al*., 1998, Antepartum risk factors for newborn encephalopathy. *Pediatr Res*, 44: 434.

https://doi.org/10.1203/00006450-199809000-00126

21. Ferriero DM, 2004, Neonatal brain injury. *N Engl J Med*, 351: 1985–1895.

https://doi.org/10.1056/nejmra041996

22. Douglas-Escobar M, Weiss MD, 2015, Hypoxic-ischemic encephalopathy: A review for the clinician. *JAMA Pediatr*, 169: 397–403.

https://doi.org/10.1001/jamapediatrics.2014.3269

23. Dirnagl U, Iadecola C, Moskowitz MA, 1999, Pathobiology of ischaemic stroke: An integrated view. *Trends Neurosci*, 22: 391–397.

https://doi.org/10.1016/S0166-2236(99)01401-0

24. Kurinczuk JJ, White-Koning M, Badawi N, 2010, Epidemiology of neonatal encephalopathy and hypoxic-ischaemic encephalopathy. *Early Hum Dev*, 86: 329–338

https://doi.org/10.1016/j.earlhumdev.2010.05.010

25. Allen KA, Brandon DH, 2011, Hypoxic ischemic encephalopathy: Pathophysiology and experimental treatments. *Newborn Infant Nurs Rev*, 11: 125–133.

https://doi.org/10.1053/j.nainr.2011.07.004

26. Drury PP, Bennet L, Gunn AJ, 2010, Mechanisms of hypothermic neuroprotection. *Semin Fetal Neonatal Med*, 15: 287–292.

https://doi.org/10.1016/j.siny.2010.05.005

27. Wassink G, Lear CA, Gunn KC, *et al*., 2015, Analgesics, sedatives, anticonvulsant drugs, and the cooled brain. *Semin Fetal Neonatal Med*, 20: 109–114.

https://doi.org/10.1016/j.siny.2014.10.003

28. Chen W, Xu B, Xiao A, *et al*., 2015, TRPM7 inhibitor carvacrol protects brain from neonatal hypoxic-ischemic injury. *Mol Brain*, 8: 11.

https://doi.org/10.1186/s13041-015-0102-5

29. Turlova, E, Wong R, Xu B, *et al*., 2021, TRPM7 mediates neuronal cell death upstream of calcium/calmodulin-dependent protein kinase II and calcineurin mechanism in neonatal hypoxic-ischemic brain injury. *Transl Stroke Res*, 12: 164–184.

https://doi.org/10.1007/s12975-020-00810-3

30. Ovcjak A, Xiao A, Kim JS, *et al*., 2022, Ryanodine receptor inhibitor dantrolene reduces hypoxic-ischemic brain injury in neonatal mice. *Exp Neurol*, 351: 113985.

https://doi.org/10.1016/j.expneurol.2022.113985

31. Fatemi A, Wilson MA, Johnston MV, 2009, Hypoxic-ischemic encephalopathy in the term infant. *Clin Perinatol*, 36: 835–858, vii.

https://doi.org/10.1016/j.clp.2009.07.011

32. Felix JF, Badawi N, Kurinczuk JJ, *et al*., 2000, Birth defects in children with newborn encephalopathy. *Dev Med Child Neurol*, 42: 803–808.

https://doi.org/10.1017/s0012162200001493

33. Badawi N, Felix JF, Kurinczuk JJ, *et al*., 2005, Cerebral palsy following term newborn encephalopathy: A population-based study. *Dev Med Child Neurol*, 47: 293–298.

https://doi.org/10.1017/s0012162205000575

34. Nelson KB, 2008, Causative factors in cerebral palsy. *Clin Obstet Gynecol*, 51: 749–762.

https://doi.org/10.1097/grf.0b013e318187087c

35. Hesse S, Werner C, 2003, Poststroke motor dysfunction and spasticity: Novel pharmacological and physical treatment strategies. *CNS Drugs*, 17: 1093–1107.

https://doi.org/10.2165/00023210-200317150-00004

36. Booth AT, Buizer AI, Meyns P, *et al*., 2018, The efficacy of functional gait training in children and young adults with cerebral palsy: A systematic review and meta-analysis. *Dev Med Child Neurol*, 60: 866–883.

https://doi.org/10.1111/dmcn.13708

37. Deeks JJ, Higgins JP, 2010, Statistical Algorithms in Review Manager 5 on Behalf of the Statistical Methods Group of The Cochrane Collaboration Data structure Individual Study Estimates: Dichotomous Outcomes, p1–11. Available from: https://scholar.google.com/scholar_lookup?title=Statistical%20algorithms%20in%20review%20manager%205&author=J.%20Deeks&publication_year=2007

38. Yamada T, Akaishi R, Yamada T, *et al*., 2014, Risk of cerebral palsy associated with neonatal encephalopathy in macrosomic neonates. *J Obstet Gynaecol Res*, 40: 1611–1617.

https://doi.org/10.1111/jog.12367

39. Ellis M, Manandhar N, Shrestha PS, *et al*., 1999, Outcome at 1 year of neonatal encephalopathy in Kathmandu, Nepal. *Dev Med Child Neurol*, 41: 689–695.

https://doi.org/10.1017/s0012162299001413

40. Evans K, Rigby AS, Hamilton P, *et al*., 2001, The relationships between neonatal encephalopathy and cerebral palsy: A cohort study. *J Obstet Gynaecol*, 21: 114–120.

https://doi.org/10.1080/01443610020025967

41. Gaffney G, Flavell V, Johnson A, *et al*., 1994, Cerebral palsy and neonatal encephalopathy. *BMJ*, 308: 1507.

https://doi.org/10.1136/bmj.308.6942.1507

42. Kyriakopoulos P, Oskoui M, Dagenais L, *et al*., 2013, Term neonatal encephalopathy antecedent cerebral palsy: A retrospective population-based study. *Eur J Paediatr Neurol*, 17: 269–273.

https://doi.org/10.1016/j.ejpn.2012.11.001

43. Freire G, Shevell M, Oskoui M, 2015, Cerebral palsy: Phenotypes and risk factors in term singletons born small for gestational age. *Eur J Paediatr Neurol*, 19: 218–225.

https://doi.org/10.1016/j.ejpn.2014.12.005

44. Gurbuz A, Karateke A, Yilmaz U, *et al*., 2006, The role of perinatal and intrapartum risk factors in the etiology of cerebral palsy in term deliveries in a Turkish population. *J Matern Fetal Neonatal Med*, 19: 147–155.

https://doi.org/10.1080/14767050500476212

45. Stelmach T, Pisarev H, Talvik T, 2005, Ante-and perinatal factors for cerebral palsy: Case-control study in Estonia. *J Child Neurol*, 20: 654–661.

https://doi.org/10.1177/08830738050200080401

46. Sandoval Karamian, AG, Mercimek-Andrews S, Mohammad K, *et al*., 2021, Neonatal encephalopathy: Etiologies other than hypoxic-ischemic encephalopathy. *Semin Fetal Neonatal Med*, 26: 101272.

https://doi.org/10.1016/j.siny.2021.101272

47. Russ JB, Simmons R, Glass HC, 2021, Neonatal encephalopathy: Beyond hypoxic-ischemic encephalopathy. *Neoreviews*, 22: e148–e162.

https://doi.org/10.1542/neo.22-3-e148

48. Sadowska M, Sarecka-Hujar B, Kopyta I, 2020, Cerebral palsy: Current opinions on definition, epidemiology, risk factors, classification and treatment options. *Neuropsychiatr Dis Treat*, 16: 1505–1518.

https://doi.org/10.2147/ndt.S235165

49. Johnson A, Surveillance of Cerebral Palsy in Europe (SCPE), 2007, Prevalence and characteristics of children with cerebral palsy in Europe. *Dev Med Child Neurol*, 44: 633–640.

50. Himpens E, Van Den Broeck C, Oostra A, *et al*., 2008, Prevalence, type, distribution, and severity of cerebral palsy in relation to gestational age: A meta-analytic review. *Dev Med Child Neurol*, 50: 334–340.

https://doi.org/10.1111/j.1469-8749.2008.02047.x

51. Novak I, Morgan C, Adde L, *et al*., 2017, Early, accurate diagnosis and early intervention in cerebral palsy: Advances in diagnosis and treatment. *JAMA Pediatr*, 171: 897–907.

https://doi.org/10.1001/jamapediatrics.2017.1689

52. Al Mamun A, Yu H, Romana S, *et al*., 2018, Inflammatory responses are sex specific in chronic hypoxic-ischemic encephalopathy. *Cell Transplant*, 27: 1328–1339.

https://doi.org/10.1177/0963689718766362

53. Murden S, Borbélyová V, Laštůvka Z, *et al*., 2019, Gender differences involved in the pathophysiology of the perinatal hypoxic-ischemic damage. *Physiol Res*, 68: S207–S217.

https://doi.org/10.33549/physiolres.934356

54. Rees P, Callan C, Chadda KR, *et al*., 2022, Preterm brain injury and neurodevelopmental outcomes: A meta-analysis. *Pediatrics*, 150: e2022057442.

https://doi.org/10.1542/peds.2022-057442

55. Andersen G, Mjøen TR, Vik T, 2010, Prevalence of speech problems and the use of augmentative and alternative communication in children with cerebral palsy: A registry-based study in Norway. *Perspect Augment Altern Commun*, 19: 12–20.

https://doi.org/10.1044/aac19.1.12

56. Himmelmann K, Lindh K, Hidecker MJ, 2013, Communication ability in cerebral palsy: A study from the CP register of Western Sweden. *Eur J Paediatr Neurol*, 17: 568–574.

https://doi.org/10.1016/j.ejpn.2013.04.005

57. Smith AL, Hustad KC, 2015, AAC and early intervention for children with cerebral palsy: Parent perceptions and child risk factors. *Augment Altern Commun*, 31: 336–350.

https://doi.org/10.3109/07434618.2015.1084373

58. Mei C, Fern B, Reilly S, *et al*., 2020, Communication behaviours of children with cerebral palsy who are minimally verbal. *Child Care Health Dev*, 46: 617–626.

https://doi.org/10.1111/cch.12792

59. Arvedson JC, 2013, Feeding children with cerebral palsy and swallowing difficulties. *Eur J Clin Nutr*, 67: S9–S12.

https://doi.org/10.1038/ejcn.2013.224

60. Morgan AT, Dodrill P, Ward EC, 2012, Interventions for oropharyngeal dysphagia in children with neurological impairment. *Cochrane Database Syst Rev*, 10: CD009456.

https://doi.org/10.1002/14651858.CD009456

61. Rogers B, 2004, Feeding method and health outcomes of children with cerebral palsy. *J Pediatr*, 145: S28–S32.

https://doi.org/10.1016/j.jpeds.2004.05.019

62. Snider L, Majnemer A, Darsaklis V, 2011, Feeding interventions for children with cerebral palsy: A review of the evidence. *Phys Occup Ther Pediatr*, 31: 58–77.

https://doi.org/10.3109/01942638.2010.523397

63. Stadskleiv K, 2020, Cognitive functioning in children with cerebral palsy. *Dev Med Child Neurol*, 62: 283–289.

https://doi.org/10.1111/dmcn.14463

64. Novak I, McIntyre S, Morgan C, *et al*., 2013, A systematic review of interventions for children with cerebral palsy: State of the evidence. *Dev Med Child Neurol*, 55: 885–910.

https://doi.org/10.1111/dmcn.12246

65. Jenks KM, de Moor J, van Lieshout EC, *et al*., 2007, The effect of cerebral palsy on arithmetic accuracy is mediated by working memory, intelligence, early numeracy, and instruction time. *Dev Neuropsychol*, 32: 861–879.

https://doi.org/10.1080/87565640701539758

66. Jenks KM, van Lieshout EC, de Moor JM, 2012, Cognitive correlates of mathematical achievement in children with cerebral palsy and typically developing children. *Br J Educ Psychol*, 82: 120–135.

https://doi.org/10.1111/j.2044-8279.2011.02034.x

67. Wahyuni LK, 2023, Multisystem compensations and consequences in spastic quadriplegic cerebral palsy children. *Front Neurol*, 13: 1076316.

https://doi.org/10.3389/fneur.2022.1076316

68. Edwards AD, Brocklehurst P, Gunn AJ, *et al*., 2010, Neurological outcomes at 18 months of age after moderate hypothermia for perinatal hypoxic ischaemic encephalopathy: synthesis and meta-analysis of trial data. *BMJ*, 340: c363.

https://doi.org/10.1136/bmj.c363

69. Drury PP, Gunn ER, Bennet L, *et al*., 2014, Mechanisms of hypothermic neuroprotection. *Clin Perinatol*, 41: 161–175.

https://doi.org/10.1016/j.clp.2013.10.005

70. McLaren J, Holmes GL, Berg MT, 2019, Functional connectivity in term neonates with hypoxic-ischemic encephalopathy undergoing therapeutic hypothermia. *Pediatr Neurol*, 94: 74–79.

https://doi.org/10.1016/j.pediatrneurol.2019.01.006

71. Shepherd E, Salam RA, Middleton P, *et al*., 2018, Neonatal interventions for preventing cerebral palsy: An overview of cochrane systematic reviews. *Cochrane Database Syst Rev*, 3: 7–15.

72. Zhou WH, Cheng GQ, Shao XM, *et al*., 2010, Selective head cooling with mild systemic hypothermia after neonatal hypoxic-ischemic encephalopathy: A multicenter randomized controlled trial in China. *J Pediatr*, 157: 367–372.e3.

https://doi.org/10.1016/j.jpeds.2010.03.030

73. Simbruner G, Mittal RA, Rohlmann F, *et al*., 2010, Systemic hypothermia after neonatal encephalopathy: Outcomes of neo.nEURO.network RCT. *Pediatrics*, 126: e771–e778.

https://doi.org/10.1542/peds.2009-2441

74. Shankaran S, Pappas A, McDonald SA, *et al*., 2012, Childhood outcomes after hypothermia for neonatal encephalopathy. *Obstet Gynecol Surv*, 67: 617–619.

https://doi.org/10.1097/01.ogx.0000419766.08585.32

75. Ovcjak A, Pontello R, Miller SP, *et al*., 2023, Hypothermia combined with neuroprotective adjuvants shortens the duration of hospitalization in infants with hypoxic ischemic encephalopathy: Meta-analysis. *Front Pharmacol*, 13: 1037131.

https://doi.org/10.3389/fphar.2022.1037131

ACCSCIENCE PUBLISHING

Advanced Neurology

ORIGINAL RESEARCH ARTICLE

Predicting futile recanalization risk in acute basilar artery occlusion: Combination of collateral status and pre-procedural systemic inflammation response index

Yao-Wu Liu[1†], Bo Du[1,2,3†], Bilal Muhammad[2], Qi-Yang Yuan[1], Shuo Li[1], Jin-Jin Yang[1], Yan-Bo Cheng[1,2], Shi-Guang Zhu[1,2], Dian-Shuai Gao[1,3*], and De-Qin Geng[1,2,3*]

[1]Department of Neurology, Faculty of First Clinical Medical, Xuzhou Medical University, Xuzhou, Jiangsu Province, China

[2]Department of Neurology, Affiliated Hospital of Xuzhou Medical University, Xuzhou, Jiangsu Province, China

[3]Department of Neurology, Faculty of Xuzhou Medical University, Nanjing Medical University, Nanjing, Jiangsu Province, China

Abstract

Acute basilar artery occlusion (ABAO) is a rare form of acute ischemic stroke (AIS). Endovascular treatment (EVT) has emerged as a primary therapeutic approach for achieving early reperfusion of the ischemic area. However, a favorable prognosis remains elusive for a considerable number of patient post-recanalization. The assessment of disparities in hematological and radiological indicators is of notable significance for predicting the prognosis of AIS patients. Our study aimed to predict futile recanalization (FR) by analyzing inflammation levels and collateral status in ABAO patients treated with EVT. Clinical data were collected from January 2019 to March 2023. The angiographic collateral grading system for basilar artery occlusion (ACGS-BAO) and the systemic inflammation response index (SIRI) was employed to assess the collateral status and inflammation levels, respectively. FR was defined as patients experiencing an unfavorable functional outcome (modified Rankin Scale >2) at 3-month post-EVT, despite successful recanalization (modified Thrombolysis in Cerebral Infarction 2b or 3). Logistic regression models were utilized to analyze the association of ACGS-BAO and SIRI with FR. A total of 72 (65.5%) patients developed FR. Multivariate logistic analysis revealed that ACGS-BAO (odds ratio [OR]: 0.343, 95% confidence interval [CI]: 0.179 – 0.658, $P = 0.001$), procedure time (OR: 1.028, 95% CI: 1.007 – 1.050, $P = 0.01$), and natural logarithm-transformed of the SIRI (Ln[SIRI]) (OR: 2.857, 95% CI: 1.518 – 5.380, $P = 0.001$) were independently associated with FR. In receiver operating characteristic analysis, the area under the curve for ACGS-BAO combined SIRI was 0.789 (95% CI: 0.699 – 0.878; $P < 0.001$). The effects of ACGS-BAO and Ln(SIRI) on FR were similar in all subgroups ($P > 0.10$ for all interactions). In conclusion, poor collateral status and high inflammatory levels are independent predictors of FR after EVT in patients with ABAO.

Keywords: Futile recanalization; Collateral status; Inflammatory; Thrombectomy; Ischemic stroke

[†]These authors contributed equally to this work.

***Corresponding authors:**
Dian-Shuai Gao
(gds@xzhmu.edu.cn)
De-Qin Geng
(gengdeqin@126.com)

Citation: Liu Y, Du B, Muhammad B, *et al.*, 2023, Predicting futile recanalization risk in acute basilar artery occlusion: Combination of collateral status and pre-procedural systemic in lammation response index. *Adv Neuro,* 2(4): 1641. https://doi.org/10.36922/an.1641

Received: August 20, 2023

Accepted: November 28, 2023

Published Online: December 12, 2023

1. Introduction

Acute basilar artery occlusion (ABAO) accounts for approximately 10% of all strokes[1] and is distinguished as the most severe type due to its high morbidity and mortality[2]. In the early stages of ABAO, endovascular treatment (EVT) was employed to achieve vascular recanalization and reinstate blood perfusion, thus becoming the primary treatment modality[3]. Previous multi-center cohort studies demonstrated that EVT could increase the recanalization rate of ABAO to over 80%. Despite this, nearly half of the patients with successful recanalization still exhibited poor prognosis and futile recanalization (FR)[4-6]. Hussein *et al.* introduced the concept of FR in a multicenter study, defining it as Thrombolysis in Myocardial Infarction (TIMI) grade 3 in patients after EVT with a modified Rankin Scale (mRS) >2 at 3 months[7]. Subsequently, the concept of FR changed due to the modification of TIMI to modified Thrombolysis in Cerebral Infarction (mTICI)[8]. It is currently defined as the occluded vessel achieving complete recanalization (mTICI 2b or 3), but patients are unable to achieve functional independence (mRS >2) at 3 months[9,10].

The mechanisms of FR remain obscure, but many theories are inseparable from reperfusion injury[11,12]. The rapid reperfusion of ischemic brain tissue initiates a sequence of inflammatory reactions and oxidative stress, resulting in cellular and blood–brain barrier damage, ultimately culminating in neurological deterioration[13]. In recent years, multiple studies have shown that the level of systemic inflammatory response caused by acute ischemic stroke (AIS) can be evaluated through peripheral blood-based markers. The systemic inflammation response index (SIRI), composed of neutrophil count, platelet count, and lymphocyte count, offers a novel inflammatory marker that reflects the body's inflammatory status and immune function. It is widely applied to evaluate the prognosis of various diseases, such as malignancies, cardiovascular diseases, infections, stroke, and neuroimmune diseases. Furthermore, robust collateral status plays a vital role in maintaining blood perfusion in the ischemic area, including reducing core infarction and alleviating reperfusion injury[14,15]. With an increasing volume of research dedicated to appraising posterior circulation collateral status, several evaluation techniques have emerged. Digital subtraction angiography (DSA) is the recognized gold standard for diagnosing cerebrovascular diseases and provides a superior assessment method of collateral circulation quality. The angiographic collateral grading system for basilar artery occlusion (ACGS-BAO) is a novel DSA-based system for assessing collateral circulation in the basilar artery[16] and has demonstrated efficacy in predicting the clinical prognosis of ABAO patients. In this study, we evaluated the neurological function of patients at 3 months and explored the relationship between the level of inflammatory response, collateral status, and FR.

2. Materials and methods

2.1. Participants

We conducted a retrospective analysis of the clinical and imaging data collected from patients diagnosed with ABAO and treated with EVT at our institution between January 2019 and March 2023. Patients were included in the study based on the following inclusion criteria: (i) ≥18 years old, (ii) diagnosed with ABAO, (iii) underwent EVT, and (iv) completed a successful 3-month follow-up. Exclusion criteria comprised recanalization failure, incomplete clinical data, time from onset to puncture completion exceeding 24 h, patients with anterior circulation stroke, contrast agent allergy, severe active bleeding, known bleeding tendency, essential organ dysfunctions (such as heart, liver, kidney), severe hypertension uncontrollable by drugs, and pregnant or lactating women. A total of 17 patients were excluded based on these criteria. This study was carried out in compliance with the Declaration of Helsinki and was approved by the ethics committees of The Affiliated Hospital of Xuzhou Medical University.

2.2. EVT methods

All patients underwent prompt pre-operative examinations upon admission. Intravenous thrombolysis treatment was administered within the appropriate time window to patients without contraindications for venous thrombolysis. EVT comprised two main procedures:

(i) Aspiration thrombectomy: The thrombus was aspirated using a 50 mL syringe or aspiration pump as the intermediate catheter approached its core.

(ii) Stent thrombectomy: A microcatheter was navigated through the occluded segment with a micro guide wire, and thrombectomy was performed through negative pressure aspiration following stent release.

In cases where the vessels remained occluded, the aforementioned procedures could be repeated. However, stent thrombectomy was limited to a maximum of three attempts. Remedial measures, including intra-arterial thrombolysis, balloon angioplasty, stent implantation, or intra-arterial administration of tirofiban, could be employed as needed.

2.3. Clinical and imaging assessment

Demographic and clinical data were collected, including information on age, gender, hypertension, coronary heart disease, diabetes, atrial fibrillation, previous stroke history, pre-operative systolic and diastolic blood pressure,

pre-operative alkaline phosphatase, cholinesterase, red blood cell distribution width (RDW), platelet, neutrophil, monocytes, and lymphocyte counts. Additionally, patient details were gathered based on the Trial of Org 10172 in Acute Stroke Treatment (TOAST) criteria, National Institutes of Health Stroke Scale (NIHSS), Posterior Circulation Acute Stroke Prognosis Early Computed Tomography Score (pc-ASPECTS) derived from non-contrast computed tomography, occlusion site, surgical modalities, onset-to-groin puncture time (OPT), onset-to-recanalization time (ORT), and intravenous thrombolysis (IVT). The ACGS-BAO was utilized to assess collateral circulation, employing four grades: Grade 1 defined as neither posterior communicating artery (PComA) nor leptomeningeal collaterals were present, without filling to the top of the basilar artery (BA); grade 2 defined as the presence of either PComA or leptomeningeal collaterals but without filling to the top of BA; grade 3 defined as the presence of either PComA or leptomeningeal collaterals, with partial filling to the top of BA; and grade 4 defined as the presence of either PComA or leptomeningeal collaterals, with complete filling to the top of BA. Poor collateral status, based on ACGS-BAO, is defined as a grade of 1–2, intermediate status as grade 3, and good status as grade 4. In addition, SIRI was calculated as follows:

$$\text{Monocyte count} \times \frac{\text{Neutrophil count}}{\text{Lymphocyte count}} \quad \text{(I)}$$

The SIRI value was determined using hemogram parameters measured preprocedurally.

Neuro-interventional experts, independent of this study, evaluated relevant imaging data. Patient follow-ups were conducted by trained professionals who were not aware of the details of this experimental study. These follow-ups occurred either over the telephone or in the clinic, involving the patient or their family.

2.4. Outcome assessment

The mRS score was employed to assess neurologic functional outcomes at the 3-month mark. This scale spans from 0 (no residual stroke symptoms) to 6 (death). The primary outcome of this study pertained to FR subsequent to EVT. FR was defined as an mRS rating falling within the range of 3 – 6 at the 3-month assessment, even in cases where successful recanalization had been achieved.

2.5. Statistical analysis

Patients were divided into two groups based on the occurrence of FR. The normality of variables was assessed using the Shapiro–Wilk test. Continuous variables with a normal distribution were expressed as mean ± standard deviation (SD) and compared using the independent sample *t*-test. For continuous variables lacking a normal distribution, the median (25^{th} – 75^{th} interquartile range) was reported, and comparisons were made using the Mann–Whitney *U*-test. Categorical variables were expressed as counts and percentages (%) and compared using the Chi-square test. To address skewed original values, natural logarithm-transformed values were applied in the statistical analyses of SIRI. A multivariable logistic regression model, controlling for potential confounders, was employed to determine adjusted odds ratios (OR) with corresponding 95% confidence intervals (CI), assessing ACGS-BAO and natural logarithm-transformed of the SIRI (Ln[SIRI]) as independent predictors of FR. Confounders were defined as baseline variables exhibiting a difference at a level of $P < 0.05$ in univariable analysis. Receiver operating characteristic (ROC) curves were generated to calculate sensitivity and specificity, determining the cutoff value. At the same time, DeLong's test was utilized for pairwise comparison of the ROC between SIRI, ACGS-BAO, and their combination. The predictive power of ACGS-BAO and Ln(SIRI) for FR was explored across different subgroups defined by sex (male and female), age (≤60 years and >60 years), OPT (≤6 h and >6 h), stroke severity (NIHSS ≤20 and >20), and etiology (*in situ* stenosis and embolism). All tests were two-tailed, and statistical significance was defined as $P < 0.05$.

3. Results

3.1. Clinical characteristics of patients at baseline

In this study, we collected data from 127 patients with ABAO, and among them, 11 patients did not achieve successful recanalization. Ultimately, our study included a total of 110 patients with ABAO. The enrollment flow is illustrated in Figure 1.

The mean age of the participants was 63.35 ± 12.10 years, with 78 (70.9%) of them being men. Common comorbidities observed among the patients included hypertension (66 [60%]), diabetes mellitus (34 [62.1%]), coronary heart disease (19 [17.3%]), atrial fibrillation (34 [30.9%]), and prior stroke (40 [36.4%]). Further details on baseline characteristics are summarized in Table 1.

During the follow-up period, 72 patients (65.45%) exhibited a 90-day mRS score from 3 to 6 points, indicating FR and 34 patients (30.90%) succumbed to the condition.

Comparisons between the FR and non-FR groups revealed significant differences in various parameters. Specifically, the FR group scored higher systemic immune inflammation index (SII) (1589.82 [794.72 – 2515.65]) vs. 771.30 [399.17 – 1518.11], $P = 0.001$) and SIRI

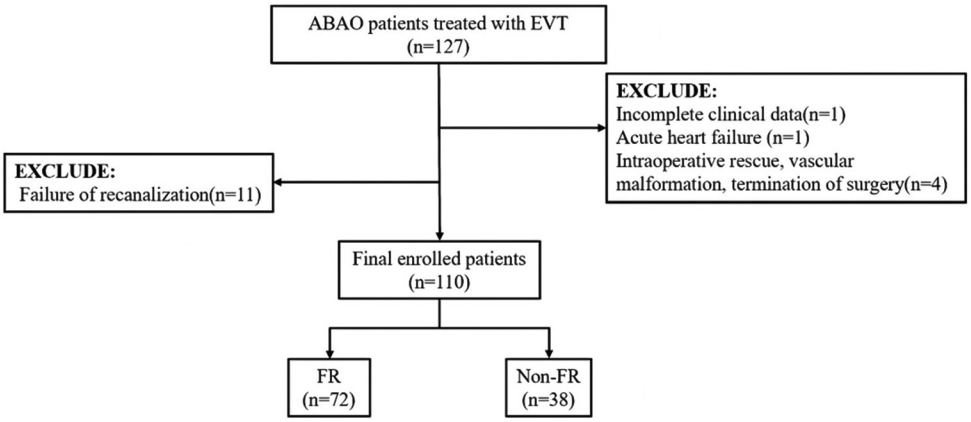

Figure 1. Flow chart of the enrollment of the study cohort.
Abbreviations: ABAO: Acute basilar artery occlusion; EVT: Endovascular therapy; FR: Futile recanalization.

(3.02 [1.54 – 6.05] vs. 1.45 [0.77 – 3.43], $P = 0.001$), as well as NIHSS scores (29 [19 – 35] vs. 19 [10 – 35], $P = 0.013$). Operation time (102.85 ± 42.12 vs. 75.82 ± 27.84, $P = 0.001$), malignant brain edema (17 [23.6%] vs. 0 [0%]), $P = 0.001$), and the incidence of hemorrhagic transformation (HT) (23 [31.9%] vs. 2 [5.3%], $P = 0.001$) were also significantly higher in the FR group. On the contrary, the collateral status, as assessed by ACGS-BAO, was lower in the FR group (2 [2 – 3] vs. 3 [2 – 4], $P < 0.001$), indicating a poorer collateral status in patients experiencing FR.

3.2. Associations of SIRI and ACGS-BAO with FR in ABAO patients following EVT

Multivariate regression analysis was performed on factors exhibiting statistical significance in the univariate regression analysis. Ln(SIRI) (OR: 2.857; 95% CI: 1.518 – 5.380, $P = 0.001$), procedure time (OR: 1.028; 95% CI: 1.007 – 1.050, $P = 0.010$), and ACGS-BAO (OR: 0.0.343; 95% CI: 0.179 – 0.658, $P = 0.001$) emerged as independent predictors for functional outcome (Table 2). The result underscored that lower ACGS-BAO and higher SIRI were associated with an increased probability of FR (Figure 2). To further elucidate, two representative cases are presented, categorized based on collateral status and SIRI (Figure 3). The distribution of the 90-day mRS scores, based on ACGS-BAO and SIRI, is presented in Figure 4.

3.3. Predicting power of SIRI and ACGS-BAO for FR using ROC curve analysis

To further validate the sensitivity and specificity, the ROC curve analysis was performed (Figure 5). The results of the ROC curve analysis indicated that the area under the curve (AUC) for ACGS-BAO was 0.717 (95% CI: 0.614 – 0.819, $P < 0.001$), for Ln(SIRI) was 0.692 (95% CI: 0.589 – 0.795, $P = 0.001$), and for procedure time was 0.696 (95% CI:0.592 – 0.801, $P = 0.001$). Setting the cutoff point at 0.730 for Ln(SIRI) and 2.5 for ACGS-BAO, sensitivity and specificity values were determined. Specifically, Ln(SIRI) exhibited a sensitivity of 65.3% and specificity of 71.1%, while ACGS-BAO demonstrated a sensitivity of 68.1% and specificity of 63.2% (Table 3). Conducting pairwise comparisons of ROC curves using the DeLong method indicated that Ln(SIRI) and ACGS-BAO alone exhibited comparable discrimination of FR ($z = 0.334$, $p = 0.738$). However, the combined use of Ln(SIRI) with ACGS-BAO resulted in superior discrimination (AUC: 0.789; 95% CI: 0.699 – 0.878; $P < 0.001$). Furthermore, no significant differences were observed between ACGS-BAO and SIRI in predicting FR across different subgroups (interaction $P > 0.10$) (Figure 6).

4. Discussion

ABAO accounts for approximately 5% of all intracranial large vessel occlusions[17], featuring a more prolonged prodrome distinct from hemispheric ischemia[18]. Early neurological deficits, such as dizziness, vertigo, maliciousness, and ataxia, are notably atypical[2,19]. These characteristics pose considerable challenges in achieving an early diagnosis of ABAO, leading to delays in treatment and extended onset-to-thrombolysis time as well as ORT. Recognizing that time is of the essence, achieving vascular recanalization in the early stages is imperative for optimal outcomes.

However, many patients encounter suboptimal prognoses due to complications such as post-operative HT, malignant cerebral edema, and pulmonary infection. Previous studies on EVT of ABAO, including BASILAR, BAOCHE, ATTENTION, BEST, and BASICS trials, have consistently reported higher rates of FR (72.6%, 61%, 67%, 66.7%, and 64.9%)[4-6,20,21]. Some research even suggests that EVT may not yield statistically significant improvements compared to standard medical therapy, posing challenges in selecting

Table 1. Demographic characteristics and clinical data of the ABAO patients treated with EVT

Variables	FR (*n*=72)	Non-FR (*n*=38)	*P*-value
Age (mean±SD year)	64.71±10.77	60.76±14.07	0.104
Male (n [%])	48 (66.7%)	30 (78.9%)	0.177
Hypertension (n [%])	45 (62.5%)	21 (55.3%)	0.461
Diabetes mellitus (n [%])	23 (31.9%)	11 (28.9%)	0.746
Coronary heart disease (n [%])	14 (19.4%)	5 (13.2%)	0.407
Atrial fibrillation (n [%])	24 (33.3%)	10 (26.3%)	0.449
Prior stroke (n [%])	28 (38.9%)	12 (31.6%)	0.449
Systolic pressure (mean±SD mm Hg)	147.18±27.71	142.84±25.15	0.426
Diastolic pressure (mean±SD mm Hg)	83.89±14.69	86.54±13.21	0.358
SII (median, IQR)	1589.82 (794.72 – 2515.65)	771.30 (399.17 – 1518.11)	0.001
Ln (SII) (mean±SD)	7.27±0.89	6.65±0.82	<0.001
SIRI (median [IQR])	3.02 (1.54 – 6.05)	1.45 (0.77 – 3.43)	0.001
Ln (SIRI) (mean±SD)	1.09±0.89	0.47±0.87	0.001
RPR	0.06 (0.05 – 0.08)	0.07 (0.06 – 0.08)	0.211
ALP (U/L)	84.64±25.43	72.32±18.62	0.01
ChE (U/L)	7740.46±1791.61	7396.11±1703.88	0.332
TOAST			0.048
LAA (n [%])	44 (61.1%)	19 (50%)	
CE (n [%])	20 (27.8%)	7 (18.4%)	
SAA (n [%])	2 (2.8%)	7 (18.4%)	
SOE (n [%])	3 (4.2%)	3 (7.9%)	
SUE (n [%])	3 (4.2%)	2 (5.3%)	
Intravenous rt-PA (n [%])	25 (34.7%)	5 (13.2%)	0.016
NIHSS score (median, IQR)	29 (19 – 35)	19 (10 – 35)	0.013
OPT (mean±SD min)	365.04±184.75	445.43±172.01	0.219
ORT (mean±SD min)	445.43±172.01	384.05±156.42	0.069
Procedure time (min)	102.85±42.12	75.82±27.84	0.001
Occlusion site			0.971
Proximal BA (n [%])	27 (37.5%)	16 (42.1%)	
Middle BA (n [%])	16 (22.2%)	8 (21.1%)	
Distal BA (n [%])	13 (18.1%)	6 (15.8%)	
Tandem lesions (n [%])	16 (22.2%)	8 (21.1%)	
ACGS-BAO (median [IQR])	2 (2 – 3)	3 (2 – 4)	<0.001
pc-ASPECTS on NCCT (median [IQR])	8 (7 – 10)	9 (8 – 10)	0.083
Infusion of tirofiban (n [%])	30 (41.7%)	19 (50%)	0.403
Surgical modalities			0.003
Aspiration thrombectomy (n [%])	15 (20.8%)	11 (28.9%)	
Stent-retriever thrombectomy (n [%])	41 (56.9%)	9 (23.7%)	
Intra-arterial thrombolysis (n [%])	16 (22.2%)	18 (47.4%)	
Malignant cerebral edema (n [%])	17 (23.6%)	0 (0%)	0.001
HT (n [%])	23 (31.9%)	2 (5.3%)	0.001

Abbreviations: ABAO: Acute basilar artery occlusion; ACGS-BAO: Angiographic Collateral Grading System for Basilar Artery Occlusion; ALP: Alkaline phosphatase; BA: Basilar artery; CE: Cardioembolism; ChE: Cholinesterase; EVT: Endovascular treatment; FR: Futile recanalization; HT: Hemorrhagic transformation; IQR: Interquartile range; LAA: Large-artery atherosclerosis; Ln (SII): Natural logarithm-transformed of systemic immune inflammation index; Ln (SIRI): Natural logarithm-transformed of systemic inflammation response index; NCCT: Non-contrast computed tomography; NIHSS: National Institutes of Health Stroke Scale; OPT: Onset-to-groin puncture time; ORT: Onset-to-recanalization time; pc-ASPECTS: Posterior Circulation Acute Stroke Prognosis Early Computed Tomography Score; RPR: Red blood cell distribution width-platelet ratio; rt-PA: Recombinant tissue plasminogen activator; SAA: Small-artery occlusion lacunar; SD: Standard deviation; SII: Systemic immune inflammation index; SIRI: Systemic inflammation response index; SOE: Stroke of other determined etiology; SUE: Stroke of undetermined etiology; TOAST: Trial of Org 10172 in Acute Stroke Treatment.

Table 2. Independent predictors of futile recanalization in ABAO patients

Variables	Univariate logistic regression analysis				Multivariate logistic regression analysis			
	β	OR	95% CI	*P*	*β*	OR	95% CI	*P*
Ln (SII)	0.835	2.306	1.398 – 3.804	0.001				
Ln (SIRI)	0.793	2.211	1.365 – 3.581	0.001	1.050	2.857	1.518 – 5.380	0.001
ALP	0.025	1.025	1.005 – 1.046	0.013				
Intravenous rt-PA	1.256	3.511	1.218 – 10.116	0.020	2.194	8.974	2.315 – 34.788	0.002
NIHSS score	0.058	1.060	1.017 – 1.104	0.005				
Procedure time	0.026	1.026	1.010 – 1.042	0.001	0.027	1.028	1.007 – 1.050	0.010
ACGS-BAO	-1.048	0.350	0.206 – 0.597	<0.001	-1.070	0.343	0.179 – 0.658	0.001
HT	2.134	8.449	1.871 – 38.155	0.006				
Surgical modalities								
Intra-arterial thrombolysis			Reference					
Stent-retriever thrombectomy	1.634	5.125	1.910 – 13.750	0.001				
aspiration thrombectomy	0.428	1.534	0.548 – 4.293	0.415				

Abbreviations: ABAO: Acute basilar artery occlusion; ACGS-BAO: Angiographic Collateral Grading System for Basilar Artery Occlusion; ALP: Alkaline phosphatase; HT: Hemorrhagic transformation; CI: Confidence interval; Ln (SII): Natural logarithm-transformed of systemic immune inflammation index; Ln (SIRI): Natural logarithm-transformed of systemic inflammation response index; OR: Odds ratio; rt-PA: Recombinant tissue plasminogen activator; NIHSS: National Institutes of Health Stroke Scale.

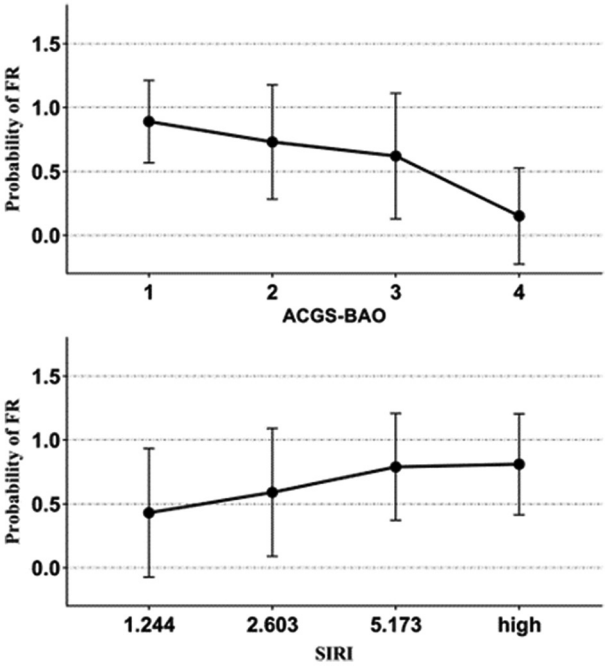

Figure 2. Probability of FR according to ACGS-BAO and SIRI. Abbreviations: ACGS-BAO: Angiographic Collateral Grading System for Basilar Artery Occlusion; FR: Futile recanalization; SIRI: Systemic inflammation response index.

optimal treatment methods for ABAO. An ongoing debate surrounds the appropriateness of administering intravenous thrombolysis before EVT. The Italian Registry of EVT in Acute Stroke (IRETAS) study indicated that, for patients within 6 h of ABAO onset, the combination of IVT and EVT (IVT + EVT) can potentially reduce mortality rates[22]. Coincidentally, another study demonstrated that, compared to direct EVT, patients with ABAO who received IVT+EVT treatment within 24 h of onset had better functional outcomes at 90 days[23]. However, in this study, patients receiving EVT + IVT treatment exhibited a higher rate of FR. We attribute this observation to the increased rate of HT (26.7% vs. 21.3%) and a higher rate of severe stroke (NIHSS > 20) (63.3% vs. 31.5%) in the IVT+EVT group. Additionally, several patients were transferred to our hospital after receiving intravenous thrombolysis at a primary stroke center, implying a longer OPT. Therefore, it is particularly important to choose a more appropriate vascular recanalization method and predict FR in these complex cases.

Few studies have delved into the mechanisms of FR. Existing research suggests that reperfusion injury and the "no-reflow" phenomenon are intricately linked to the prognosis of acute cerebral infarction, with considerable influence from the opening of collateral circulation and inflammatory factors. This paper aims to investigate the prediction of FR from two aspects: Collateral circulation status evaluation and inflammatory response level.

Collateral circulation serves as an auxiliary vascular structure that supplements cerebral blood flow in ischemic areas when the primary cerebral artery is severely narrowed or occluded. The robustness of collateral circulation plays a crucial role in identifying reperfusion, determining infarct

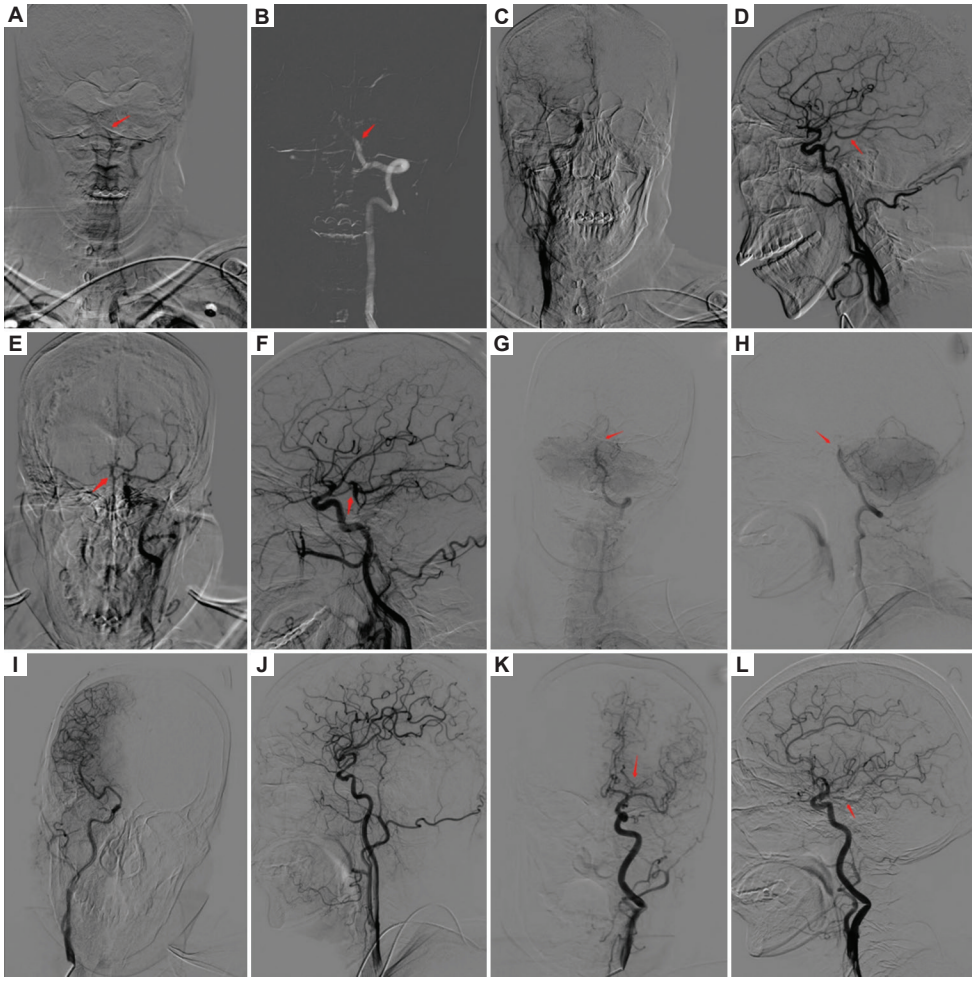

Figure 3. Representative cases of acute basilar artery occlusion. Case 1 (A-F): (A and B) Proximal basilar artery occlusion without leptomeningeal collaterals. (C and D) The right posterior communicating artery was open. (E and F) Notably, robust perfusion from the left posterior communicating artery was observed, supplying the distal basilar artery, bilateral posterior cerebral arteries, and superior cerebellar arteries. The patient had ACGS-BAO grade 4, SIRI 0.6244, and a 90-day mRS of 1 point, indicating a good prognosis. Case 2 (G-L): (G and H) Poor leptomeningeal collaterals with no visualization of the top of the basilar artery. (I and J) The right posterior communicating artery was not observed. (K and L) Although the patient's left posterior communicating artery was open, it did not perfuse the top of the basilar artery. The patient had ACGS-BAO grade 2, SIRI 3.7776, and a 90-day mRS of 4 points, indicating a poor prognosis.

Abbreviations: ACGS-BAO: Angiographic Collateral Grading System for Basilar Artery Occlusion; mRS: modified Rankin Scale; SIRI: Systemic inflammation response index.

size and even influencing the clinical outcome of AIS[24]. According to an early study, the angiographic collateral grade determines the recanalization rate after EVT. In cases of successful recanalization, patients with poor collateral circulation exhibited greater infarct growth compared to those with well-developed collaterals (P = 0.012)[25]. However, it is important to note that this study was limited to patients with acute occlusion of the middle cerebral artery, leaving a niche for studies comprehending collateral circulation in patients who have suffered an acute stroke resulting from BAO.

Owing to its unique anatomical structure, basal artery collateral circulation primarily consists of compensatory blood supply through the internal carotid artery–PComA pathway or the external carotid artery–occipital artery–vertebral artery route. Additionally, certain collateral circulation originates from pial collateral circulation, which is furnished by the superior cerebellar artery, anterior inferior cerebellar artery, and posterior inferior cerebellar artery of the vertebrobasilar arterial system. Several collateral scoring systems for the posterior circulation have emerged in recent years, such as the posterior circulation collateral score (PC-CS)[26], posterior circulation computed tomography angiography (pc-CTA)[27], basilar artery on computed tomography angiography (BATMAN)[28], and pc-ASPECTS[29]. With advancements in neuro-interventional

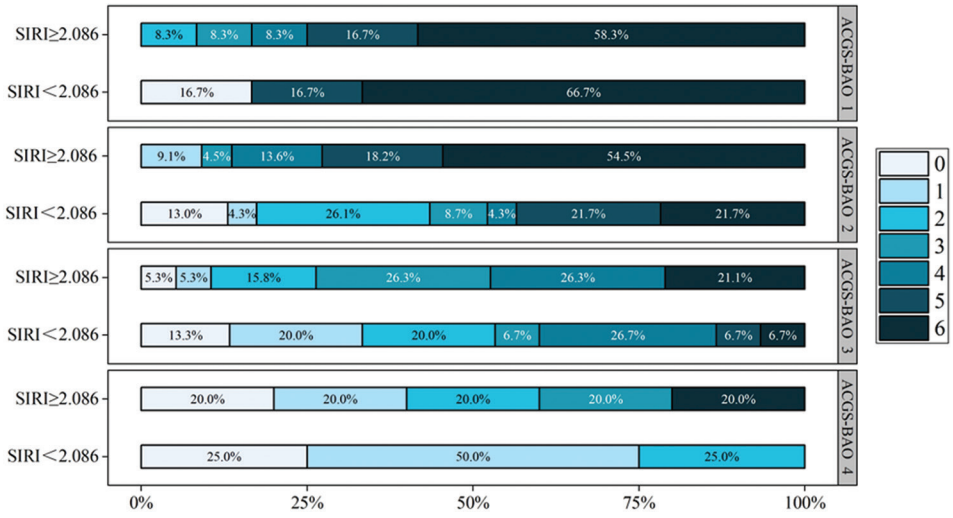

Figure 4. The distribution of 90-day mRS based on ACGS-BAO and SIRI. The numbers within the bars represent the percentage of patients. Scores range from 0 to 6, with higher scores indicating greater disability.
Abbreviations: ACGS-BAO: Angiographic Collateral Grading System for Basilar Artery Occlusion; mRS: modified Rankin Scale; SIRI: Systemic inflammation response index.

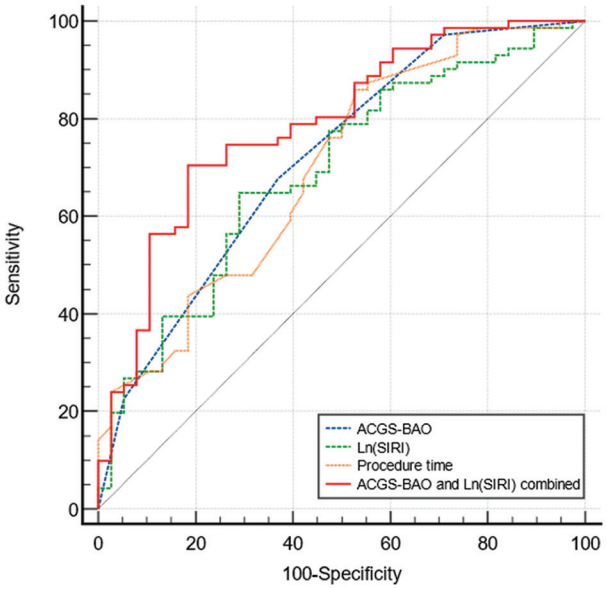

Figure 5. ROC curves for ACGS-BAO and Ln(SIRI) in predicting FR of patients with ABAO treated with EVT.
Abbreviations: ABAO: Acute basilar artery occlusion; ACGS-BAO: Angiographic Collateral Grading System for Basilar Artery Occlusion; EVT: Endovascular therapy; ROC: Receiver operating characteristic; SIRI: Systemic inflammation response index.

technology leading to an increasing number of patients undergoing EVT, collateral circulation evaluation extends beyond computed tomography/computed tomography angiography (CT/CTA). DSA allows for dynamic observation of blood perfusion, playing an irreplaceable role in collateral circulation evaluation. ACGS-BAO leverages DSA to visualize the extent of the posterior circulation, pial branches, and the basilar artery tip. This system enables a reasonably accurate evaluation of collateral compensation within the basilar artery[16].

Inflammation constitutes an essential factor affecting the severity and prognosis of AIS[30]. Following vascular occlusion, a cascade of neuronal necrosis and inflammation is immediately activated[13]. In the presence of fibrin and the adhesion molecule P-selectin, leukocytes and platelets aggregate, forming blood-platelet-leukocyte clusters that induce microvascular embolism, thereby exacerbating ischemic injury[31,32]. Neutrophils inflict damage upon the blood–brain barrier by releasing matrix metalloproteinases and a plethora of free radicals, along with discharging inflammatory mediators, thereby further intensifying and promoting brain injury[33,34]. Animal studies have revealed a continuous decline in T cells for several weeks post-occlusion of the middle cerebral artery in mice, potentially attributed to systemic immunosuppression. In addition, the decrease in lymphocytes weakens the protective effect on neurons[35,36]. Prior studies have demonstrated a strong association between higher neutrophil-to-lymphocyte ratio (NLR) and lymphocyte-to-monocyte ratio (LMR) with the prognosis of AIS[37]. However, relying on a single indicator of inflammation is insufficient for predicting the severity of inflammation. SIRI used in this study incorporates three indicators – neutrophils, monocytes, and lymphocytes – providing a reflection of both overactive coagulation and inflammatory pathways concurrently. In comparison with NLR and LMR, SIRI offers a more comprehensive depiction of a patient's inflammatory status

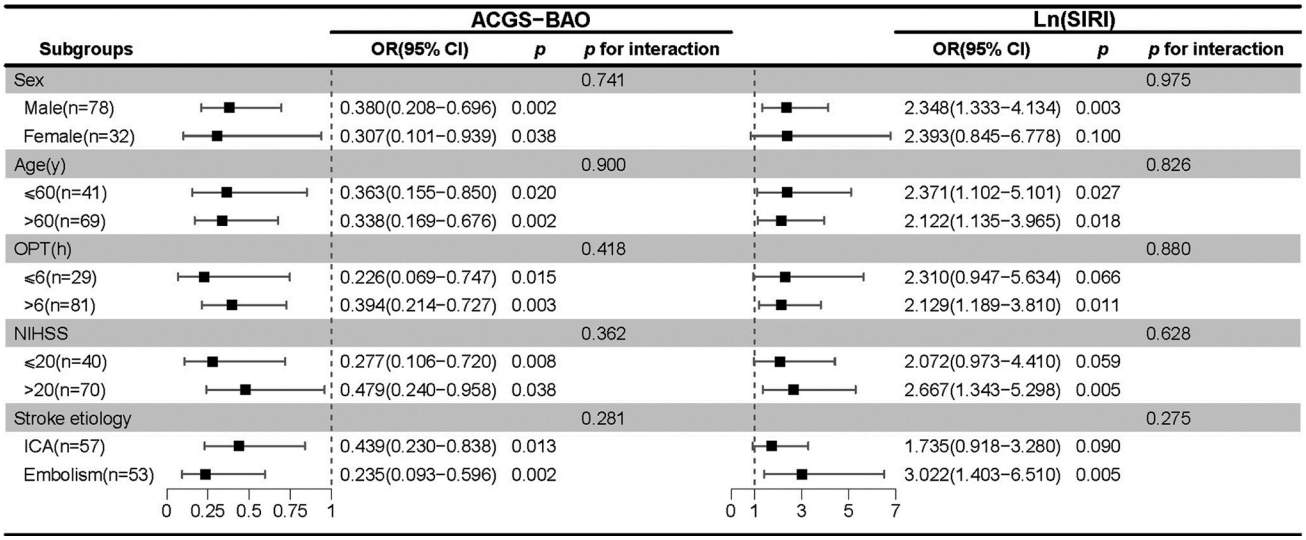

Figure 6. Association of ACGS-BAO and Ln(SIRI) with futile recanalization in subgroup analysis.
Abbreviations: ACGS-BAO: Angiographic Collateral Grading System for Basilar Artery Occlusion; CI: Confidence interval; ICA: Intracranial atherosclerotic; NIHSS: National Institutes of Health Stroke Scale; OPT: Onset-to-groin puncture time; OR: Odds ratio; SIRI: Systemic inflammation response index.

Table 3. ROC curve analysis of ACGS-BAO and Ln (SIRI)

Variables	AUC	Cutoff	95% CI	Sensitivity	Specificity	*P*
ACGS-BAO	0.717	2.5	0.614 – 0.819	0.681	0.632	<0.001
Ln (SIRI)	0.692	0.730	0.589 – 0.795	0.653	0.711	0.001
Procedure time	0.696	67	0.592 – 0.801	0.859	0.474	0.001
ACGS-BAO and Ln (SIRI) combined	0.789	0.700	0.699 – 0.878	0.708	0.816	<0.001

Abbreviations: ACGS-BAO: Angiographic Collateral Grading System for Basilar Artery Occlusion; Ln (SIRI): Natural logarithm-transformed of systemic inflammation response index; OR: Odds ratio; ROC: Receiver operating characteristic; SIRI: Systemic inflammation response index.

and the correlation between stroke and inflammation. Consequently, SIRI has the potential to serve as a more sensitive predictor of inflammation.

The effectiveness of SIRI in reflecting the state of inflammation and immune balance has been validated across various vascular diseases and cancers. Yun *et al.* conducted an analysis of 680 patients with aneurysmal subarachnoid hemorrhage (aSAH) and demonstrated that a SIRI value ≥3.2 × 10^9/L (OR: 1.82, 95% CI: 1.46 – 3.24; P = 0.021) independently predicted poor prognosis after aSAH[38]. In the cardiovascular domain, higher SIRI has proven effective in predicting major adverse cardiovascular events in patients with acute coronary syndrome undergoing percutaneous coronary intervention[39]. A retrospective study identified SIRI as an independent predictor of prognosis in gallbladder cancer[40]. Zhang *et al.* reported that elevated SIRI was associated with a higher risk of mortality and sepsis, along with higher stroke severity. Notably, SIRI outperformed other inflammation biomarkers, including NLR, platelet-to-lymphocyte ratio, LMR, and RDW (AUC: 0.6216 vs. 0.5349, 0.6216 vs. 0.5628, 0.6216 vs. 0.5579, and 0.6216 vs. 0.5865, respectively)[41]. Furthermore, higher SIRI had proven valuable in predicting poor clinical outcomes for patients with mild AIS following IVT (OR: 2.938, 95% CI: 1.805 – 4.782, P < 0.001)[42]. Yi *et al.* demonstrated that a SIRI threshold <2.9 (OR: 2.27, 95% CI: 1.29 – 5.17, P = 0.019) was an independent predictor of good prognosis in EVT for large artery occlusion[43]. The pre-procedural application of SIRI as an auxiliary method for predicting prognosis has proven effective and holds promise for future clinical application.

This study is not without its limitations. First, it is imperative to acknowledge that this study is a single-center retrospective study characterized by a small sample size (n = 110). This intrinsic limitation may introduce a degree of selection bias. Second, a notable constraint lies in the exclusive focus on SIRI without concurrent consideration of pivotal inflammatory markers such as high-sensitivity C-reactive protein, interleukin-1, interleukin-6, and tumor necrosis factors. The absence of these markers in the

analytical framework may compromise a comprehensive assessment of the inflammation status among the study participants. Finally, it is essential to underscore that all procedures within the purview of this study were executed by multiple neuro-intervention specialists. The variability in operators' experience levels and distinct operational methodologies potentially introduces an element of subjectivity that may impact vessel recanalization.

5. Conclusion

In conclusion, ACGS-BAO and pre-procedural SIRI stand as standard, readily available metrics in clinical practice. They respectively evaluate the condition of basilar collateral circulation and the extent of the inflammatory response, both intrinsically linked to the occurrence of FR post-EVT. Our study affirms a negative correlation between collateral circulation status and FR while conversely establishing a positive correlation with inflammation levels. The combined use of these two biomarkers proves more predictive of post-operative FR than the isolated use of either marker. This finding holds significant implications for tailoring individualized treatment strategies and mitigating the risk of additional injuries.

Acknowledgments

None.

Funding

The study supported by the National Health Commission Brain Prevention Committee, under the grant "Research and Promotion Project of Appropriate Technology Intervention for High-risk Groups of Stroke in China" (GN-2018R0009), and "Xuzhou Promoting Science and Technology Innovation Project" (KC22241).

Conflict of interest

The authors declare that they have no competing interests.

Author contributions

Conceptualization: Yao-Wu Liu, Bo Du, De-Qin Geng
Data curation: Yao-Wu Liu, Qi-Yang Yuan, Shuo Li, Jin-Jin Yang
Formal analysis: Yao-Wu Liu, Qi-Yang Yuan, Bo Du
Investigation: Dian-Shuai Gao, De-Qin Geng
Methodology: Yao-Wu Liu, Shi-Guang Zhu, De-Qin Geng
Writing – original draft: Yao-Wu Liu, Qi-Yang Yuan, Bo Du
Writing – review & editing: Yao-Wu Liu, Bilal Muhammad, Yan-Bo Cheng, Shi-Guang Zhu, De-Qin Geng

All authors read and approved the final manuscript.

Ethics approval and consent to participate

This study was approved by the Medical Ethics Committee of the Affiliated Hospital of Xuzhou Medical University (approval number: XYFY2018-KL078). Written informed consent was individually obtained from all patients. We affirm that all methods conducted in our study adhered to the pertinent guidelines and regulations.

Consent for publication

Not applicable.

Availability of data

The datasets used and analyzed during the current study are available from the corresponding author upon reasonable request.

References

1. Israeli-korn SD, Schwammenthal Y, Yonash-Kimchi T, *et al*., 2010, Ischemic stroke due to acute basilar artery occlusion: proportion and outcomes. *Isr Med Assoc J*, 12: 671–675.
2. Mattle HP, Arnold M, Lindsberg PJ, *et al*., 2011, Basilar artery occlusion. *Lancet Neurol*, 10: 1002–1014.
3. Gory B, Eldesouky I, Sivan-Hoffmann R, *et al*., 2016, Outcomes of stent retriever thrombectomy in basilar artery occlusion: An observational study and systematic review. *J Neurol Neurosurg Psychiatry*, 87: 520–525.
   https://doi.org/10.1136/jnnp-2014-310250
4. Zi W, Qiu Z, Wu D, *et al*., 2020, Assessment of endovascular treatment for acute basilar artery occlusion via a nationwide prospective registry. *JAMA Neurol*, 77: 561–573.
   https://doi.org/10.1001/jamaneurol.2020.0156
5. Jovin TG, Li C, Wu L, *et al*., 2022, Trial of thrombectomy 6 to 24 hours after stroke due to basilar-artery occlusion. *N Engl J Med*, 387: 1373–1384.
   https://doi.org/10.1056/NEJMoa2207576
6. Tao C, Nogueira RG, Zhu Y, *et al*., 2022, Trial of endovascular treatment of acute basilar-artery occlusion. *N Engl J Med*, 387: 1361–1372.
   https://doi.org/10.1056/NEJMoa2206317
7. Hussein HM, Georgiadis AL, Vazquez G, *et al*., 2010, Occurrence and predictors of futile recanalization following endovascular treatment among patients with acute ischemic stroke: A multicenter study. *AJNR Am J Neuroradiol*, 31: 454–458.
   https://doi.org/10.3174/ajnr.A2006
8. Tomsick T, Broderick J, Carrozella J, *et al*., 2008, Revascularization results in the interventional management of stroke II trial. *AJNR Am J Neuroradiol*, 29: 582–587.

https://doi.org/10.3174/ajnr.A0843

9. Tateishi Y, Wisco D, Aoki J, *et al*., 2015, Large deep white matter lesions may predict futile recanalization in endovascular therapy for acute ischemic stroke. *Interv Neurol*, 3: 48–55.

https://doi.org/10.1159/000369835

10. Tomsick TA, Yeatts SD, Liebeskind DS, *et al*., 2015, Endovascular revascularization results in IMS III: Intracranial ICA and M1 occlusions. *J Neurointerv Surg*, 7: 795–802.

https://doi.org/10.1136/neurintsurg-2014-011318

11. Sun MS, Jin H, Sun X, *et al*., 2018, Free radical damage in ischemia-reperfusion injury: An obstacle in acute ischemic stroke after revascularization therapy. *Oxid Med Cell Longev*, 2018: 3804979.

https://doi.org/10.1155/2018/3804979

12. Nie X, Leng X, Miao Z, *et al*., 2023, Clinically ineffective reperfusion after endovascular therapy in acute ischemic stroke. *Stroke*, 54: 873–881.

https://doi.org/10.1161/STROKEAHA.122.038466

13. Iadecola C, Anrather J, 2011, The immunology of stroke: From mechanisms to translation. *Nat Med*, 17: 796–808.

https://doi.org/10.1038/nm.2399

14. Tariq N, Khatri R. 2008, Leptomeningeal collaterals in acute ischemic stroke. *J Vasc Interv Neurol*, 1: 91–95.

15. Venema SM, Dankbaar JW, Van der Lugt A, *et al*., 2022, Cerebral collateral circulation in the era of reperfusion therapies for acute ischemic stroke. *Stroke*, 53: 3222–3234.

https://doi.org/10.1161/STROKEAHA.121.037869

16. Gao F, Tong X, Sun X, 2021, A new angiographic collateral grading system for acute basilar artery occlusion treated with endovascular therapy. *Transl Stroke Res*, 12: 559–568.

https://doi.org/10.1007/s12975-020-00856-3

17. Kayan Y, Meyers PM, Prestigiacomo CJ, *et al*., 2019, Current endovascular strategies for posterior circulation large vessel occlusion stroke: Report of the society of neurointerventional surgery standards and guidelines committee. *J Neurointerv Surg*, 11: 1055–1062.

https://doi.org/10.1136/neurintsurg-2019-014873

18. Voetsch B, DeWitt LD, Pessin MS, *et al*., 2004, Basilar artery occlusive disease in the New England medical center posterior circulation registry. *Arch Neurol*, 61: 496–504.

https://doi.org/10.1001/archneur.61.4.496

19. Nouh A, Remke J, Ruland S, 2014, Ischemic posterior circulation stroke: A review of anatomy, clinical presentations, diagnosis, and current management. *Front Neurol*, 5: 30.

https://doi.org/10.3389/fneur.2014.00030

20. Liu X, Dai Q, Ye R, *et al*., 2020, Endovascular treatment versus standard medical treatment for vertebrobasilar artery occlusion (BEST): An open-label, randomised controlled trial. *Lancet Neurol*, 19: 115–122.

https://doi.org/10.1016/S1474-4422(19)30395-3

21. Langezaal L, Van der Hoeven E, Mont'Alverne F, *et al*., 2021, Endovascular therapy for stroke due to basilar-artery occlusion. *N Engl J Med*, 384: 1910–1920.

https://doi.org/10.1056/NEJMoa2030297

22. Nappini S, Arba F, Pracucci G, *et al*., 2021, Bridging versus direct endovascular therapy in basilar artery occlusion. *J Neurol Neurosurg Psychiatry*, 92: 956–962.

https://doi.org/10.1136/jnnp-2020-325328

23. Nie X, Wang D, Pu Y, *et al*., 2022, Endovascular treatment with or without intravenous alteplase for acute ischaemic stroke due to basilar artery occlusion. *Stroke Vasc Neurol*, 7: 190–199.

https://doi.org/10.1136/svn-2021-001242

24. Ginsberg MD, 2018, The cerebral collateral circulation: Relevance to pathophysiology and treatment of stroke. *Neuropharmacology*, 134: 280–292.

https://doi.org/10.1016/j.neuropharm.2017.08.003

25. Bang OY, Saver JL, Kim SJ, *et al*., 2011, Collateral flow predicts response to endovascular therapy for acute ischemic stroke. *Stroke*, 42: 693–699.

https://doi.org/10.1161/STROKEAHA.110.595256

26. Van der Hoeven EJ, McVerry F, Vos JA, *et al*., 2016, Collateral flow predicts outcome after basilar artery occlusion: The posterior circulation collateral score. *Int J Stroke*, 11: 768–775.

https://doi.org/10.1177/1747493016641951

27. Da Ros V, Meschini A, Gandini R, *et al*., 2016, Proposal for a vascular computed tomography-based grading system in posterior circulation stroke: A single-center experience. *J Stroke Cerebrovasc Dis*, 25: 368–377.

https://doi.org/10.1016/j.jstrokecerebrovasdis.2015.10.008

28. Alemseged F, Shah DG, Diomedi M, *et al*., 2017, The basilar artery on computed tomography angiography prognostic score for basilar artery occlusion. *Stroke*, 48: 631–637.

https://doi.org/10.1161/STROKEAHA.116.015492

29. Puetz V, Sylaja PN, Coutts SB, *et al*., 2008, Extent of hypoattenuation on CT angiography source images predicts functional outcome in patients with basilar artery occlusion. *Stroke*, 39: 2485–2490.

https://doi.org/10.1161/STROKEAHA.107.511162

30. Parikh NS, Merkler AE, Iadecola C. Inflammation, autoimmunity, infection, and stroke: Epidemiology and lessons from therapeutic intervention. *Stroke*, 51: 711–718.

https://doi.org/10.1161/STROKEAHA.119.024157

31. De Meyer SF, Denorme F, Langhauser F, *et al*., 2016, Thromboinflammation in stroke brain damage. *Stroke*, 47: 1165–1172.

https://doi.org/10.1161/STROKEAHA.115.011238

32. Anrather J, Iadecola C, 2016, Inflammation and stroke: An overview. *Neurotherapeutics*, 3: 661–670.

https://doi.org/10.1007/s13311-016-0483-x

33. Justicia C, Panés J, Solé S, *et al*., 2003, Neutrophil infiltration increases matrix metalloproteinase-9 in the ischemic brain after occlusion/reperfusion of the middle cerebral artery in rats. *J Cereb Blood Flow Metab*, 23: 1430–1440.

https://doi.org/10.1097/01.WCB.0000090680.07515.C8

34. Amantea D, Nappi G, Bernardi G, *et al*., 2009, Post-ischemic brain damage: Pathophysiology and role of inflammatory mediators. *FEBS J*, 276: 13–26.

https://doi.org/10.1111/j.1742-4658.2008.06766.x

35. Prass K, Meisel C, Höflich C, *et al*., 2003, Stroke-induced immunodeficiency promotes spontaneous bacterial infections and is mediated by sympathetic activation reversal by poststroke T helper cell type 1-like immunostimulation. *J Exp Med*, 198: 725–736.

https://doi.org/10.1084/jem.20021098

36. Offner H, Vandenbark AA, Hurn PD, 2009, Effect of experimental stroke on peripheral immunity: CNS ischemia induces profound immunosuppression. *Neuroscience*, 158: 1098–1111.

https://doi.org/10.1016/j.neuroscience.2008.05.033

37. Gong P, Liu Y, Gong Y, *et al*., 2021, The association of neutrophil to lymphocyte ratio, platelet to lymphocyte ratio, and lymphocyte to monocyte ratio with post-thrombolysis early neurological outcomes in patients with acute ischemic stroke. *J Neuroinflammation*, 18: 51.

https://doi.org/10.1186/s12974-021-02090-6

38. Yun S, Yi HJ, Lee DH, *et al*., 2021, Systemic inflammation response index and systemic immune-inflammation index for predicting the prognosis of patients with aneurysmal subarachnoid hemorrhage. *J Stroke Cerebrovasc Dis*, 30: 105861.

https://doi.org/10.1016/j.jstrokecerebrovasdis.2021.105861

39. Han K, Shi D, Yang L, *et al*., 2022, Prognostic value of systemic inflammatory response index in patients with acute coronary syndrome undergoing percutaneous coronary intervention. *Ann Med*, 54: 1667–1677.

https://doi.org/10.1080/07853890.2022.2083671

40. Sun L, Hu W, Liu M, *et al*., 2020, High systemic inflammation response index (SIRI) indicates poor outcome in gallbladder cancer patients with surgical resection: A single institution experience in China. *Cancer Res Treat*, 52: 1199–1210.

https://doi.org/10.4143/crt.2020.303

41. Zhang Y, Xing Z, Zhou K, *et al*., 2021, The predictive role of systemic inflammation response index (SIRI) in the prognosis of stroke patients. *Clin Interv Aging*, 16: 1997–2007.

https://doi.org/10.2147/CIA.S339221

42. Chu M, Luo Y, Wang D, *et al*., 2023, Systemic inflammation response index predicts 3-month outcome in patients with mild acute ischemic stroke receiving intravenous thrombolysis. *Front Neurol*, 14: 1095668.

https://doi.org/10.3389/fneur.2023.1095668

43. Yi HJ, Sung JH, Lee DH, 2021, Systemic inflammation response index and systemic immune-inflammation index are associated with clinical outcomes in patients treated with mechanical thrombectomy for large artery occlusion. *World Neurosurg*, 153: e282–e289.

https://doi.org/10.1016/j.wneu.2021.06.113

ACCSCIENCE PUBLISHING

Advanced Neurology

ORIGINAL RESEARCH ARTICLE

Evoked potential response in patients with idiopathic Parkinson's disease and atypical parkinsonian syndromes: A comparative study

Manoj Roy, Amar Kumar Misra, Joydeep Mukherjee*, Manamita Mandal, Jasodhara Chaudhuri, Kartik Chandra Ghosh, and Bijendra Mohanty

Department of Neurology, Nil Ratan Sircar Medical College and Hospital, AJC Bose Road, Kolkata, West Bengal, India

Abstract

Patients with idiopathic Parkinson's disease (IPD) and atypical parkinsonian syndromes (APSs) suffer from a range of disorders, especially in balance and locomotion, which necessitate visual, auditory, and somatosensory inputs. In this study, IPD patients, APS patients, and healthy controls (HCs) ($n = 50$ per group) underwent a series of assessments for visual evoked potentials (VEP), brainstem auditory evoked response (BAER), and short-latency somatosensory evoked potentials (SSEP). Results showed that VEP P100 latency was prolonged in multiple system atrophy-cerebellar type (MSA-C), multiple system atrophy-parkinsonian type (MSA-P), and corticobasal ganglionic degeneration (CBD) patients. The latency of peaks III and V was prolonged in IPD, MSA-C, dementia with Lewy bodies (DLB), and Parkinson's disease dementia (PDD). BAER I-III and I-V interpeak latency were prolonged in IPD, DLB, and PDD, whereas BAER I-III, III-V, and I-V interpeak latencies were increased and the V/I amplitude ratio was decreased in MSA-C. The central sensory conduction time (N20-N13) was increased in MSA-P and MSA-C in SSEP. IPD patients had prolonged VEP P100 latency ($P < 0.001$), lower VEP N75-P100 amplitude ($P < 0.001$), prolonged BAER I, II, II, IV, V peak latencies ($P < 0.001$), I-III, I-V interpeak latencies ($P < 0.001$), lower BAER V/I amplitude ratio ($P < 0.001$), and prolonged SSEP N13, N20, central sensory conduction time (N20-N13) ($P < 0.001$) than HCs. IPD patients also had prolonged BAER I, II, II, IV, V peak latencies ($P < 0.001$), prolonged I-III, I-V interpeak latencies ($P < 0.001$), and shorter SSEP N13, N20, central sensory conduction time (N20-N13) ($P < 0.001$) than APS patients. Moreover, APS patients had prolonged VEP P100 and N145 latencies ($P < 0.001$) and decreased N75-N145 amplitude ($P < 0.001$) compared to HCs. APS patients also had prolonged BAER II, II, IV, V peak latencies ($P < 0.001$), prolonged I-III, III-V, I-V interpeak latencies ($P < 0.001$), decreased V/I amplitude ratio, and prolonged SSEP N13, N20, central sensory conduction time (N20-N13) ($P < 0.001$) than HCs. Postural instability and gait disorder (PIGD) IPD had significantly prolonged BAER III, V peak latencies ($P < 0.05$), and prolonged III-V interpeak latencies ($P < 0.05$) compared to tremor-dominant IPD. Overall, the IPD and APS patients had significant VEP, BAER, and SSEP abnormalities of demyelination and axonal variety in the visual, auditory, and somatosensory pathways. The changes were also correlated with the disease duration and severity. Although the diseases are predominantly motor disorders with significant non-motor components, these electrophysiological abnormalities might open a new avenue to assess the non-motor symptoms.

Keywords: Idiopathic Parkinson's disease; Atypical parkinsonian syndromes; Visual evoked potentials; P100; Brainstem auditory evoked response; Short-latency somatosensory evoked potentials

***Corresponding author:**
Joydeep Mukherjee
(joydeepdoc@gmail.com)

Citation: Roy M, Misra AK, Mukherjee J, *et al.*, 2023, Evoked potential response in patients with idiopathic Parkinson's disease and atypical parkinsonian syndromes: A comparative study. *Adv Neuro,* 2(4): 1907.
https://doi.org/10.36922/an.1907

Received: September 25, 2023

Accepted: November 28, 2023

Published Online: December 14, 2023

1. Introduction

Idiopathic Parkinson's disease (IPD) is a neurodegenerative disorder affecting old and late middle-aged populations. The characteristic clinical features of IPD include tremors, muscular rigidity, bradykinesia, and impairment of postural reflexes[1,2]. In addition, IPD is characterized by several defining pathological features, such as specific degeneration of nigral and other pigmented brain stem nuclei and inclusion of Lewy bodies in the nerve cells[3].

Atypical parkinsonian syndromes (APS) represent a group of heterogeneous degenerative neurological disorders that differ from the classical IPD in terms of the associated clinical features. Progressive supranuclear palsy (PSP), multiple system atrophy (MSA), and dementia with Lewy body disease (DLB) are common disorders. Less frequent disorders include corticobasal ganglionic degeneration (CBD), frontotemporal dementia with chromosome 17 (FTDP-17), Pick's disease, and the parkinsonian-dementia complex of Guam[3]. Evoked potentials, or evoked responses such as visual evoked potentials (VEPs), short-latency somatosensory evoked potentials (SSEP), short-latency brainstem auditory evoked response (BAER), are measurements used to assess the electrophysiologic responses of the nervous system to a variety of stimuli.

Based on the positive correlation between latency and disease severity discovered by Gawel *et al.*, VEP proves valuable in the assessment of Parkinson's disease[4]. The SSEP test could show the sensory electrical signals from the different organs to the brain or spinal cord. On the other hand, waves III and V in the BAER test reflect the postsynaptic activity in structures such as superior olive and colliculus. Therefore, the postsynaptic changes caused by these diseases could be corroborated with the BAER study. At present, evoked potentials in APS have not been evaluated thoroughly. This study was designed under the hypothesis that APS presents altered evoked potentials, which provides a new avenue for differentiating between IPD and APS.

2. Materials and methods

2.1. Study subjects

This is a cross-sectional, observational study conducted in the inpatient and outpatient clinics of the Department of Neurology in a multispecialty teaching hospital from September 2017 to August 2020. We enrolled patients of both genders of various age groups. Healthy controls (HCs) were selected from age and gender-matched asymptomatic medical college staff. The study participants were categorized into IPD, APS, and HC groups, with 50 patients per group. Detailed neurological examinations were performed. HCs were only recruited if their clinical examination results were normal. The study participants were required to provide all relevant information related to this study. Informed consent was obtained before recruiting them. This study was approved by the institutional ethics committee.

Inclusion criteria of this study are as follows:

(i). All IPD cases were diagnosed in adherence with the UK Parkinson's Disease Society Brain Bank Clinical Diagnostic Criteria[5].

(ii). All APS cases were diagnosed using the validated clinical criteria[6-9].

Exclusion criteria of this study are as follows:

(i). Cases of secondary parkinsonism

(ii). Patients with previously known ophthalmological disorders (uncorrected refractive errors, glaucoma, retinopathies, etc.) and hearing difficulties after thorough evaluation by ophthalmologist and otorhinolaryngologist, respectively.

2.2. Study design

This is a cross-sectional, observational study. The flowchart of the study is depicted in Figure 1.

2.3. Parameters for evaluation

Evoked potentials were recorded using Nihon Kohden Neuropack II plus.

2.3.1. VEPs

Patients and normal controls with no ocular pathology and a visual acuity of not more than 6/9 were selected. The recording was made with Nihon Kohden Neuropack II plus for Checkboard patterned reversal VEP (CBPR VEP). VEP was recorded from each eye separately with surface electrodes, with the reference electrode placed on Fz, the active electrode on Oz, and other electrodes in O1 and O2 as per the International 10-20 system. The analysis time was 500 msec, and 256 sweeps were averaged. N75 latency, P100 latency, and P100 amplitude were recorded. P100 latency is the interval between the stimulus and the peak of the major positive component.

2.3.2. Brainstem auditory evoked potential

Auditory evoked responses were obtained by brief acoustic click stimuli delivering monophasic square pulses of 100-msec duration to headphones with a monoaural stimulus intensity of 60 – 65 dB HL. Given that there were many patients experiencing subclinical hearing loss in this sample, we resorted to gradually increasing the decibel if a BAER waveform was not obtained. The patients

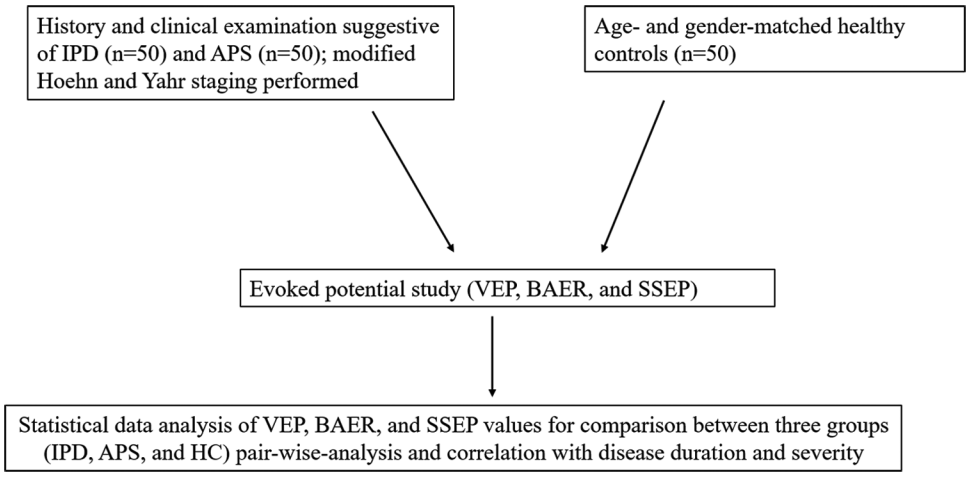

Figure 1. Flow chart of the study.
Abbreviations: IPD: Idiopathic Parkinson's disease; APS: Atypical parkinsonian syndromes; HC: Healthy control; VEP: Visual evoked potentials; BAER: Brainstem auditory evoked response; SSEP: Short-latency somatosensory evoked potentials.

with known hearing loss, after being confirmed by an otorhinolaryngologist, were excluded. The contralateral ear was masked with continuous white noise at 30 to 40 dB below the BAER stimulus. Recording electrodes were placed at the vertex (location Cz of the International 10–20 System) and the mastoids (Mi and Mc). Amplitude and latency of waves I to V were recorded.

2.3.3. Somatosensory evoked potential

The median nerves were stimulated at the wrists using the standard technique. The anode was placed just proximal to the palmar crease, and the cathode was placed between the tendons of the palmaris longus muscle, 3 cm proximal to the anode. Recording amplifier filter settings for SEPs were 5 – 30 Hz (low-cut or high-pass filter) to 3,000 Hz (high-cut or low-pass filter). Electrodes were placed over Erb's point (*i.e.*, the angle between the clavicular head of the sternocleidomastoid muscle and the clavicle), both ipsilateral and contralateral to the stimulus (labeled EPi and EPc, respectively). Recording electrodes over the spine were placed in the midline labeled as C5S using the international 10 – 20 system. Electrode CP3 was midway between C3 and P3, and electrode CP4 was midway between C4 and P4. CPi was ipsilateral to the stimulated limb, and CPc was the contralateral centroparietal scalp electrode. According to the guidelines of the American Clinical Neurophysiology Society, following channels were used. Recordings were obtained from the neck at the C-5 level (the N13 potential) and the contralateral scalp (the N20 potential). Each run was repeated and superimposed. The peak latencies of the cervical (N13) and scalp (N20) potentials were used to calculate the "central conduction time" (CCT).

2.4. Statistical analysis

We performed standard statistical methods using IBM SPSS software version 26. Kolmogorov–Smirnov test was conducted to evaluate the normality of data distribution. Since the data were not normally distributed, Mann–Whitney *U*-test was performed to compare the median between the groups and $P < 0.05$ was considered statistically significant.

3. Results

3.1. Patient demography

The demographical parameters are tabulated in Table 1. The age at onset and presentation were nearly similar in the IPD and APS categories. The HCs were also enrolled after matching for ages. There were more male patients than female patients both IPD and APS groups, with the percentage of the male population higher in APS than in IPD. In this study, the number of IPD cases of tremor-predominant variety surpassed that of postural instability and gait disorder (PIGD) (74% vs. 26%). Meanwhile, progressive supranuclear palsy (PSP) patients accounted for the majority of cases in the APS group. Among the IPD subclasses, the PIGD patients scored higher in the modified Hoehn and Yahr staging scale than the tremor-predominant variety patients did (1.84 ± 0.9 vs. 1.74 ± 1).

3.2. VEP, BAER, and SSEP values in patients and HCs

The means and standard deviations of VEP, BAER, and SSEP in IPD, different variants of APS, and HCs were recorded (Table 2). IPD patients had increased waves III and V latency and interpeak latency in I-III and I-V bilaterally. SSEP was in the normal range in IPD. PSP patients had normal mean values in VEP, BAER, and

Table 1. Demographic summary of the patients and HC

Parameter	IPD	APS	HC	Modified Hoehn and Yahr staging
Total cases	50	50	50	
Age at onset (year)	57.4±6.8	58.2±6.2		
Age at presentation (year)	60.4±6.9	60.8±6	60.0±4.2	
Duration of disease (year)	3.0±1.4	2.6±0.8		
Gender (male %)	58	64	50	
IPD categories				
PIGD (*n*=13)	26%			1.84±0.9
Tremor-dominant variety (*n*=37)	74%			1.74±1
APS categories				
PSP (*n*=25)		50%		
MSA-C (*n*=9)		18%		
MSA-P (*n*=6)		12%		
CBD (*n*=5)		10%		
DLB (*n*=3)		6%		
PDD (*n*=2)		4%		

Abbreviations: IPD: Idiopathic Parkinson's disease; APS: Atypical parkinsonian syndromes; HC: Healthy control; PIGD: Postural instability and gait disorder Parkinson's disease; PSP: Progressive supranuclear palsy; MSA: Multiple system atrophy (C: Cerebellar variety, P: Parkinsonian variety); CBD: Corticobasal degeneration; DLB: Dementia with Lewy bodies; PDD: Parkinson's disease dementia; n: Number.

SSEP. MSA-cerebellar type (MSA-C), MSA-parkinsonian type (MSA-P), and CBD patients had bilateral VEP P100-pronged latency. MSA-C, DLB, and Parkinson's disease dementia (PDD) patients had prolonged latency in waves III and V and interpeak latency in I-V bilaterally. In addition, MSA-C patients had prolonged interpeak latency of III-V and an increased amplitude ratio of V/I wave. The central sensory conduction time (N20-N13) was prolonged in MSA-C and MSA-P patients.

3.3. Comparison between IPD and HCs

IPD patients had significantly higher P100 latency and significantly lower N75-P100 amplitude on the right side compared to HCs. On the contrary, IPD patients had higher P100 and P145 latency and significantly lower N75-P100 amplitude on the right side compared to HCs. In contrast to the VEP asymmetry, BAER had more symmetrical differences between the IPD and HCs. Except for the reduced latency of wave I in IPD patients compared to HCs, all other BAER wave latencies and interpeak latencies were prolonged bilaterally in the IPD group. Moreover, the V/I amplitude ratio was also decreased in IPD. SSEP did not show any statistically significant difference between these two groups (Table 3).

3.4. Comparison between APS and HCs

VEP, BAER, and SSEP showed prolonged bilateral latencies and reduced amplitudes in most of the waves in the APS group compared to the HCs (Table 3). Thus, the relative symmetry and extensive abnormalities were presented in APS compared to IPD. Interestingly, wave I of BAER did not show any significant difference between APS and HC.

3.5. Comparison between IPD and APS

Table 3 also depicts the head-to-head comparison between IPD and APS patients. The two groups had no statistically significant difference in VEP latency and amplitude. BAER showed reduced latency of wave I and prolonged latency of waves II, II, IV, and V on both sides in IPD compared to APS. The interpeak latencies of I-III and I-V were significantly higher in IPD compared to APS bilaterally. The V/I amplitude ratio did not have a statistically significant difference in the IPD than in the APS bilaterally. Compared to IPD patients, APS patients had prolonged latency of N13, N20, and prolonged central sensory conduction time (N13–N20) bilaterally (Table 3).

3.6. Comparison between IPD subgroups

The comparison between IPD subgroups is presented in Table 3. The PIGD variant had significantly prolonged latency in BAER wave III bilaterally and wave V on the left side compared to the tremor-predominant variety. Moreover, the inter-peak latency of III-V in the left side was significantly prolonged in the former. These results

Table 2. VEP, BAER, and SSEP values in healthy controls, idiopathic Parkinson's disease, and atypical parkinsonian syndromes patients

VEP, BAER, SSEP in various parkinsonism patients	IPD	PSP	MSA-C	MSA-P	CBD	DLB	PDD	HC
VEP								
P 100								
L	106.26±14.55	100.06±13.20	**114.32±10.27**	**119.88±12.58**	**119.66±5.54**	99.00±4.76	105.95±1.20	90.75±4.67
R	106.26±15.88	99.20±12.50	**113.50±12.33**	**118.31±12.62**	**119.06±6.04**	101.60±12.78	104.70±12.28	91.00±4.66
BAER								
I								
L	1.56±0.061	1.57±0.054	1.57±0.046	1.64±0.044	1.57±0.030	1.60±0.011	1.58±0.049	1.59±0.051
R	1.55±0.052	1.57±0.049	1.54±0.051	1.62±0.042	1.58±0.040	1.60±0.037	1.58±0.063	1.59±0.056
III								
L	**3.84±0.150**	3.56±0.131	**3.95±0.039**	3.76±0.059	3.64±0.063	**3.93±0.026**	**3.92±0.042**	3.53±0.109
R	**3.84±0.152**	3.55±0.122	**3.94±0.043**	3.77±0.066	3.61±0.109	**3.92±0.055**	**3.94±0.035**	3.53±0.129
V								
L	**5.86±0.239**	5.55±0.145	**6.28±0.093**	5.66±0.047	5.66±0.133	**5.79±0.043**	**5.83±0.056**	5.46±0.122
R	**5.85±0.250**	5.52±0.161	**6.24±0.127**	5.68±0.027	5.66±0.145	**5.78±0.020**	**5.78±0.070**	5.47±0.104
I-III								
L	**2.28±0.169**	2.07±0.072	**2.37±0.053**	2.12±0.033	2.07±0.072	**2.32±0.015**	**2.33±0.007**	1.93±0.103
R	**2.28±0.163**	1.97±0.121	**2.39±0.045**	2.15±0.026	2.05±0.120	**2.32±0.036**	**2.36±0.028**	1.93±0.117
III-V								
L	2.03±0.149	2.08±0.481	**2.33±0.091**	1.90±0.092	2.01±0.129	1.86±0.070	1.91±0.099	1.93±0.099
R	2.00±0.142	1.96±0.071	**2.30±0.111**	1.90±0.072	2.05±0.107	1.85±0.075	1.83±0.176	1.93±0.093
I-V								
L	**4.30±0.257**	3.98±0.153	**4.71±0.071**	4.02±0.077	4.08±0.129	**4.18±0.055**	**4.24±0.106**	3.86±0.119
R	**4.29±0.264**	3.94±0.158	**4.69±0.122**	4.06±0.050	4.08±0.136	**4.17±0.055**	**4.19±0.134**	3.91±0.283
V/I								
L	1.64±0.037	1.63±0.030	**1.37±0.032**	1.67±0.000	1.67±0.061	1.62±0.005	1.62±0.000	1.65±0.043
R	1.62±0.047	1.62±0.041	**1.38±0.043**	1.69±0.010	1.64±0.048	1.59±0.005	1.59±0.007	1.65±0.045
SSEP								
N13								
L	13.14±0.60	13.21±0.50	14.24±1.13	14.00±0.90	14.19±0.88	13.12±0.48	12.89±0.57	13.10±0.56
R	13.14±0.60	13.22±0.51	14.24±1.15	13.98±0.48	14.18±0.15	13.08±0.52	12.88±0.6	13.11±0.56
N20								
L	19.03±0.66	19.14±0.56	20.87±1.54	20.61±1.37	20.94±1.26	19.06±0.45	18.87±0.52	18.98±0.64
R	19.05±0.66	19.17±0.58	20.83±1.58	20.75±1.00	21.13±0.40	18.98±0.48	18.83±0.56	18.99±0.64
N13-N20								
L	5.89±0.12	5.92±0.11	**6.63±0.10**	**6.60±0.48**	6.75±0.39	5.93±0.14	5.98±0.13	5.87±0.13
R	5.90±0.12	5.94±0.11	**6.59±0.50**	**6.77±0.50**	6.96±0.26	5.96±0.06	5.92±0.07	5.88±0.12

Note: Abnormal values are in bold fonts.
Abbreviations: IPD: Idiopathic Parkinson's disease; APS: Atypical parkinsonian syndromes; HC: Healthy control, H & Y: Hoehn and Yahr, PSP: Progressive supranuclear palsy; MSA: Multiple system atrophy (C: Cerebellar variety; P: Parkinsonian variety); CBD: Corticobasal degeneration; DLB: Dementia with Lewy bodies; PDD: Parkinson's disease dementia; L: Left; R: Right.

indicated significantly more brainstem dysfunction in the PIGD group mainly in the lower midbrain and pons. However, the VEP and SSEP values showed no statistically significant difference between the two groups of IPD.

Table 3. Comparisons between different patient categories

VEP, BAER, SSEP parameters	IPD (*n*=50) versus HC (*n*=50)		APS (*n*=50) versus HC (*n*=50)		IPD (*n*=50) versus APS (*n*=50)		TV (*n*=37) versus PIGD (*n*=13)	
	Mann–Whitney *U*-test Z score	*P*-value (2-tailed)	Mann-Whitney *U*-test Z score	*P*-value (2-tailed)	Mann–Whitney *U*-test Z score	*P*-value (2-tailed)	Mann–Whitney *U*-test Z score	*P*-value (2-tailed)
N75 (ms) R_VEP	−0.427	0.669	−2.620	0.009	−1.231	0.218	−0.166	0.868
P100 (ms) R_VEP	−4.561	**<0.001**	−6.374	**<0.001**	−0.038	0.970	−0.188	0.851
N145 (ms) R_VEP	−2.365	0.018	−1.903	0.057	−0.479	0.632	−1.272	0.203
N75-P100 AMPLITUDE (μv) R_VEP	−4.136	**<0.001**	−4.311	**<0.001**	−0.390	0.697	−1.217	0.223
N75 (ms) L_VEP	−0.586	0.558	−3.092	0.002	−1.551	0.121	−0.332	0.740
P100 (ms) L_VEP	−5.371	**<0.001**	−6.571	**<0.001**	−0.483	0.629	−0.431	0.666
N145 (ms) L_VEP	−3.575	**<0.001**	−2.772	**0.006**	−0.972	0.331	−0.984	0.325
N75-P100 AMPLITUDE (μv) L_VEP	−3.290	**0.001**	−4.324	**<0.001**	−0.741	0.459	−0.896	0.370
I (ms) R_BAER	−3.551	**<0.001**	−1.379	0.168	−2.425	**0.015**	−1.897	0.058
IIR_BAER	−6.125	**<0.001**	−2.778	**0.005**	−4.867	**<0.001**	−1.737	0.082
IIIR_BAER	−7.219	**<0.001**	−4.267	**<0.001**	−3.694	**<0.001**	−2.570	**0.010**
IVR_BAER	−6.019	**<0.001**	−3.011	**0.003**	−4.039	**<0.001**	−1.429	0.153
VR_BAER	−6.492	**<0.001**	−4.450	**<0.001**	−2.521	**0.012**	−1.738	0.082
I-IIIR_BAER	−7.655	**<0.001**	−4.549	**<0.001**	−4.241	**<0.001**	−1.350	0.177
III-VR_BAER	−4.226	**<0.001**	−1.573	0.116	−1.383	0.167	−1.107	0.268
I-VR_BAER	−6.469	**<0.001**	−4.683	**<0.001**	−2.731	**0.006**	−1.051	0.293
V/I (AMPLITUDE μv) R_BAER	−3.278	**0.001**	−3.314	**0.001**	−0.651	0.515	−0.656	0.512
I (ms) L_BAER	−2.792	**0.005**	−1.248	0.212	−1.606	0.108	−0.920	0.358
IIL_BAER	−6.598	**<0.001**	−3.898	**<0.001**	−4.705	**<0.001**	−1.451	0.147
IIIL_BAER	−7.491	**<0.001**	−4.492	**<0.001**	−3.580	**<0.001**	−2.226	**0.026**
IVL_BAER	−6.517	**<0.001**	−3.649	**<0.001**	−3.784	**<0.001**	−0.843	0.399
VL_BAER	−6.803	**<0.001**	−5.411	**<0.001**	−2.394	**0.017**	−2.331	**0.020**
I-IIIL_BAER	−7.735	**<0.001**	−4.972	**<0.001**	−4.224	**<0.001**	−1.350	0.177
III-VL_BAER	−4.381	**<0.001**	−2.815	**0.005**	−1.128	0.259	−2.503	**0.012**
I-VL_BAER	−6.882	**<0.001**	−5.780	**<0.001**	−2.513	**0.012**	−1.095	0.273
V/I (AMPLITUDE μv) L_BAER	−2.069	**0.039**	−3.582	**<0.001**	−1.846	0.065	−1.203	0.229
N9R_SSEP	−1.187	0.235	−1.983	**0.047**	−1.038	0.299	−0.365	0.715
N13R_SSEP	−0.414	0.679	−3.048	**0.002**	−2.661	**0.008**	−0.929	0.353
N20R_SSEP	−0.658	0.510	−3.792	**0.000**	−3.199	**0.001**	−0.951	0.342
N13-N20R_SSEP	−0.770	0.441	−3.884	**0.000**	−3.327	**0.001**	−0.155	0.877
N9L_SSEP	−1.231	0.218	−1.538	0.124	−0.535	0.593	−0.343	0.732
N13L_SSEP	−0.479	0.632	−2.993	**0.003**	−2.510	**0.012**	−0.841	0.400
N20L_SSEP	−0.686	0.493	−3.809	**<0.001**	−3.234	**0.001**	−1.062	0.288
N13-N20L_SSEP	−0.822	0.411	−4.060	**<0.001**	−3.516	**<0.001**	−0.599	0.549

Note: Statistically significant values are in bold font.
Abbreviations: IPD: Idiopathic Parkinson's disease; APS: Atypical parkinsonian syndromes; TV: Tremor-predominant Parkinson's disease; PIGD: Postural instability and gait disorder Parkinson's disease; L: Left, R: Right.

Table 4. Spearman's correlation of VEP, BAER, and SSEP parameters with the duration and clinical severity in IPD and APS

Spearman's correlation in IPD (*n*=50) and APS (*n*=50)	IPD-Duration	IPD-Modified Hoehn and Yahr Staging	APS-Duration	APS-Modified Hoehn and Yahr Staging
N75(ms) R_VEP				
Correlation coefficient	0.730**	0.625**	0.361**	0.283*
Sig. (2-tailed)	**<0.001**	**<0.001**	**0.010**	**0.046**
P100(ms) R_VEP				
Correlation coefficient	0.826**	0.738**	0.265	0.114
Sig. (2-tailed)	**<0.001**	**<0.001**	0.063	0.432
N145(ms) R_VEP				
Correlation coefficient	0.744**	0.675**	0.138	0.079
Sig. (2-tailed)	**<0.001**	**<0.001**	0.338	0.584
N75-P100 AMPLITUDE (μv) R_VEP				
Correlation coefficient	−0.627**	−0.529**	−0.154	−0.204
Sig. (2-tailed)	**<0.001**	**<0.001**	0.285	0.156
N75 (ms) L_VEP				
Correlation coefficient	0.550**	0.498**	0.319*	0.220
Sig. (2-tailed)	**<0.001**	**<0.001**	**0.024**	0.126
P100 (ms) L_VEP				
Correlation coefficient	0.749**	0.687**	0.344*	0.139
Sig. (2-tailed)	**<0.001**	**<0.001**	**0.015**	0.337
N145 (ms) L_VEP				
Correlation coefficient	0.559**	0.472**	0.122	-0.026
Sig. (2-tailed)	**<0.001**	**0.001**	0.401	0.858
N75-P100 AMPLITUDE (μv) L_VEP				
Correlation coefficient	−0.575**	−0.549**	−0.149	−0.231
Sig. (2-tailed)	**<0.001**	**<0.001**	0.300	0.106
I (ms) R_BAER				
Correlation coefficient	−0.340*	−0.273	0.278	0.418**
Sig. (2-tailed)	**0.016**	0.055	0.051	**0.003**
IIR_BAER				
Correlation coefficient	0.865**	0.818**	0.069	−0.029
Sig. (2-tailed)	**<0.001**	**<0.001**	0.635	0.842
IIIR_BAER				
Correlation coefficient	0.789**	0.701**	0.109	−0.149
Sig. (2-tailed)	**<0.001**	**<0.001**	0.451	0.301
IVR_BAER				
Correlation coefficient	0.629**	0.630**	0.011	−0.113
Sig. (2-tailed)	**<0.001**	**<0.001**	0.942	0.433
VR_BAER				
Correlation coefficient	0.756**	0.670**	0.050	−0.126
Sig. (2-tailed)	**<0.001**	**<0.001**	0.729	0.385
I-IIIR_BAER				
Correlation coefficient	0.836**	0.724**	0.025	−0.270
Sig. (2-tailed)	**<0.001**	**<0.001**	0.863	0.058

(Cont'd...)

Table 4. ***(Continued)***

Spearman's correlation in IPD (*n*=50) and APS (*n*=50)	IPD-Duration	IPD-Modified Hoehn and Yahr Staging	APS-Duration	APS-Modified Hoehn and Yahr Staging
III-VR_BAER				
Correlation coefficient	0.683**	0.574**	0.036	0.023
Sig. (2-tailed)	**<0.001**	**<0.001**	0.802	0.873
I-VR_BAER				
Correlation coefficient	0.823**	0.716**	−0.016	−0.252
Sig. (2-tailed)	**<0.001**	**<0.001**	0.912	0.078
V/I (AMPLITUDE µv) R_BAER				
Correlation coefficient	−0.167	−0.124	−0.051	−0.017
Sig. (2-tailed)	0.248	0.390	0.726	0.906
I (ms) L_BAER				
Correlation coefficient	−0.320*	−0.196	0.217	0.372**
Sig. (2-tailed)	**0.023**	0.173	0.130	**0.008**
IIL_BAER				
Correlation coefficient	0.782**	0.756**	0.124	0.052
Sig. (2-tailed)	**<0.001**	**<0.001**	0.392	0.721
IIIL_BAER				
Correlation coefficient	0.815**	0.754**	0.044	−0.222
Sig. (2-tailed)	**<0.001**	**<0.001**	0.761	0.121
IVL_BAER				
Correlation coefficient	0.615**	0.653**	0.115	−0.127
Sig. (2-tailed)	**<0.001**	**<0.001**	0.426	0.380
VL_BAER				
Correlation coefficient	0.749**	0.697**	0.130	−0.157
Sig. (2-tailed)	**<0.001**	**<0.001**	0.367	0.276
I-IIIL_BAER				
Correlation coefficient	0.877**	0.761**	−0.017	−0.298*
Sig. (2-tailed)	**<0.001**	**<0.001**	0.907	**0.035**
III-VL_BAER				
Correlation coefficient	0.477**	0.351*	0.130	0.018
Sig. (2-tailed)	**<0.001**	**0.012**	0.367	0.904
I-VL_BAER				
Correlation coefficient	0.837**	0.735**	0.043	−0.269
Sig. (2-tailed)	**<0.001**	**<0.001**	0.766	0.059
V/I (AMPLITUDE µv) L_BAER				
Correlation coefficient	−0.294*	−0.265	−0.243	−0.167
Sig. (2-tailed)	**0.038**	0.063	0.088	0.245
N9R_SSEP				
Correlation coefficient	0.163	0.233	−0.012	0.147
Sig. (2-tailed)	0.257	0.103	0.937	0.307
N13R_SSEP				
Correlation coefficient	0.220	0.310*	0.397**	0.352*
Sig. (2-tailed)	0.124	**0.029**	**0.004**	**0.012**

(Cont'd...)

Table 4. *(Continued)*

Spearman's correlation in IPD (*n*=50) and APS (*n*=50)	IPD-Duration	IPD-Modified Hoehn and Yahr Staging	APS-Duration	APS-Modified Hoehn and Yahr Staging
N20R_SSEP				
Correlation coefficient	0.254	0.313*	0.384**	0.315*
Sig. (2-tailed)	0.075	**0.027**	**0.006**	**0.026**
N13-N20R_SSEP				
Correlation coefficient	0.170	0.105	0.210	0.140
Sig. (2-tailed)	0.237	0.468	0.143	0.333
N9L_SSEP				
Correlation coefficient	0.143	0.204	−0.005	0.175
Sig. (2-tailed)	0.322	0.156	0.972	0.224
N13L_SSEP				
Correlation coefficient	0.204	0.311*	0.331*	0.358*
Sig. (2-tailed)	0.155	**0.028**	**0.019**	**0.011**
N20L_SSEP				
Correlation coefficient	0.255	0.327*	0.320*	0.309*
Sig. (2-tailed)	0.074	**0.020**	**0.024**	**0.029**
N13-N20L_SSEP				
Correlation coefficient	0.193	0.148	0.179	0.108
Sig. (2-tailed)	0.179	0.306	0.212	0.455

Note: Statistically significant values are in bold font.
Abbreviations: IPD: Idiopathic Parkinson's disease; APS: Atypical parkinsonian syndromes; L: Left; R: Right.

3.7. SSEP in CBD

In patients with CBD on the apraxic side, the latency of N13, N20, and central sensory conduction time (N13 – N20) was increased compared to the non-apraxic side. The mean values of N13, N20, and CCT (msec) are 14.596 ± 1.0 vs. 13.77 ± 0.9, 21.74 ± 1.0 vs. 20.33 ± 0.9, and 7.144 ± 0.9 vs. 6.56 ± 0.8, respectively ($P < 0.05$).

3.8. Correlation with disease duration

As shown in Table 4, the VEP latency of N75, P100, and N145 showed a good positive correlation and the V/I amplitude ratio showed a good negative correlation bilaterally with the disease duration in IPD patients. On the other hand, only a few parameters of the APS patients (N75 bilaterally and P100 on the left side) showed positive correlations with the disease duration. The BAER latency of wave I showed a negative correlation, and waves II, III, IV, and V along with interpeak latency of I-III, III-V, and I-V showed a good positive correlation with the disease duration of IPD. On the contrary, APS patients did not show any statistically significant BAER correlation with their disease duration. Although the IPD group did not have any statistically significant SSEP correlation, the APS group showed a positive correlation of SSEP N13 and N20 latency bilaterally with the disease duration.

3.9. Correlation with disease severity

Modified Hoehn and Yahr staging was performed to determine disease severity in IPD patients. The similar staging procedure was also applied to the APS group. We found the VEP latency of N75, P100, and N145 having a good positive correlation and the V/I amplitude ratio having a good negative correlation bilaterally with the disease severity in IPD patients. Besides, IPD patients also showed good positive correlations of BAER latency of wave II, III, IV, V, interpeak I-III, III-V, and I-V with disease severity. VEP right N75 wave latency and BAER bilateral wave I and left I-III interpeak latency were positively correlated with the disease severity. The SSEP of both IPD and APS patients was positively correlated with bilateral N13 and N20 latency.

4. Discussion

The VEP changes suggested a dysfunctional visual pathway in our patients. VEP P100, N145 latency was increased bilaterally and N75-P100 amplitude was reduced bilaterally in IPD compared to HCs. Thus, there were both demyelinating and axonal changes in the visual cortical areas, with normal N75 latency denoting a relatively normal anterior visual pathway in IPD. Optical coherence

tomography studies in Parkinson's disease patients showed the thinning of the retinal nerve fiber layer, macula, and annular zone around the fovea[10-12]. The post-mortem study of IPD patients showed a decrease in dopamine in retinal cells[13]. The possible mechanism of visual dysfunction in Parkinson's disease patients could be pathological changes in the caudal nuclei, putamen nuclei, hypothalamus, and pontine nucleus coeruleus[12]. It could result in cholinergic system dysfunction that diffusely affects the brainstem auditory pathway. The degenerative pathology in these regions causes dopaminergic neuron degeneration and a decrease in dopamine production and secretion, which may cause dysfunction of the inter-plexiform cells and horizontal cells in the retina, contributing to the abnormal changes of VEP[14]. Long-term dopamine deficiency could trigger a compensatory decrement of acetylcholine and lead to changes in VEP latency. A retinal dopaminergic deficiency could also underlie some visual changes. Besides, the expression of alpha-synuclein (α-syn) in the vertebrate retina may shed light on the pathological mechanism behind the visual changes[15].

By investigating the structural changes in the retina using spectral-domain optical coherence tomography, Ma *et al.* found that the patterns of retinal involvement in of IPD, MSA, and PSP were different and also correlated with disease duration[16]. Another study showed that dopaminergic amacrine cell loss leads to activation of the rod pathway, which subsequently results in reduced contrast sensitivity in IPD[17]. Retinal thinning, which started in the early stage of IPD, correlated with disease severity and might be related to dopaminergic degeneration in the substantia nigra[18]. Moreover, smaller thickness of parafoveal ganglion cell-inner plexiform layer complex and peripapillary retinal nerve fiber layer in IPD constitutes an increased risk for cognitive decline at 3 years[19]. In this study, we found that the duration and severity of the disease had a positive correlation with greater extent of damage in the visual pathway. Both ventral and dorsal visual streams are involved in IPD. IPD patients with freezing of gait had significantly reduced dopamine levels in the nigrostriatal system and low metabolism of primary visual cortex[20]. A recent functional connectivity study using functional magnetic resonance imaging (fMRI) and Visual Object and Space Perception battery (VOSP) by Kawabata *et al.*[21] found that IPD patients had visual perceptual disturbance due to decreased connectivity in the ventral visual feedback pathway. Overall, visual abnormalities in IPD encompass changes in visual acuity, contrast sensitivity, color vision, retinal function, eye movements, cortical visual processing, peripheral vision, object perception, visuospatial construction, motion perception, facial neglect, and face and emotion recognition[22]. The IPD patients exhibited more pronounced latency and amplitude changes in P100 and N145, indicating bilateral higher cortical involvement in occipital-temporal-parietal lobes. Our study corroborated findings of many studies by showing extensive bilateral involvement in visual pathways correlating with the severity of the disease.

VEP N75, P100, and N145 latency were increased bilaterally and N75-P100 amplitude was reduced bilaterally in APS compared to HCs. So, there were both demyelinating and axonal changes in the visual cortical areas, as well as in anterior visual pathways in APS in our study. We noted a prolonged P100 latency in the MSA group in our study, consistent with findings reported by Abele *et al.*[23] At present, the mechanisms underlying the slowed conduction in the visual pathways remain unclear. The probable hypothesis of increased latency and decreased amplitude may be related to the involvement of the nigrostriatal system, which leads to manifestations such as gliosis, vacuolation, and glial cytoplasmic inclusion (GCI) mainly in the putamen and substantia nigra, causing dopamine deficiency and possibly abnormal function of the retinal cells. In this study, CBD patients showed increased latency. A previous study demonstrated that in CBD patients, subcortical and deep gray matter involvement leads to basal ganglia dysfunction, especially posterior putamen, which causes visual dysfunction[24]. An earlier study by Bak *et al.* on APS using VOSP neuropsychological tests[25] confirmed that visuospatial function was intact in the MSA patients, whereas profound visuospatial deficits, not correlated with MMSE score, were detected in the CBD patients. On the contrary, PSP patients had milder visuospatial involvement, which was also correlated with the decline in MMSE scores.

BAER wave I represented the auditory nerve compound action potential from the most distal portion of the auditory nerve. Wave II was generated mainly in the proximal auditory nerve but probably included a contribution from the intra-axial part of the nerve and the cochlear nucleus. The wave III potential was generated in the lower pons in the superior olive and trapezoid regions. Finally, the generators of waves IV and V lay in the upper pons and the midbrain, as high as the inferior colliculus. In this study, increased absolute latency of waves I, III, and V and interpeak latency of I-III, III-V were noted on both sides in the patients with IPD, MSA-C, DLB, and PDD. A decreased V/I amplitude ratio was noted in patients with MSA-C.

Liu *et al.*[10] noted prolonged latency of waves III, V, III-V, and I-V in IPD patients. In their respective studies, Hassan *et al.*[26] and Shalash *et al.*[27] found prolonged latency of waves V and I-V. Daniel *et al.*[28] noted that waves II, III, IV, V, and III-V were bilaterally prolonged, and Shalash *et al.*[27]

also noted rigidity and bradykinesia correlating with BAER abnormalities contralateral to the clinically more affected side in IPD. In another study, a prolonged III-V latency on the symptomatic brainstem side was found in IPD[29]. In the current study, we found that BAER increased latency of waves III, IV, V, I-III, III-V, I-V and decreased V/I amplitude in IPD compared to HCs with relative sparing of wave I, corroborating a demyelination and axonal involvement of central brainstem pathways in IPD. The occurrence of dysfunction of alpha-synuclein, which is expressed in the inner ear, could explain a peripheral mechanism of hearing loss[30]. Functional study of the brain by single-photon emission computerized tomography (SPECT) and fMRI showed basal ganglia involvement in auditory stimulation. Dysfunctional outputs from basal ganglia to the inferior colliculus, medial geniculate nucleus, and temporal cortex may explain the probable abnormality observed in the BAER study[31-34].

Several studies have reported BAER anomalies in patients with MSA[35,36]. In our study, absolute and interpeak latency was increased along with a decreased amplitude ratio of V/I waves. In pathological studies on MSA patients, degenerative changes were found in several nuclei and tracts close to the brainstem auditory pathway, including the substantia nigra, locus coeruleus, pontocerebellar tracts, pontine nuclei, dorsal vagal nuclei, and inferior olivary nuclei[37-41]. This may explain the auditory pathway abnormality in patients with MSA-C. Brainstem neuropathology may underline BAER abnormality in DLB and PDD patients, as described by Braak *et al.*[42]

The current SSEP study showed that the central sensory conduction time latency was increased in patients with MSA-C and MSA-P, while the rest of the patients' SSEP values are within normal limits (Table 2). N13 reflects postsynaptic activity in the central gray matter of the cervical cord. The N20 waveform is a composite made of signals from multiple generators within or close to the primary cortical receiving area. Pramstaller *et al.*[43] and Abbruzzese *et al.*[44] reported that they did not find any SSEP latency abnormalities in patients with MSA, whereas Takeda *et al.*[45] reported increased N13 and N20 latency in patients with CBD. As previously discussed, patients with degenerative changes were noted in brainstem nuclei, which may cause abnormal SSEP response in MSA patients, but further research is needed for underlying pathology.[41] APS patients had significantly prolonged N13 and N20 latency and increased somatosensory CCT compared to HCs in our study.

On the contrary, IPD patients did not manifest these changes. The head-to-head comparison also showed significantly prolonged somatosensory CCT and prolonged N13 and N20 latency in APS patients compared to IPD. However, the PIGD and tremor-predominant IPD do not differ in terms of SSEP. Regarding the sensory pathway abnormality in Parkinson's disease, Conte *et al.* postulate that disease-related dopaminergic denervation in parkinsonian syndromes results in the transmission of noisy and poorly differentiated sensory information to cortical regions and suggest that abnormalities in the periaqueductal gray matter and non-dopaminergic neurotransmitter systems also play a role in contributing to the pathway abnormality.[46] Of note, the measurement of CCT is well-validated and reproducible approach.[47]

The VEP, BAER, and SSEP changes correlated well in IPD, but a few parameters in APS exhibited a good correlation with the duration and severity of the disease. Compared to IPD, APS has diverse findings, which can probably be ascribed to the heterogenous etiologies. The progression of electrophysiologic changes with the disease duration denoted a probable degenerative pathology in the diseases. A negative correlation between the latency of BAER wave I with disease duration and severity in IPD probably pointed out the relative sparing of peripheral connections of auditory pathways even in the late disease course. A progressively increasing positive feedback in wave I in gradually deteriorating brainstem connections in the later course of IPD may account for the relative sparing of peripheral connections of auditory pathways. Overall, results from the correlation analysis indicated that progressive central nervous system degeneration is a hallmark in progressive disease.

The changes in specific parts registered by the electrophysiological tests, which denote damage to specific parts of the midbrain, pons, anterior visual, and thalamocortical pathways in the brain allow us to identify severe involvement in these areas. Although the IPD is known to primarily affect the striatum and midbrain dopaminergic system, the involvement of these areas would denote a widespread nature of the disease, which is accompanied by non-motor symptoms such as sleep disorders and visual hallucinations and motor symptoms such as postural instability. Even if these areas show normal brain magnetic resonance imaging (MRI) results, other assessments such as VEP, BAER, and SSEP tests might generate abnormal results, which are indicative of the disease. Thus, more in-depth studies on evoked potentials are warranted to establish distinct pathological profiles for both IPD and APS.

5. Conclusion

Overall, the IPD and APS patients had significant VEP, BAER, and SSEP abnormalities of demyelination and

axonal variety in the visual, auditory, and somatosensory pathways. Despite being predominantly motor disorders, these diseases are also tied with profound non-motor components, necessitating assessments of the electrophysiological abnormalities, which have been found to correlate with disease severity and disease duration. The visual pathways, from the anterior visual pathways to the higher visual processing centers, are heavily impacted in IPD and APS.

The evoked potential tests are able to detect the relevant abnormalities, especially in the early stages of the disease while the brain MRI fails to pick up any abnormal findings. Contrary to the popular belief that only nigrostriatal dopaminergic pathway is involved, IPD is characterized by a widespread brain involvement. PIGD and tremor-dominant IPD patients are significantly different in terms of BAER findings, denoting a significantly higher brainstem involvement in the PIGD variant.

Acknowledgments

None.

Funding

None.

Conflict of interest

The authors declare that they have no competing interests.

Author contributions

Conceptualization: Manoj Roy, Amar Kumar Misra,
Formal analysis: Joydeep Mukherjee, Jasodhara Chaudhuri
Investigation: Manoj Roy, Manamita Mandal, Bijendra Mohanty
Methodology: Manoj Roy, Amar Kumar Misra, Joydeep Mukherjee
Writing – original draft: Manoj Roy, Joydeep Mukherjee
Writing – review & editing: Amar Kumar Misra, Joydeep Mukherjee, Kartik Chandra Ghosh

Ethics approval and consent to participate

This study was approved by the NRS Medical College Institutional Ethics Committee (NMC/958).

Informed consent was taken from all participants before enrolment.

Consent for publication

We obtained informed consent of the study subjects for publishing their data without revealing their identity in scientific research articles.

Availability of data

Data used in this work are available from the corresponding author upon reasonable request.

References

1. Jankovic J, Mcdermott M, Carter J, *et al*., 1990, Variable expression of Parkinson's disease: A base-line analysis of the DATATOP cohort, The Parkinson study group, *Neurology*, 40: 1529–1534.

   https://doi.org/10.1212/wnl.40.10.1529

2. Marsden CD, 1990, Parkinson's disease, *Lancet*, 335: 948–952.

   https://doi.org/10.1016/0140-6736(90)91006-v

3. Jankovic J, 1989, Parkinsonism plus syndromes, *Mov Disord*, 4: 95119.

   https://doi.org/10.1002/mds.870040512

4. Gawel MJ, Das P, Vincent S, *et al*., 19881, Visual and auditory evoked responses in patients with Parkinson's disease, *J Neurol Neurosurg Psychiatry* 44: 227–232.

   https://doi.org/10.1136/jnnp.44.3.227

5. Gelb DJ, Oliver E, Gilman S, 1999, Diagnostic criteria for Parkinson's disease, Arch Neurol, 56: 33–39.

   https://doi.org/10.1001/archneur.56.1.33

6. Williams DR, Lees AJ, 2009, Progressive supranuclear palsy: Clinicopathological concepts and diagnostic challenges, *Lancet Neurol*, 8: 270–279.

   https://doi.org/10.1016/S1474-4422(09)70042-0

7. Gilman S, Wenning GK, Low PA, *et al*., 2008, Second consensus statement on the diagnosis of multiple system atrophy, *Neurology*, 71: 670–676.

   https://doi.org/10.1212/01.wnl.0000324625.00404.15

8. Kertesz A, Blair M, McMonagle P, *et al*., 2007, The diagnosis and course of frontotemporal dementia, *Alzheimer Dis Assoc Disord*, 21: 155–163.

   https://doi.org/10.1097/WAD.0b013e31806547eb

9. McKeith IG, Galasko D, Kosaka K, *et al*., 1996, Consensus guidelines for the clinical and pathologic diagnosis of dementia with Lewy bodies (DLB): Report of the consortium on DLB international workshop, *Neurology*, 47: 1113–1124.

   https://doi.org/10.1212/wnl.47.5.1113

10. Liu C, Zhang Y, Tang W, *et al*., 2017, Evoked potential changes in patients with Parkinson's disease, *Brain Behav*, 7: e00703.

    https://doi.org/10.1002/brb3.703

11. Inzelberg R, Ramirez JA, Nisipeanu P, *et al*., 2004, Retinal nerve fiber layer thinning in Parkinson disease, *Vision Res*, 44: 279.

https://doi.org/10.1016/j.visres.2004.06.009

12. Savy C, Simon A, Nguyenlegros J, 1991, Spatial geometry of the dopamine innervation in the avascular area of the human fovea, *Visual Neurosci*, 7: 487–498.

https://doi.org/10.1017/S0952523800009779

13. Harnois C, Di PT, 1990, Decreased dopamine in the retinas of patients with Parkinson's disease, *Invest Ophthalmol Visual Sci*, 31: 2473–2475.

14. Miri S, Glazman S, Mylin L, *et al*., 2016, A combination of retinal morphology and visual electrophysiology testing increases diagnostic yield in Parkinson's disease, *Parkinsonism Relat Disord*, 1:134–137.

https://doi.org/10.1016/j.parkreldis.2015.09.015

15. Mart´ınez-navarrete GC, Mart´ınnieto J, Esteverudd J, *et al*., 2007, Alpha synuclein gene expression profile in the retina of vertebrates, *Mol Vis*, 13: 949–961.

16. Ma X, Li S, Zheng B, *et al*., 2023, Retinal structure abnormalities in Parkinson's disease and atypical parkinsonism, *Biomolecules*, 13: 218.

https://doi.org/10.3390/biom13020218

17. Ortuño-Lizarán I, Sánchez-Sáez X, Lax P, *et al*., 2020, Dopaminergic retinal cell loss and visual dysfunction in Parkinson's disease, *Ann Neurol*, 88: 893–906.

https://doi.org/10.1002/ana.25897

18. Ahn J, Lee JY, Kim TW, *et al*., 2018, Retinal thinning associates with nigral dopaminergic loss in de novo Parkinson's disease, *Neurology*, 91: e1003–12.

https://doi.org/10.1212/WNL.0000000000006157

19. Murueta-Goyena A, Del Pino R, Galdós M, *et al*., 2021, Retinal thickness predicts the risk of cognitive decline in Parkinson's disease, *Ann Neurol*, 89: 165–176.

https://doi.org/10.1002/ana.25944

20. Zhou Y, Zhao J, Hou Y, *et al*., 2019, Dopaminergic pathway and primary visual cortex are involved in the freezing of gait in Parkinson's disease: A PET-CT study, *Neuropsychiatr Dis Treat*, 15: 1905–1914.

https://doi.org/10.2147/NDT.S197879

21. Kawabata K, Ohdake R, Watanabe H, *et al*., 2020, Visuoperceptual disturbances in Parkinson's disease, *Clin Park Relat Disord*, 3: 100036.

https://doi.org/10.1016/j.prdoa.2020.100036

22. Weil RS, Schrag AE, Warren JD, *et al*., 2016, Visual dysfunction in Parkinson's disease, *Brain*, 139: 2827–2843.

https://doi.org/10.1093/brain/aww175

23. Abele M, Schulz JB, Bu¨rk K, *et al*., 2000, Evoked potentials in multiple system atrophy (MSA), *Acta Neurol Scand*, 101: 111–115.

https://doi.org/10.1034/j.1600-0404.2000.101002111.x

24. Gibb WR, Luthert PJ, Marsden CD, 1989, Corticobasal degeneration, *Brain*, 112: 1171–1192.

https://doi.org/10.1093/brain/awq173

25. Bak TH, Caine D, Hearn VC, *et al*., 2006, Visuospatial functions in atypical Parkinsonian syndromes, *J Neurol Neurosurg Psychiatry*, 77: 454–456.

https://doi.org/10.1136/jnnp.2005.068239

26. Hassan DM, Shalash A, 2017, Auditory brainstem evoked responses and vestibular evoked myogenic potentials: Potential biomarkers in Parkinson's disease, *Egypt J Otolaryngol*, 33: 508–517.

https://doi.org/10.4103/1012-5574.206023

27. Shalash AS, Hassan DM, Elrassas HH, *et al*., 2017, Auditory- and vestibular-evoked potentials correlate with motor and non-motor features of Parkinson's disease, *Front Neurol*, 8: 55.

https://doi.org/10.3389/fneur.2017.00055

28. Alexa D, Alexa L, Popa L, *et al*., 2013, Brainstem auditory evoked potentials in Parkinson's disease, *Rom J Neurol*, 12: 198–201.

https://doi.org/10.37897/RJN.2013.4.7

29. Venhovens J, Meulstee J, Bloem BR, *et al*., 2016, Neurovestibular analysis and falls in Parkinson's disease and atypical parkinsonism, *Eur J Neurosci*, 43: 1636–1646.

https://doi.org/10.1111/ejn.13253

30. Akil CM, Weber SN, Park SN, *et al*., 2008, Localization of synucleins in the mammalian cochlea, *J Assoc Res Otoloaryngol*, 9: 452–463.

htttps://doi.org/10.1007/s10162-008-0134-y

31. Carpenter M, 1985, Core Text of Neuroanatomy, Baltimore, MD: Williams and Wilkins, p137–149.

32. Yeterian EH, Pandya DN, 1998, Corticostriatal connections of the superior temporal region in rhesus monkeys, *J Comp Neurol*, 399: 384–402.

https://doi.org/10.1002/(SICI)1096-9861(19980928)399:3<384:AID-CNE7>3.0.CO;2-X

33. Selemon LD, Goldman-Rakic PS, 1985, Longitudinal topography and interdigitation of corticostriatal projections in the rhesus monkey, *J Neurosci*, 5: 776–794.

https://doi.org/10.1523/JNEUROSCI.05-03-00776.1985

34. Shammah-Lagnado SJ, Alheid GF, Heimer L, 1996, Efferent connections of the caudal part of the globus pallidus in the rat, *J Comp Neurol*, 376: 489–507.

https://doi.org/10.1002/(SICI)1096-9861(19961216)376:3<489:AID-CNE10>3.0.CO;2-H

35. Uematsu D, Hamada J, Gotoh F, 1987, Brainstem auditory

evoked responses and CT findings in multiple system atrophy, *J Neurol Sci*, 77: 161–171.

https://doi.org/10.1016/0022-510X(87)90119-5

36. Prasher D, Bannister R, 1986, Brain stem auditory evoked potentials in patients with multiple system atrophy with progressive autonomic failure (Shy-Drager syndrome), *J Neurol Neurosurg Psychiatry*, 49: 278–289.

https://doi.org/10.1136/jnnp.49.3.278

37. Shy GM, Drager GA, 1960, A neurological syndrome associated with orthostatic hypotension, A clinical pathologic study, *Arch Neurol*, 2: 511–527.

https://doi.org/10.1001/archneur.1960.03840110025004

38. Schwarz GA, 1967, The orthostatic hypotension syndrome of shy-drager, A clinicopathologic report, *Arch Neurol*, 16: 123–139.

https://doi.org/10.1001/archneur.1967.00470200011002

39. Nick J, Contamin F, Escourolle R, *et al*., 1967, Idiopathic orthostatic hypotension with a complex neurological syndrome of extrapyramidal predominance, *Rev Neurol (Paris)*, 116: 213–227.

40. Johnson RH, Lee GD, Oppenheimer DR, *et al*., 1966, Autonomic failure with orthostatic hypotension due to intermediolateral column degeneration, A report of two cases with autopsies, *Q J Med*, 35: 276–292.

41. Bannister R, Oppenheimer DR, 1972, Degenerative disease of the nervous system associated with autonomic failure, *Brain*, 95: 457–474.

https://doi.org/10.1093/brain/95.3.457

42. Braak H, Tredici KD, Rüb U, *et al*., 2003, Staging of brain pathology related to sporadic Parkinson's disease, *Neurobiol Aging*, 24: 197–211.

https://doi.org/10.1016/s0197-4580(02)00065-9

43. Pramstaller PP, Wenning GK, Smith SJ, *et al*., 1995, Nerve conduction studies, skeletal muscle EMG, and sphincter EMG in multiple system atrophy, *J Neurol Neurosurg Psychiatry*, 58: 618–621.

https://doi.org/10.1136/jnnp.58.5.618

44. Abbruzzese G, Marchese R, Trompetto C, 1997, Sensory and motor evoked potentials in multiple system atrophy: A comparative study with Parkinson's disease. *Mov Disord*, 12, 315–321.

https://doi.org/10.1002/mds.870120309

45. Takeda M, Tachibana H, Okuda B, *et al*., 1998, Electrophysiological comparison between corticobasal degeneration and progressive supranuclear palsy, *Clin Neurol Neurosurg*, 100: 94–98.

https://doi.org/10.1016/s0303-8467(98)00007-9

46. Conte A, Khan N, Defazio G, *et al*., 2013, Pathophysiology of somatosensory abnormalities in Parkinson's disease, *Nat Rev Neurol*, 9: 687–697.

https://doi.org/10.1038/nrneurol.2013.224

47. De Beyl ZD, Delberghe X, Herbaut AG, *et al*., 1988, The somatosensory central conduction time: Physiological considerations and normative data, *Electroencephalogr Clin Neurophysiol*, 71: 17–26.

https://doi.org/10.1016/0168-5597(88)90015-9

ACCSCIENCE PUBLISHING

Advanced Neurology

ORIGINAL RESEARCH ARTICLE

Ethnogenetic-specific mutations in Alzheimer's disease: A marker of clinical outcomes

Georgia Uebergang, Mourad Tayebi, and Utpal K. Adhikari*

Neuroimmunology Laboratory, School of Medicine, Western Sydney University, Campbelltown, New South Wales, Australia

Abstract

Alzheimer's disease (AD) presents a substantial global health challenge, with its pathogenesis influenced by a complex interplay of genetic and molecular factors. Approximately 1% of AD cases are attributed to early onset autosomal dominant familial AD (fAD), with genetics contributing to about 70% of overall AD risk. Understanding the genetic basis and molecular mechanisms is paramount for early diagnosis and prognosis improvement. This study explores a previously underexplored area of fAD, examining how different mutations within the same gene, encoding a single protein, may influence the clinical features and progression of fAD subtypes. Our investigation focuses on distinct fAD subtypes — Iranian (T714A), Swedish (KM670/671NL), and Australian (L723P) — and their associated mutations within the C-terminus domain of amyloid precursor protein (APP). Through an extensive analysis of existing literature encompassing clinical severity, pathogenicity, neuropathology, and biological processes, we reveal critical insights into these fAD subtypes. Leveraging bioinformatics tools, we correlate the physicochemical properties of translated mutant proteins with clinical and neuropathological features. Notably, our findings demonstrate that mutations occurring between codons 714 and 717 of the *APP* gene share a higher similarity, resulting in lower root mean squared deviation scores. These mutations are associated with a broader spectrum of clinical symptoms, including myoclonus and seizures, and an earlier age of onset. Moreover, we observe a direct correlation between the location of genetic mutations on the protein sequence and specific physicochemical properties, clinical presentations, and neuropathological features among fAD subtypes. Mutations with higher structural similarity tend to manifest similar clinical and physical characteristics. While certain neuropathological findings correlate with an increasing epitope toxicity burden, our analysis indicates that epitope toxicity does not significantly impact clinical outcomes. In summary, our study provides novel insights into the heterogeneous nature of fAD subtypes, illuminating the intricate relationship between genetic mutations, physicochemical properties, and clinical manifestations. These findings offer a foundation for further research into tailored therapeutic approaches and personalized medicine for fAD.

Keywords: Alzheimer's disease; Amyloid precursor protein mutations; Ethnogenetic; Epitopes; Bioinformatics; Epitope toxicity

***Corresponding author:**
Utpal K. Adhikari
(U.Adhikari@westernsydney.edu.au)

Citation: Uebergang G, Tayebi M, Adhikari UK, 2023, Ethnogenetic-specific mutations in Alzheimer's disease: A marker of clinical outcomes. *Adv Neuro,* 2(4): 1734. https://doi.org/10.36922/an.1734

Received: August 31, 2023

Accepted: November 28, 2023

Published Online: December 15, 2023

1. Introduction

Alzheimer's disease (AD) represents a major health-care challenge, notably as the predominant cause of dementia in the elderly[1,2]. Despite significant progress

in understanding this neurodegenerative disorder, numerous aspects of its pathogenesis remain elusive. AD is characterized by the aggregation of misfolded proteins, precipitating the degeneration of specific brain regions and culminating in dementia[3]. This pathological hallmark has been pivotal in advancing our molecular and genetic comprehension of the disease[4].

Genetics play a substantial role in AD, contributing to an estimated 70% of the disease's risk[1]. This impact of genetics highlights the critical importance of elucidating the genetic mutations and underlying molecular mechanisms that govern the recognition and prognosis of AD[1,3]. However, it is worth noting that, when considering causality, approximately 90% of AD cases remain sporadic. Nevertheless, a comprehensive understanding of the genetics and molecular mechanisms across all AD subtypes is essential for the development, testing, and utilization of novel treatments designed to target these specific mutations or causal pathways[5].

AD manifests in two primary forms: late-onset and early-onset AD (EOAD). The more common late-onset AD is often sporadic but may have an increased risk associated with the ApoE4 genotype[6]. Conversely, EOAD, constituting <10% of cases, includes familial AD (fAD) cases, of which 5 – 10% are attributed to genetic mutations in three key genes: Presenilin-1 (*PSEN1*), amyloid precursor protein (*APP*), and rarely Presenilin-2 (*PSEN2*)[6,7]. While autosomal dominant mutations in the *PSEN1*, *PSEN2*, and *APP* genes account for a relatively small proportion of AD cases, gaining insights into the mechanisms behind fAD and its causative mutations is instrumental in understanding other forms of EOAD and even the more prevalent sporadic late-onset AD. The accumulation of Aβ peptide deposits in the brain is a recognized hallmark in both sporadic AD (sAD) and fAD[8]. This concept, known as the amyloid cascade hypothesis, postulates that Aβ deposition leads to neuronal cell death, often through Tau protein aggregation, though the precise mechanisms remain elusive[5].

The *APP* gene encodes the Aβ peptide, a crucial substrate following enzymatic cleavage by β-secretase and γ-secretase enzymes[9]. While α secretase enzyme typically facilitates normal Aβ cleavage, the inclusion of β- and γ-secretase can result in pathological Aβ peptide deposition in the brain[9,10]. Certain mutations in the *APP* gene can disrupt this cleavage pathway, resulting in pathological outcomes. Notably, not all *APP* mutations are pathogenic, as some appear to confer a protective effect by reducing Aβ42/Aβ40 ratios[10].

Similarly, the *PSEN1* and *PSEN2* genes exert influence on the amyloid cascade through their impact on the function of the γ-secretase enzyme. Mutations in these genes can lead to abnormal cleavage of the *APP* gene, resulting in excessive Aβ peptide deposition[8,9]. Understanding the diverse clinical effects of pathogenic mutations on the *APP* gene can also inform our understanding of other genetic mutation subtypes, including those on *PSEN1* and *PSEN2* genes, such as Glu126fs and Lys306fs[11], which share similar mechanisms.

Furthermore, comprehension of these mutations and their effects indirectly contributes to our understanding of sporadic AD, augmenting our insights into the broader landscape of AD, regardless of subtype[8]. The identification of Aβ depositions, amyloid plaques, and neurofibrillary tangles in most fAD cases has significantly advanced our understanding of the amyloid cascade and shed light on other potential pathogenic mechanisms.

The previous research has indicated that specific mutations may influence clinical features, as observed in comparisons between patients with *PSEN1* mutations (often presenting with seizures, spastic paraparesis, myoclonus, and cerebellar signs), patients with *APP* mutations (frequently displaying aggression), and patients with *PSEN2* mutations (typically experiencing a longer disease duration and more frequent disorientation)[12].

The influence of mutations extends to varying pathogenic mutations within the same gene, a phenomenon particularly observed when examining mutations in different regions of the *APP*, *PSEN1*, and *PSEN2* genes. Autosomal mutations in the *APP* gene associated with fAD have been observed across multiple ethnic populations[13], each manifesting unique clinical features and characteristics[14].

For example, mutations occurring at the *APP* residue V717, such as the London mutation (V717I), V717G, and V717L, present similar phenotypes with clinical symptoms including dyscalculia, myoclonus, and seizures[15]. In contrast, mutations occurring at different residue locations lead to heterogeneous phenotypes, exemplified by the Flemish subtype (A692G) compared to variants at residue V717. Unlike the V717 variants, the A692G variant does not induce seizures and myoclonus but instead results in cerebrovascular events, a feature less frequently observed in patients with other mutation subtypes[15,16].

Moreover, even variants occurring at the same residue can manifest diverse phenotypes, as evidenced by the comparison of the Arctic mutation (E693G) with the Dutch mutation (E693Q). While both mutations result in amyloid angiopathy, the Dutch mutation is characterized by recurrent cerebrovascular events, whereas patients with the Arctic mutation exhibit a purely cognitive phenotype[16].

This phenotypic heterogeneity may also be influenced by the mutation type, as observed in the Osaka mutation (E693Del), which primarily presents as a neurological disease with progressive cognitive decline and focal neurological symptoms, such as loss of movement and spastic quadriplegia[17,18]. These clinical symptoms are not commonly observed in patients with mutations occurring at this residue location.

Identifying the genes and subsequent mutations responsible for fAD is crucial for advancing our understanding of AD's underlying mechanisms. This knowledge not only informs future disease treatment but also fosters interest in the application of genetic testing and counseling in clinical practice[19]. Despite this importance, limited investigation has been conducted concerning the diverse effects of different mutations within the same gene that encodes a single protein on the clinical features and progression of fAD subtypes. The multitude of mutation subtypes within the *APP* gene provides a unique opportunity to explore this connection.

Herein, we undertook a comprehensive comparison of the clinical and neuropathological severity observed in fAD ethno-genetic subtypes. Our study involved an extensive analysis aimed at investigating whether the specific location of mutations on the *APP* gene and the physicochemical properties of the encoded protein contribute to variations in clinical and neuropathological presentations within these subtypes. This analysis considers clinical severity, pathogenicity, neuropathology, biological processes, and the relationship between the properties of each *APP* mutation and the severity of the disease. Strikingly, our findings reveal the most significant disparities in mutations occurring between amino acids 714 – 723 on the C-terminal region of the *APP* gene compared to mutations occurring toward the N-terminal region. Mutations within the 714 – 717 region exhibit the greatest diversity of symptoms, including seizures and/or myoclonus, and are associated with an earlier average disease onset, coupled with a slightly higher *APP* instability index. These results underscore the important role of disease-specific mutations within the *APP* gene in shaping the clinical and neuropathological outcomes, as well as the onset and severity of AD. Consequently, our study underscores the need for an ethno-genetic assessment when formulating diagnostic and therapeutic strategies.

2. Materials and methods

2.1. Materials

The flow chart depicting the overall materials and methods for sequence retrieval from the protein database, bioinformatics analysis of the sequences, and identification of correlations between protein physicochemical properties and clinical phenotype is illustrated in Figure 1.

2.2. Analysis of the physicochemical properties of wild-type and mutated human amyloid precursor proteins

Initially, the FASTA-formatted human APP sequence (P05067) was obtained from the UniProtKB/SwissProt (www.uniprot.org/uniprotkb) database[20]. Subsequently, *APP* sequences were copied and altered to represent all mutations (21 *APP* mutations) categorized as pathogenic for AD according to the AlzForum (www.alzforum.org) *APP* mutation database at the time of access in 2020. AlzForum serves as a new platform and information database regularly updated to include the most up-to-date research findings, fostering discovery and advancements in treatment[21].

To analyze the physicochemical properties of both the wild-type and each mutated human APP sequence, the ExPASy ProtParam tool (web.expasy.org/protparam/) was employed. This tool facilitates the calculation of various physical and chemical parameters based on the provided FASTA format, including molecular weight (MW), theoretical isoelectric point (pI), extinction coefficient (EC), instability index (II), aliphatic index (AI), and grand average of hydropathicity (GRAVY)[22].

2.3. Prediction and refinement of three-dimensional (3D) structures of the wild-type and mutated human APP sequences

Protein 3D structures for both the wild-type and mutated human APP sequences were generated using each FASTA-formatted sequence through the I-TASSER (Iterative Threading Assembly Refinement) Server (seq2fun.dcmb.med.umich.edu//I-TASSER/). I-TASSER, a protein 3D structure prediction server, operates by predicting protein structures from linear sequences. This process involves the initial identification of structural templates from the Protein Data Bank (PDB), followed by the construction of full-length protein models through iterative template-based fragment assembly simulations[23-25]. Subsequent to structure prediction, each model was refined using the Galaxy Web's GalaxyRefine server (galaxy.seoklab.org). This server enhances structural quality through repeated structural disturbances and subsequent relaxations facilitated by molecular dynamics simulations, ultimately improving the overall quality of the protein structures[26,27].

2.4. Evaluation of the quality of the predicted initial and refined protein models

The quality assessment of both initial and refined protein models involved the utilization of various tools, including

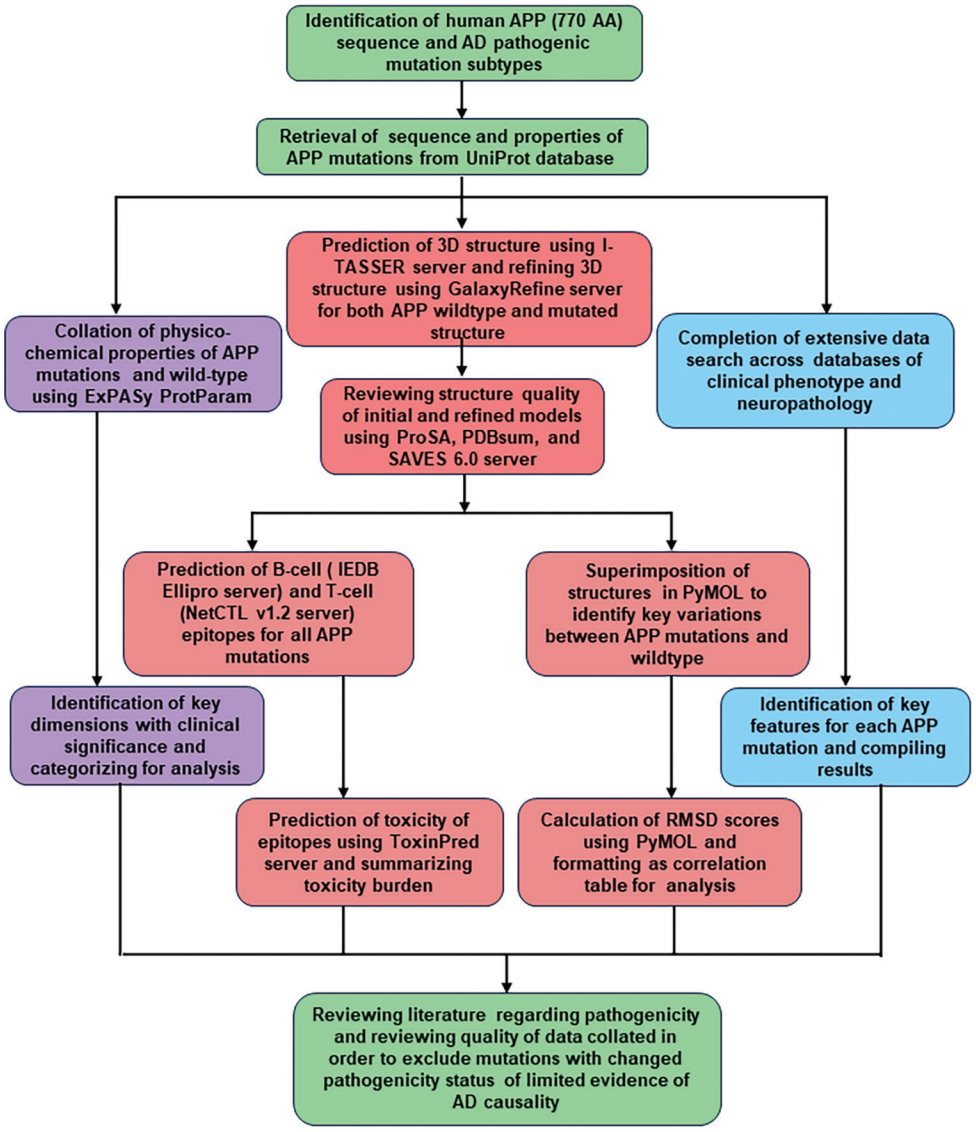

Figure 1. Schematic representation of the workflow employed in this study.
Abbreviations: AA: Amino acid; APP: Amyloid precursor protein; RMSD: Root mean square deviation.

Ramachandran plot, Verify3D, ERRAT, and ProSA. The Ramachandran Plot diagrams were generated using the PDBsum database (www.ebi.ac.uk/thornton-srv/databases/cgi-bin/pdbsum/)[28], illustrating structure quality by comparing psi and phi values to identify disallowed and stable/allowed conformations. A structure was considered of good quality if over 90% of residues resided in the most favored region. These diagrams were collected for all initial and refined protein structures to facilitate a comprehensive comparison of protein structure quality. Verify3D and ERRAT quality analyses were performed via the SAVES v6.0 server (saves.mbi.ucla.edu/). Verify3D determines the compatibility of a 3D model with its amino acid sequence, assigning a structural class and comparing results to statistically sound structures. A good structure, as determined by Verify3D, exhibited a score of approximately 90% or higher[29,30]. On the other hand, ERRAT tools analyze statistics of non-bonded interactions between different atom types, with a good score defined as above 80 for protein structure[31]. The ProSA protein structure analysis software (prosa.services.came.sbg.ac.at) was employed to calculate the overall protein model quality (z-score) and local model quality (residue scores) for each initial and refined protein model[32,33]. Local model quality, assessed on a residue-by-residue basis, deemed each residue as of good quality if window size 40 was below 0.0[32]. Visual comparison of the number of residues below the 0.0 mark determined whether

the initial or refined model exhibited superior quality. Conversely, the overall model quality, represented by a z-score, was calculated based on the model's similarity to other experimentally valid structures. Visual examination and consolidation were performed based on the negative state of each Z-score[33]. Notably, all models demonstrated higher average quality scores in the refined structures compared to the initial ones. Furthermore, all mutations demonstrated comparable results in the refined structures in terms of quality.

The protein model visualization software PyMOL (software version 2.5.4) was employed to visualize and superimpose the 3D structures of both the wild-type and mutated human APP protein[34]. The degree of differentiation between superimposed protein models was quantified using the root mean square deviation (RMSD) score[34].

2.5. Identification of T-cell epitopes in the wild-type and mutated human APP sequences

The NetCTL v1.2 server (https://services.healthtech.dtu.dk/service.php?NetCTL-1.2)[35] served as the tool for predicting cytotoxic T lymphocyte (CTL) epitopes within protein sequences, integrating peptide prediction through MHC Class 1 binding, proteasomal C terminal cleavage, and transporter associated with antigen processing (TAP) transport efficiency. In this study, parameters for identifying T-cell epitopes from both wild-type and mutated human APP sequences included a weight of 0.15 on C terminal cleavage, a weight of 0.05 on TAP transport efficiency, and a threshold for epitope identification set at 0.75. Finally, epitopes were predicted and collected based on the combined score generated by the NetCTL v1.2 server.

2.6. Identification of the linear and conformational B-cell epitopes in the wild-type and mutated human APP sequences

Both linear and conformational B-cell epitopes were predicted from the structures of both the wild-type and mutated human APP sequences using the Ellipro server (http://tools.iedb.org/ellipro/)[36] under the IEDB database (https://www.iedb.org/)[37]. Finally, the BepiPred v2.0 server (https://services.healthtech.dtu.dk/service.php?BepiPred-2.0)[38] was used to predict linear B-cell epitopes from the linear sequences, providing validation for the linear B-cell epitopes predicted by the Ellipro server.

2.7. Toxicity prediction of B-cell and T-cell epitopes

The toxicity of the predicted T-cell epitopes and the linear B-cell epitopes was assessed using the ToxinPred server (http://crdd.osdd.net/raghava/toxinpred/)[39,40]. In this study, both support vector machines (SVM) and quantitative matrix (QM) methods were used for predicting the toxicity of each B- and T-cell epitope.

2.8. Retrieval of genetic properties for each *APP* mutation

Data concerning the position and codon changes for each *APP* mutation were collated from the AlzForum database. This database provided comprehensive information on chromosomal position, coding or non-coding properties, mutation type, codon and amino acid alterations, reference isoform, and genomic region for each mutation[21]. In addition, more detailed information about each amino acid related to APP mutations was gathered, encompassing the codon sequence, R group charge, and molecular mass.

2.9. Literature review for the identification of *APP* mutation-related clinical phenotype, pathogenicity, and neuropathology

An extensive literature review was conducted to elucidate the clinical and neuropathological phenotypes associated with each genetic subtype of fAD. The initial phase of the literature review involved the utilization of diverse conjunctions of keywords and Boolean operators such as "AND," "OR," and "NOT" on the PubMed (pubmed.ncbi.nlm.nih.gov) and Embase (embase.com) databases. The comprehensive list of keywords and terms employed in the search included: "Alzheimer's Disease," "familial AD," "amyloid precursor protein," "clinical phenotype," "clinical symptoms," "neuropathology," and "ethno-genetic subtype." This literature search was conducted using various combinations of keywords and Boolean operators across both databases, encompassing relevant abbreviations and truncations (*).

After the initial review, relevant data were selectively chosen based on research quality and validity. Subsequently, a list of mutations on the *APP* gene associated with fAD was created, drawing information from the ALZForum database. The previously mentioned keywords and terms were then combined with mutation subtype descriptions, which included ethno-genetic names (e.g., "Flemish" and "E693G"). This combination aimed to identify all relevant mutation-specific research papers. The searches were conducted through Google Scholar, as well as Medline and Cochrane Library, to augment the volume of results, particularly given the limited caseload available within the literature for rarer subtypes. In addition, further relevant research was identified by exploring the references of relevant systematic reviews and examining articles listed in the ALZForum database.

The data collated from the extensive literature search underwent a quality review based on the representativeness

and reliability of different studies across varying evidence levels. Given that many of the mutations under study had a low number of recorded cases, case reports, and case series were considered for certain mutations, contingent on the quality of methodology and reported results. However, preference was given to higher-level studies, including systematic reviews and case series. Given the nature of the collated data, most studies were of a quantitative nature. The results were subsequently summarized in table format for detailed analysis and inclusion in the report.

3. Results

3.1. Analysis of physicochemical properties of the wild-type and mutated human APP sequences

The analysis of physicochemical properties for the wild-type human and 20 mutated APP, conducted through the ExPASy ProtParam server, demonstrated variable MW for the mutated APPs compared to the wild-type APP. Herein, significant changes in MW were observed for the Osaka (86814.13 Da) and Arctic (86871.19) mutations when compared to the wild-type APP (86943.25) (Table 1). On the other hand, the Indiana mutation exhibited the highest MW (86991.29 Da), followed by the Iberian (86977.27 Da), French (86975.31 Da), and A673V (86971.3) mutations (Table 1). The theoretical pI, determining a protein's acidicity or basicity, was consistent among the wild-type APP and several mutations, including Flemish, A673V, Iranian, Austrian, German, French, Iberian, Indiana, V717G, London, V717L, T719N, and Australian, all sharing a pI value of 4.73. Notably, the Taiwanese mutation exhibited the highest pI (4.76), while the Swedish mutation displayed the lowest pI (4.72). Conversely, the Tottori, Osaka, Arctic, and Iowa mutations had a pI of 4.74, surpassing the threshold value of the wild-type APP (4.73) (Table 1).

The AI serves as an indicator of a protein's thermostability. Analysis of the AI revealed that both wild-type and mutated APPs generally exhibit thermostability. Notably, the Tottori, Arctic, Iowa, Taiwanese, T719N, and M722K mutations share an identical AI value of 73.18, similar to the wild-type APP. Comparatively, when assessed against the resultant threshold value, the AI value increased for the Austrian and Swedish mutations to 73.69, followed by A673V (73.43). On the other hand, the AI value decreased for the German (72.94), French, Indiana, V717G (72.81), Iberian, and Australian mutations (72.68) when compared to the wild-type APP (Table 1).

Table 1. Physicochemical properties of the wild-type and 20 mutated human amyloid precursor protein

Mutation	MW	Theoretical pI	II	AI	GRAVY
Wild-type APP	86943.25	4.73	40.69	73.18	−0.584
A673V	86971.30	4.73	40.69	73.43	−0.581
D678N (Tottori)	86942.26	4.74	40.75	73.18	−0.584
E693Δ (Osaka)	86814.13	4.74	40.37	73.28	−0.580
E693G (Arctic)	86871.19	4.74	40.44	73.18	−0.580
D694N (Iowa)	86942.26	4.74	40.44	73.18	−0.584
A692G (Flemish)	86929.22	4.73	40.59	73.05	−0.587
KM670/671NL (Swedish)	86911.15	4.72	40.31	73.69	−0.581
D678H (Taiwanese)	86965.30	4.76	40.44	73.18	−0.584
T714A (Iranian)	86913.22	4.73	40.69	73.31	−0.581
T714I (Austrian)	86955.30	4.73	40.58	73.69	−0.577
V715A (German)	86915.20	4.73	40.69	72.94	−0.587
V715M (French)	86975.31	4.73	40.69	72.81	−0.587
I716F (Iberian)	86977.27	4.73	40.80	72.68	−0.586
V717F (Indiana)	86991.29	4.73	40.80	72.81	−0.586
V717G	86901.17	4.73	40.69	72.81	−0.590
V717I (London)	86957.28	4.73	40.80	73.31	−0.584
V717L	86957.28	4.73	41.05	73.31	−0.584
T719N	86956.25	4.73	40.69	73.18	−0.588
M722K	86940.23	4.75	40.54	73.18	−0.591
L723P (Australian)	86927.21	4.73	41.37	72.68	−0.591

Abbreviations: AI: Aliphatic index; GRAVY: Grand average hydropathy; II: Instability index; MW: Molecular weight; pI: Theoretical isoelectric point.

The II serves as an indicator of a protein's stability, with a value ≤40 suggesting stability. In this study, the analysis indicated that both the wild-type APP (40.69) and all mutated APPs exhibited instability, with values ranging from 40.31 to 41.37. Notably, the Swedish mutation demonstrated the lowest II, while the Australian mutation had the highest II (Table 1).

Positive and negative GRAVY values offer insights into the protein's hydrophobic versus hydrophilic status. In this study, we observed that both wild-type and mutated APPs were hydrophilic. The GRAVY value for wild-type APP was −0.584, followed by the Taiwanese, Tottori, Iowa, London, and V717L mutations, all sharing the same threshold value of −0.584 (Table 1).

3.2. Analysis of 3D structures in predicted wild-type and mutated APPs

The full-length 3D structures of both wild-type and mutated APPs were not available in PDB. Consequently, we employed the I-TASSER server to predict the protein 3D structure. I-TASSER predicts the protein structure and chooses the optimal model based on various criteria, including the c-score, cluster density, number of decoys, estimated template modeling (TM)-score, and estimated RMSD score. The c-score typically ranges from −5 to 2, with larger values indicating better quality of the predicted protein model, and a c-score exceeding −1.5 suggests a protein model with accurate global topology[23]. In this study, the c-score ranged from −0.68 to −1.43, differing for wild-type and each mutation of APP, with the exception of the Tottori and Flemish mutations (−0.68) (Table S1).

The TM-score serves as an indicator of the correct topology of the predicted protein model, with a TM-score >0.5 considered indicative of a good model. In this study, the lowest TM-score, recorded at 0.54 ± 0.15, was associated with the V717G and V717L mutations, whereas the highest TM-score, measured at 0.63 ± 0.14, was observed for the Flemish and Tottori mutations. The TM-score for wild-type human APP was 0.60 ± 0.14 (Table S1).

Comparatively, the RMSD score represents the average distance between residues that are structurally aligned according to the TM-score[23]. In this study, the estimated lowest RMSD score, measuring 9.9 ± 4.6 Å, was identified for the Flemish and Tottori mutations, while the highest RMSD score, reaching 11.8 ± 4.5 Å, was associated with the V717G mutation. The RMSD score for the wild-type human APP was determined to be 10.5 ± 4.6 Å (Table S1).

The number of structure decoys in a unit of space is termed cluster density, and a higher cluster density with an increased structural decoys value indicates a greater level of predictability in the model[23]. The cluster density in this study ranged from 0.0862 to 0.1832, with the V717G mutation displaying the lowest density and the Flemish mutation having the highest (Table S1). Consequently, these findings reveal that all the scores fell within an acceptable range, affirming the high quality of the predicted models for further analysis. The predicted 3D protein structures of both wild-type and mutated APPs are illustrated in Figure 2.

I-TASSER identifies the templates using 10 different template prediction servers and constructs the structure based on the best-scoring template (Table S1). In this study, the template 3KTMA was identified as common among wild-type and all 21 mutations of APPs (Table S1). In addition, templates 7WB4N (wild-type, 18 out of 20 mutations [excluding Indiana and M722K]), 6N7PX (wild-type, German), 4YNOB (wild-type, 19 out of 20 mutations [excluding Indiana]), 7WOOD (wild-type, aA673V, Arctic, Flemish, French, German, London, Taiwanese, M722K, and V717L), 6AAYA (wild-type, Australian, Iberian, A673V, and V717G) were utilized for the 3D structure prediction of wild-type and mutated APPs. However, 10 templates were found to differ when used for the 3D structure prediction of different mutated APPs, not including the wild-type APP. These templates were 5IJOJ (Indiana), 51QWQ (Indiana, Austrian, Osaka, and Taiwanese), 3UMHA (Indiana), 1QBKB (Indiana), 5OWVA (Indiana), 3Q7GA (Arctic, Austrian, Flemish, Taiwanese), 51GWQ (French and A673V), 6Z91A (Arctic, Australian, Iberian, Iranian, London, Swedish, Tottori, M722K, T719N, V717G, and V717L), 7DRRD (Flemish, Iranian, Lowa, Swedish, Tottori, M722K, T719N, V717L), and 7RHQA (Australia, Austrian, Iberian, Iranian, Osaka, Swedish, T719N, and V717G) (Table S1).

3.3. Evaluation of 3D structures in predicted wild-type and mutated APPs

The evaluation of predicted protein structures was performed based on the Ramachandran plot statistics, ERRAT score, ProSA local and overall model quality, and Verify3D score. The Ramachandran plot assesses the stereochemical quality of the protein model by categorizing residues into most favored, allowed, generously allowed, and disallowed regions. A concentration of over 90% of protein residues in the core area of the Ramachandran plot implies higher stereochemical quality in the predicted protein model. Ramachandran plot statistics were obtained both before and after refining the predicted protein structures.

The results of the Ramachandran plot statistics for non-refined protein models predicted by I-TASSER revealed that ≥66.6% of residues are located in the most favored

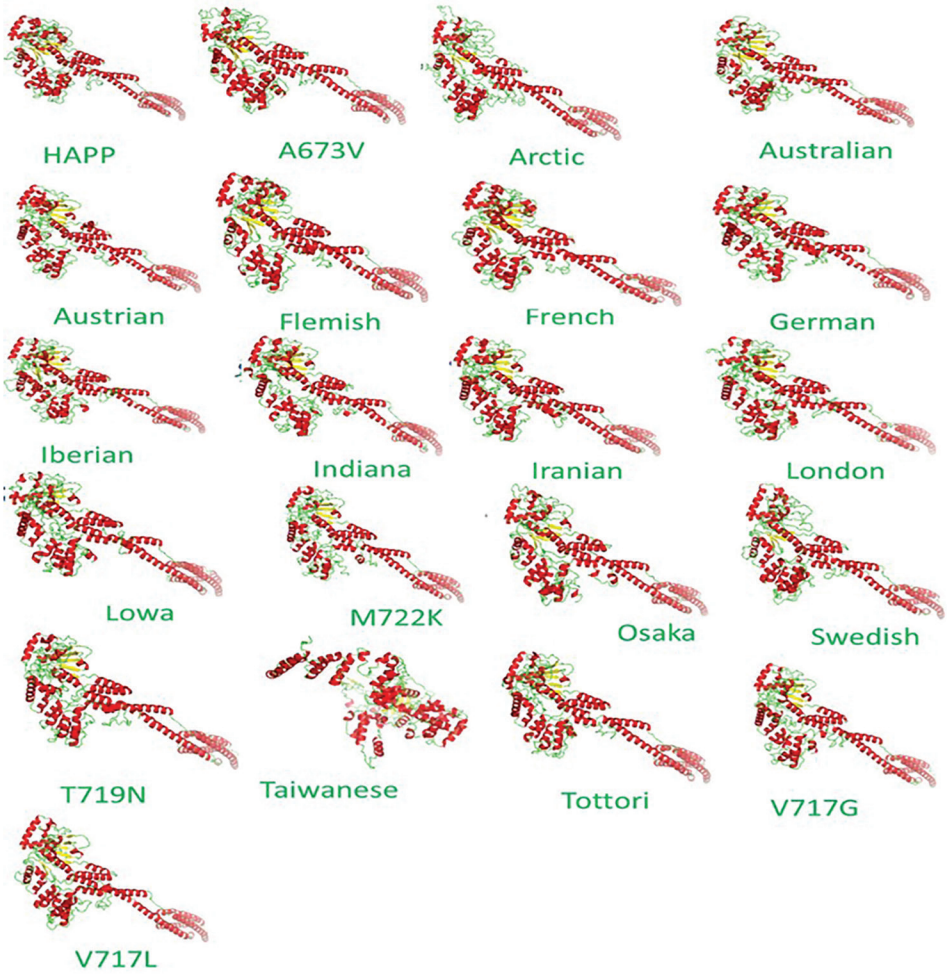

Figure 2. Refined protein 3D structures of the wild-type and 20 mutated human amyloid precursor proteins predicted through the I-TASSER server.

regions, while ≥19.0%, ≥1.70%, and ≥1.7% residues are located in the allowed, generously allowed, and disallowed regions, respectively, for both wild-type and all mutated APP models (Table S2). However, refining the protein structures through the Galaxyrefine server significantly improved structure quality. The refined structures exhibited ≥80.7% of residues in the most favored regions, ≥10.1% in the allowed regions, ≥0.70% in the generously allowed regions, and ≥1.6% residues in the disallowed regions for both wild-type and all mutated APP models (Table S2). Therefore, the refined protein structures demonstrated superior quality compared to the non-refined protein structures. The Ramachandran plots of the initial structures and refined protein structures are shown in Figure S1 and Figure 3, respectively.

Using ProSA, potential errors in both wild-type and mutated APP models were identified. The z-score on the ProSA web server represents the overall quality of the predicted protein model, with a more negative value indicating higher accuracy in the protein model. The ProSA z-score was predicted for both refined and non-refined protein structures. The z-score of the non-refined wild-type and mutated protein models ranged from −2.50 to −6.16 (Table S3). In contrast, the refined protein structures exhibited z-scores between −3.62 and −6.75, indicating an overall improvement in accuracy compared to the non-refined protein structures (Table S3). The z-scores are shown in Figure S2. Energy plots of the predicted refined and non-refined protein models for both wild-type and all mutated APPs are presented in Figure S3.

ERRAT provides an alternative method for evaluating the protein model, utilizing an atomic interaction approach to distinguish between correctly and incorrectly predicted segments of the protein model. The overall quality factor, expressed as a percentage (out of 100), serves as a measure in ERRAT, with a higher factor indicating superior predicted protein model quality. The overall quality factors predicted by ERRAT are illustrated in Table S3, confirming that both

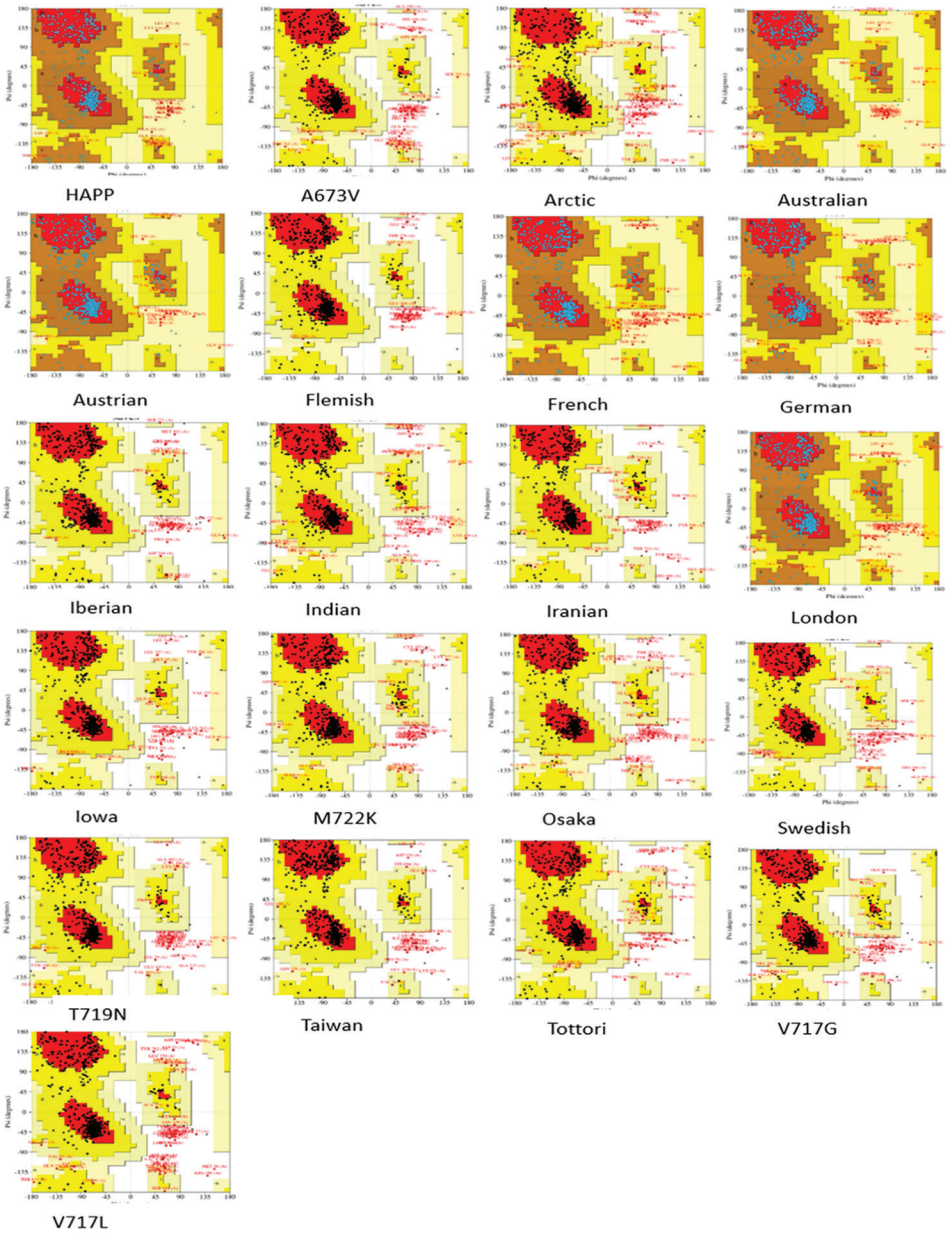

Figure 3. Ramachandran plots for the refined protein 3D structure of the wild-type and 20 mutated human amyloid precursor proteins predicted through the I-TASSER server.

refined and non-refined predicted protein models for both wild-type and all mutated APPs exhibited good quality.

For the assessment of protein models using 3D profiles, Verify3D was employed. Veryfy 3D assesses the compatibility of an atomic model (3D) with its corresponding amino acid sequence (1D) by assigning a structural class based on location and environment and comparing the results to established structures. In Verify3D, if 80.0% of the amino acids in the protein model have a score of ≥0.2 in the 3D/1D profile, the model is considered of poor quality. The analysis of Verify3D results is presented in Table S3, revealing that all mutated and wild-type models had <80.0% of residues with a score ≥0.2 in 3D/1D profiles. This designation classifies our protein models as poor-quality models according to this specific assessment.

3.4. Structural comparison of the wild-type and mutated human APPs

All 20 mutated APPs are shown in Figure 4. The superimposition of APP structures and RMSD

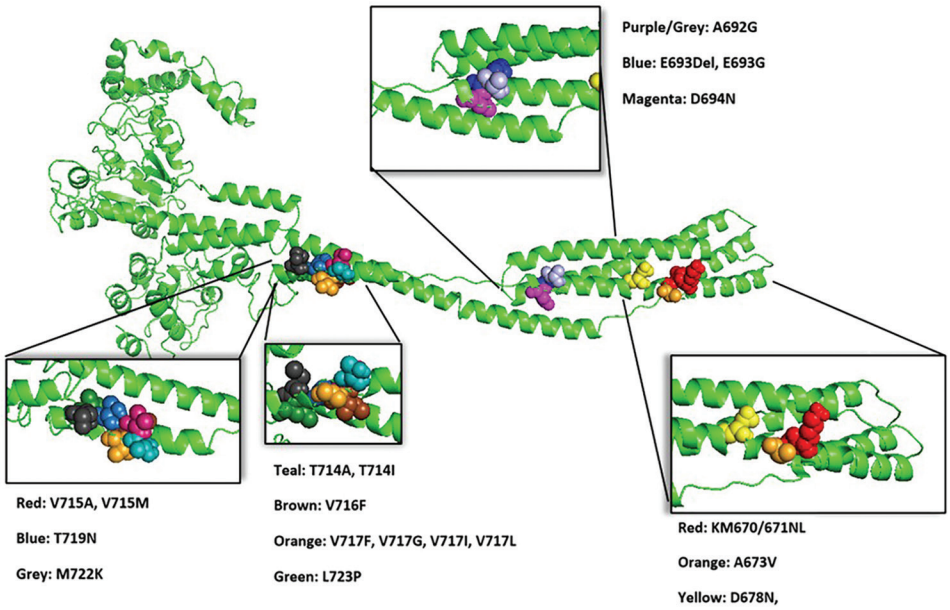

Figure 4. 3D structure of the human amyloid precursor protein and the location of the 20 different amyloid precursor protein (APP) mutations on wild-type APP structure.

calculation were performed using PyMOL software. On superimposing mutated APPs onto wild-type APP and conducting an analysis, mutated APPs with mutations at positions 714 and 717 demonstrated less visible differences compared to wild-type APP. Conversely, more pronounced differences were visualized for mutated APPs with mutations in other regions of the *APP* gene when superimposed on both wild-type and mutated APPs at positions 714 and 717. These variations were associated with a slightly lower average RMSD score (Figure 5A and B). Mutated APPs with mutations at positions 714 and 717 also demonstrated higher similarity among themselves. Notably, the structure of the Taiwanese (D678H) mutation exhibited significant variance when superimposed on wild-type and all other 20 APP mutations (Figure 5A and B).

3.5. Assessment of B- and T-cell epitopes toxicity

The identification of B-cell epitopes plays a key role in the development of epitope-based vaccines, therapeutic antibodies, and other immunodiagnostic tools. B-cell epitopes are mainly subdivided into linear (continuous) and conformational (discontinuous) forms. In this study, we utilized the ElliPro server to predict both linear and conformational B-cell epitopes from the 3D structures of APP. In addition, linear B-cell epitopes were predicted from the linear sequences of APP using the BepiPred server. A total of 658 linear B-cell epitopes were identified for wild-type and 20 mutated APPs, with 253 and 405 linear B-cell epitopes predicted by the ElliPro and BepiPred servers (Table 2).

Higher numbers of linear B-cell epitopes were observed for the Australian (34), V717L (33), Arctic (33), Austrian (32), French (32), A673V (32), and T719N (32) mutations compared to the wild-type APP (30) (Table 2). Among the 658 linear B-cell epitopes, 131 were omitted from the initial selection for toxicity prediction due to their length (sequence ≥50). Therefore, 527 linear B-cell epitopes were selected for toxicity prediction using the ToxinPred server. Out of these 527 epitopes, 220 linear B-cell epitopes were predicted to be toxic, while 307 were non-toxic. When compared to wild-type APP (8), the highest volume of toxic epitopes was linked to German (14), A673V (13), Osaka (12), Arctic (12), Austrian (12), V717G (12), M722K (12), Iowa (11), Iranian (11), French (11), Tottori (11), Iberian (10), Indiana (10), T719N (10), Australian (10), Swedish (9), Flemish (9), and London (9) mutations. On the other hand, the lowest number of toxic epitopes were associated with the Taiwanese (7) and V717L (7) mutations, indicating a lower toxicity burden compared to wild-type APP (8).

Further analysis revealed that 11 toxic linear B-cell epitopes, associated with multiple mutations, were shared among different fADs. These include epitopes 181 – 193 (Iberian, London, Flemish, V717G, T719N mutations), 200 – 210 (A673V, Arctic mutations), 54 – 74 (A673V, V717L, Swedish mutations), 94 – 119 (wild-type APP and Indiana, Iberian, London, Flemish, M722K mutations), 72 – 91 (Australian, French, Iberian, Iranian, M722K,

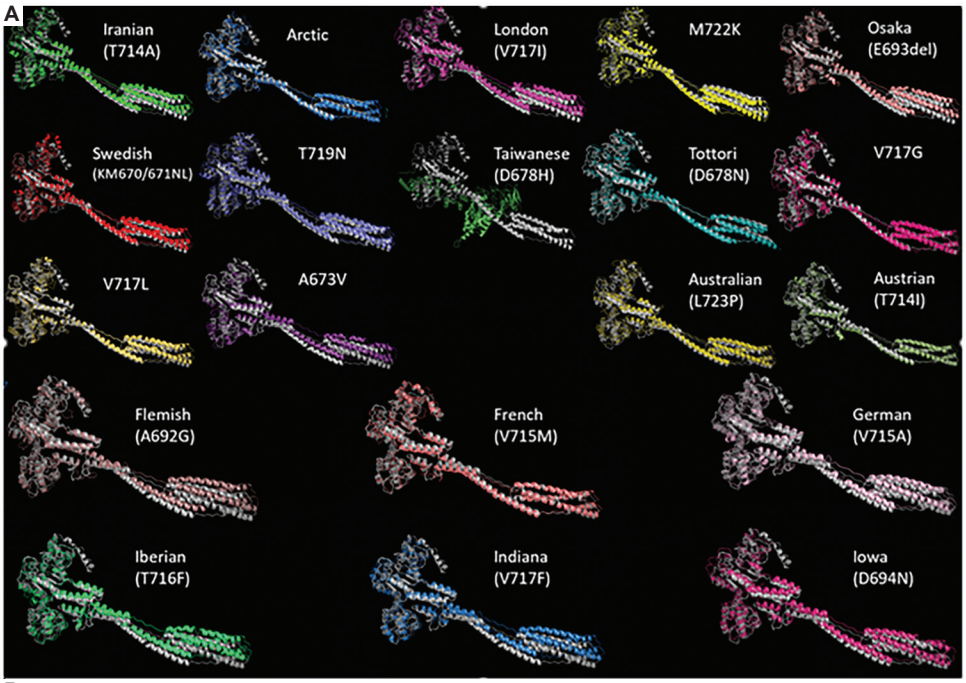

B

	APP	A673V	D678H	D678N	A692G	E693De	E693G	D694N	T714A	T714I	V715A	V715M	I716F	V717F	V717G	V717I	V717L	T719N	M722K	L723P	KM670/671NL
APP	0	1.6	42.081	0.852	1.035	1.605	1.347	0.92	0.954	0.748	0.764	0.797	0.888	0.89	0.874	0.819	0.767	0.786	0.909	0.764	1.016
A673V	1.6	0	34.901	2.289	2.533	1.134	2.089	0.869	0.841	1.091	1.293	1.862	0.818	1.928	0.753	0.794	1.201	1.226	2.375	1.409	0.826
D678H	42.081	34.901	0	53.195	51.536	50.862	54.993	40.824	48.922	40.802	46.356	41.136	48.351	45.401	47.425	44.157	54.64	58.561	52.443	45.958	53.161
D678N	0.852	2.289	53.195	0	0.991	1.487	1.811	1.499	0.891	0.928	1.014	0.888	0.786	0.808	0.719	0.997	0.839	0.887	1.085	0.883	1.15
A692G	1.035	2.533	51.536	0.991	0	1.144	1.449	1.269	0.937	0.952	0.68	0.937	0.883	0.879	1.18	0.793	0.792	0.768	0.887	0.722	0.864
E693Del	1.605	1.134	50.862	1.487	1.144	0	1.802	2.251	1.241	0.976	1.212	0.77	1.041	1.828	1.068	1.223	0.968	1.006	1.228	1.221	0.766
E693G	1.347	2.089	54.993	1.811	1.449	1.802	0	2.579	1.534	1.551	1.499	1.423	1.691	1.546	1.617	1.641	1.374	1.389	1.465	1.71	1.518
D694N	0.92	0.869	40.824	1.499	1.269	2.251	2.579	0	1.498	1.87	1.526	0.881	1.302	1.425	1.019	1.413	2.044	0.833	1.216	1.128	0.938
T714A	0.954	0.841	48.922	0.891	0.937	1.241	1.534	1.498	0	0.918	0.976	0.918	0.738	0.95	0.891	0.996	0.853	0.887	0.772	0.838	1.123
T714I	0.748	1.091	40.802	0.928	0.952	0.976	1.551	1.87	0.918	0	0.868	0.887	0.971	1.001	0.912	0.821	0.883	1.008	1.059	0.817	1.401
V715A	0.764	1.293	46.356	1.014	0.68	1.212	1.499	1.526	0.976	0.868	0	0.692	0.701	0.767	0.878	0.746	0.78	0.78	0.745	0.632	0.922
V715M	0.797	1.862	41.136	0.888	0.937	0.77	1.423	0.881	0.918	0.887	0.692	0	0.801	0.763	0.921	0.764	0.782	0.884	0.829	0.817	0.933
I716F	0.888	0.818	48.351	0.786	0.883	1.041	1.691	1.302	0.738	0.971	0.701	0.801	0	0.773	0.69	0.773	0.966	0.837	0.786	0.714	0.896
V717F	0.89	1.928	45.401	0.808	0.879	1.828	1.546	1.425	0.95	1.001	0.767	0.763	0.773	0	0.873	0.747	0.91	0.805	0.912	0.763	0.927
V717G	0.874	0.753	47.425	0.719	1.18	1.068	1.617	1.019	0.891	0.912	0.878	0.921	0.69	0.873	0	0.928	1.058	0.906	0.964	0.801	1.019
V717I	0.819	0.794	44.157	0.997	0.793	1.223	1.641	1.413	0.996	0.821	0.746	0.764	0.773	0.747	0.928	0	0.885	0.797	0.902	0.611	0.792
V717L	0.767	1.201	54.64	0.839	0.792	0.968	1.374	2.044	0.853	0.883	0.78	0.782	0.966	0.91	1.058	0.885	0	0.75	0.816	1.059	0.888
T719N	0.786	1.226	58.561	0.887	0.768	1.006	1.389	0.833	0.887	1.008	0.78	0.884	0.837	0.805	0.906	0.797	0.75	0	0.859	0.721	1.096
M722K	0.909	2.375	52.443	1.085	0.887	1.228	1.465	1.216	0.772	1.059	0.745	0.829	0.786	0.912	0.964	0.902	0.816	0.859	0	0.797	0.916
L723P	0.764	1.409	45.958	0.883	0.722	1.221	1.71	1.128	0.838	0.817	0.632	0.817	0.714	0.763	0.801	0.611	1.059	0.721	0.797	0	1.075
KM670/671NL	1.016	0.826	53.161	1.15	0.864	0.766	1.518	0.938	1.123	1.401	0.922	0.933	0.896	0.927	1.019	0.792	0.888	1.096	0.916	1.075	0

Figure 5. Superimposition of 3D structures of 20 different amyloid precursor protein (APP) mutations with wild-type APP. (A) Superimposition of the 20 different APP mutations with the human wild type of APP protein structure. Refined structures (colored) are superimposed on wild-type structures (grey). (B) Root means square deviation correlation chart for the human wild-type APP and 20 different APP mutations.

T719N, Taiwanese, V717L, Osaka, Tottori mutations), 98 – 107 (wild-type APP and all mutations except Arctic, Austrian, Flemish, and Iowa), 177 – 182 (wild-type APP and Iberian, London, Osaka, Tottori mutations), 158 – 166 (Austrian, Indiana, V717G, Flemish mutations), 177 – 184 (French, M722K, T719N, V717L mutations), 324 – 334 (wild-type APP and all mutations except Arctic, Iranian, Swedish, Tottori, and Osaka), and the epitope position 740 – 766 (wild-type APP and all mutations except Arctic and Osaka) (Table 3).

In this study, we identified 124 conformational B-cell epitopes from the 3D structure of both wild-type and 20 mutated APPs (Table 2). Notably, common epitope regions were observed between the linear and conformational B-cell epitopes (Table S4). The highest burden of conformational B-cell epitopes was associated with the Taiwanese mutation (12), followed by the V717L (7), T719N (7), and M722K (7) mutations. In contrast, the lowest number of epitopes was found with the London (4), German (4), and Osaka (4) mutations (Table 2). However, predicting the toxicity of the conformational B-cell epitopes was not feasible due to limitations in the ToxinPred Server.

A total of 3075 linear T-cell epitopes were predicted for both wild-type and 20 APP mutations using the NetCTL server (Table S5). Subsequently, these 3075 T-cell epitopes underwent toxicity prediction through the ToxinPred server, revealing that 23.45% of the epitopes (721 epitopes) were found to be toxic. Herein, the German mutation displayed the highest number of toxic T-cell epitopes (38; 26.03%) compared to the wild-type APP (31; 21.09%).

Table 2. Linear and discontinued B-cell epitopes prediction from the 3D structure of the wild-type and 20 mutated human APP

Mutation type	Linear B-cell epitope by Ellipro	Linear B-cell epitope by Bepipred	Discontinuous B-cell epitopes by Ellipro	Total
Wild-type APP	11	19	6	36
KM670/671NL (Swe)	12	19	5	36
A673V	13	19	6	38
D678N (Tot)	11	21	5	37
D678H (Tai)	12	17	12	41
A692G (Fle)	12	19	7	38
E693Del (Osa)	11	21	4	36
E693G (Arctic)	14	19	7	40
D694N (Iowa)	11	19	5	35
T714A (Ira)	11	19	6	36
T714I (Austrian)	12	20	5	37
V715A (Ger)	13	20	4	37
V715M (Fre)	13	19	5	37
I716F (Ibe)	12	19	5	36
V717F (Ind)	12	18	5	35
V717G	11	20	6	37
V717I (Lon)	10	19	4	33
V717L	14	19	7	40
T719N	12	20	7	39
M722K	12	19	7	38
L723P (Australian)	14	20	6	40

Abbreviation: APP: Amyloid precursor protein.

Table 3. Common toxic linear B-cell epitopes from the 3D structure of the human wild type and mutated APP

Common toxic B-cell epitopes	Position	Mutation subtypes
GVEFVCCPLAEES	181 – 193	I716F, V717I, A692G, V717G, T719N
DAEEDDSDVWW	200 – 210	I716V, I716T, A673V, E682K, E693G
SDPSGTKTCIDTKEGILQYCQ	54 – 74	A673V, V717L, T719P, KM670/671NL
IQNWCKRGRKQCKTHPHFVIPYRCLV	94 – 119	APP, V717F, I716F, V717I, A692G, M722K
YCQEVYPELQITNVVEANQP	72 – 91	L723P, K724N, V715M, I716M, I716F, T714A, M722K, T719N, T719P, D678H, V717L, E693Del, D678N
CKRGRKQCKT	98 – 107	APP, L723P, K724N, I716V, V715M, V715A, I716M, I716T, I716F, V717F, T714A, V717I, M722K, KM670/671NL, T719N, T719P, D678H, V717G, V717L, A673V, E693Del, D678N
DKFRGV	177 – 182	APP, I716V, I716F, V717I, E693Del, D678N
CSEKSTNLH	158 – 166	T714I, V717F, E682K, V717G, A692G
DKFRGVEF	177 – 184	K724N, V715M, M722K, T719N, T719P, V717L
CGGNRNNFDTE	324 – 334	APP, T714I, K724N, I716V, V715M, V715A, I716M, I716T, I716F, V717F, V717I, V717F, E682K, L723P, M722K, T719N, T719P, V717G, V717L, A673V, A692G, D694N, D678N
AAVTPEERHLSKMQQNGYENPTYKFFE	740 – 766	APP, L723P, T714I, K724N, I716V, V715M, V715A, I716M, I716T, I716F, V717F, V717I, V717F, T714A, E682K, M722K, KM670/671NL, T719N, T719P, D678H, V717G, V717L, A673V, A692G, D694N, D678N

Abbreviation: APP: Amyloid precursor protein.

A total of 36 toxic T-cell epitopes were linked to the M722K (24.83%), Arctic (24.66%), Austrian (24.66%), A673V (24.49%), Osaka (24.49%), and V717G (24.49%) mutations; 35 to the Tottori (24.14%), Iranian (23.97%), French (23.97%), and Iowa (23.81%) mutations; 34 to the T719N (23.45%), Indiana (22.97%), and Iberian (22.82%) mutations; 33 to the Australian (22.76%), London (22.60%), Swedish (22.45%), and Flemish (22.45%) mutations; and 31 to the Taiwanese (21.38%) and V717L (20.95%) mutations (Table S4).

3.6. Comparison of B- and T-cell epitopes toxicity burden with clinical and neuropathological outcomes

A thorough literature search was conducted to delineate the clinical symptoms and neuropathology associated with each identified APP mutation (Tables 4 and 5). Subsequently, after collating and analyzing the toxicity results of both B and T cell epitopes for each mutation (as well as wild-type APP), three distinct categories were established to define the toxicity burden based on the cumulative volume of toxic epitopes (toxicity determined according to ToxinPred server for both B and T cell linear epitopes). Mutations demonstrating more than 35 toxic epitopes were classified as having a high toxicity burden (seven mutations in total: A673V, Osaka, Arctic, Austrian, German, V717G, M722K). The remaining mutations, featuring 34 – 35 toxic epitopes, were considered to have a moderate toxicity burden (8 mutations in total: Tottori, Iowa, Iranian, French, Iberian, Indiana, T719N, Australian). All mutations with fewer than 34 toxic epitopes were categorized with a low toxicity burden (five mutations in total: Swedish, Taiwanese, Flemish, London, V717L), along with wild-type APP (toxicity burden = 31).

An increase in toxicity burden was correlated to an increase in neuropathological changes as reported in the literature, specifically an increase in Aβ deposition (identified in 57% of mutations with high toxicity burden) and the presence of amyloid plaques and neurofibrillary tangles (identified in 43% of mutations with high toxicity burden) among study participants (Table 5). However, no correlation was identified between clinical presentation (symptom presentation, disease burden, or age of onset) and the burden of epitope toxicity.

4. Discussion

fAD arises from mutations in the *APP* and *PSEN* genes[6]. The clinical presentation and neuropathological features of both sporadic AD (SAD) and fAD display a striking resemblance. Therefore, investigating the molecular events underlying fAD is critical for understanding disease pathogenesis and developing disease-modifying therapies. While 32 pathogenic mutations have been described for the *APP* gene[41], little is known about whether specific physicochemical patterns associated with these mutations directly affect clinical and neuropathological outcomes in fAD. The *APP* gene is encoded by 18 exons that undergo alternative splicing to produce APPs ranging in size from 695 to 770 amino acids. Among the 32 pathogenic mutations described for the *APP* gene, 26 are recognized as pathogenic missense mutations located within or adjacent to Aβ, generated from *APP* through the sequential cleavage of β-secretase and γ-secretases[42].

It has been demonstrated that a double mutation located at the N-terminus of Aβ, specifically at the β-secretase cleavage site in exon 16 of APP770 at codons 670 and 671, results in an increased production of total Aβ. Moreover, the pathogenic mutation APP E693Q, identified in a Dutch family with inherited cerebral hemorrhage with amyloidosis caused by Aβ[43], has been reported. Mutations within the Aβ domain have been shown to alter APP processing, leading to an increased hydrophobicity of secreted Aβ species[44,45]. Aβ42 mutations are associated with progressive dementia, senile plaques, neurofibrillary tangles, and neuronal cell loss[46]. Interestingly, mutations associated with an increase in total Aβ also contribute to cerebral amyloid angiopathy (CAA) and are associated with cerebral hemorrhages and stroke[47,48]. These findings highlight the importance of the amino acid composition of the Aβ by-products and their direct influence on the pathology and kinetic of pathological Aβ. Nonetheless, to our knowledge, little attempt has been made to study the influence of the physicochemical properties of APP/Aβ-bearing mutations on disease progression, pathogenesis, clinical presentation, Aβ kinetics, and toxicity, among other aspects.

In this study, we investigated the relationship between 20 fAD mutations and the physicochemical properties of the corresponding APPs. Our aim was to examine the specific effects of these mutations on both clinical and neuropathological outcomes. We sought to identify associations between clinical symptoms, neuropathology, and the physicochemical features of the 20 APP mutations. Various clinical symptoms, including cognitive decline, hemorrhage, seizures, myoclonus, autonomic failure, aphasia, behavioral abnormalities, dyscalculia, and pyramidal signs, were found to be associated with different APP mutations. Notably, all 20 APP mutations were linked to cognitive impairment.

Similarly, cognitive impairment, seizures, and hemorrhage have been linked to the Flemish mutation[14,15,49,50]. On the other hand, the Iranian mutation exhibited cognitive impairment, seizures, autonomic

Table 4. Clinical symptoms associated with 20 different mutations of amyloid precursor protein

Mutation subtype	AA location	Seizures	Myoclonus	Cognitive impairment	Hemorrhage	Autonomic failure	Aphasia	Behavioral changes	Dyscalculia	Pyramidal signs	Symptom count	Median age of onset
KM670/671NL (Swe)	670			Y							1	
A673V	673			Y							1	
D678N (Tot)	678			Y	N						1	
D678H (Tai)	678			Y							1	50
A692G (Fle)	692	Y		Y	Y						3	45
E693Del (Osa)	693			Y							1	
E693G (Arctic)	693			Y	N						1	55
D694N (Iowa)	694			Y	N						1	55
T714A (Ira)	714	Y		Y		Y	Y	Y			5	55
T714I (Austrian)	714	Y	Y	Y							3	32
V715A (Ger)	715			Y							1	
V715M (Fre)	715	Y	Y	Y							3	50
I716F (Ibe)	716			Y							1	31
V717F (Ind)	717	Y	Y	Y					Y		4	40
V717G	717	Y	Y	Y					Y		4	
V717I (Lon)	717	Y	Y	Y					Y		4	51
V717L	717	Y	Y	Y					Y	Y	5	44
T719N	719	N	Y	Y							2	
M722K	722			Y							1	
L723P (Australian)	723	N	Y	Y							2	62

Abbreviations: AA: Amino acid; N: Absence; Y: Presence.

https://doi.org/10.36922/an.1734

Table 5. Neuropathology and physicochemical properties associated with 20 different mutations of amyloid precursor protein

Mutation subtype	Neuropathology				Physicochemical properties		
	CAA present	Amyloid plaques	Fibrillary tangles	Aß deposition	Instability index category	Number of toxic epitopes	Structural mutation location
KM670/671NL (Swe)					1 - (40 – 40.5)	33 (B - 9 T - 24)	Aß peptide domain
A673V		Y	Y	Y-cerebellum only	2 - (40.5 – 41)	36 (B - 13 T - 23)	Aß peptide domain
D678N (Tot)	N				2 - (40.5 – 41)	35 (B - 11 T - 24)	Aß peptide domain
D678H (Tai)	Y			Y	1 - (40 – 40.5)	31 (B - 7 T - 24)	Aß peptide domain
A692G (Fle)	Y	Y	Y		2 - (40.5 – 41)	33 (B - 9 T - 24)	Aß peptide domain
E693Del (Osa)		Y	N	Y	1 - (40 – 40.5)	36 (B - 12 T - 24)	Aß peptide domain
E693G (Arctic)	Y	Y	Y	Y	1 - (40 – 40.5)	36 (B - 12 T - 24)	Aß peptide domain
D694N (Iowa)	Y	Y	Y	Y	1 - (40 – 40.5)	35 (B - 11 T - 24)	Aß peptide domain
T714A (Ira)	Y				2 - (40.5 – 41)	35 (B - 11 T - 24)	Aß peptide domain
T714I (Austrian)					2 - (40.5 – 41)	36 (B - 12 T - 24)	Aß peptide domain
V715A (Ger)					2 - (40.5 – 41)	38 (B - 14 T - 24)	Aß peptide domain
V715M (Fre)					2 - (40.5 – 41)	35 (B - 11 T - 24)	Aß peptide domain
I716F (Ibe)		Y	Y		2 - (40.5 – 41)	34 (B - 10 T - 24)	Aß precursor protein C-terminus
V717F (Ind)					2 - (40.5 – 41)	34 (B - 10 T - 24)	Aß precursor protein C-terminus
V717G					2 - (40.5 – 41)	36 (B - 12 T - 24)	Aß precursor protein C-terminus
V717I (Lon)	Y				2 - (40.5 – 41)	33 (B - 9 T - 24)	Aß precursor protein C-terminus
V717L					3 - (41+)	31 (B - 7 T - 24)	Aß precursor protein C-terminus
T719N					2 - (40.5 – 41)	34 (B - 10 T - 24)	Aß precursor protein C-terminus
M722K				Y-Increase Aß40/Aß42	2 - (40.5 – 41)	36 (B - 12 T - 24)	Aß precursor protein C-terminus
L723P (Australian)				Y-Increase Aß42	3 - (41+)	33 (B - 10 T - 23)	Aß precursor protein C-terminus

Abbreviations: CAA: Cerebral amyloid angiopathy; N: Absence; Y: Presence.

failure, aphasia, and behavioral abnormalities[11,14,51,52]. Of note, dyscalculia was associated with four different APP mutations, including Indiana, London, V717G, and V717L mutations[15]. More importantly, mutations occurring between locations 714 and 717 (Austrian, French, Indiana, London, V717G, and V717L) demonstrated the highest variety of symptoms, with seizures and/or myoclonus occurring across mutations from location 714 onwards[15,50,52-54]. The age of onset for mutations located between 714 and 717 is lower on average, while the average II is slightly higher. Interestingly, most of these mutations occur in the C-terminus of the Aβ precursor protein.

The neuropathological features associated with the Arctic and Iowa mutation (CAA, amyloid plaques, fibrillary tangles, and Aβ deposition)[14,15,49], Flemish mutation (CAA, amyloid plaques, and fibrillary tangles)[14,15,49], Osaka mutation (amyloid plaques and Aβ deposition)[18], A673V mutation (amyloid plaques, fibrillary tangles, and Aβ deposition)[16], Iranian mutation (CAA)[14], Iberian mutation (amyloid plaques and neurofibrillary tangles)[55], M722K and Australian mutation (increase Aβ42 deposition)[54,56], and London mutation (CAA)[14] were identified through extensive literature search. No such features were found in the literature for the Swedish, Austrian, German, French, Indiana, V717G, V717L, and T719N mutations.

Mutations located between positions 670 to 694 (A673V, Flemish, Osaka, Arctic, and Iowa) are generally associated with a later age of onset and a lower symptom burden. However, they exhibit a higher incidence of CAA

(with or without hemorrhage) and generally demonstrate greater Aβ deposition. These mutations predominantly occur within the Aβ peptide domain.

At present, limited research has delved into genotype-phenotype interactions across multiple mutations, as discussed above, regarding the pathogenicity of AD resulting from mutations in the *APP* gene. Two analogous studies have investigated genotype-phenotype interactions on *PSEN1*[57] and *PSEN2*[58]. Although both studies identified variations in pathogenesis and clinical outcomes for specific mutations, the scarcity of available phenotypic descriptions limited the extent of these studies, resulting in few evident clinical genotype-phenotype correlations[58].

However, genotype-phenotype interactions and correlations have been more extensively explored in various familial pathologies resulting from germline mutations. The implications of these results across a broad spectrum of pathologies underscore the importance of deepening our understanding of these interactions in AD, particularly in genetically mediated cases such as those seen in fAD.

In a review article,[59] researchers identified a definitive link between the location of mutations in breast cancer gene 1 (*BRCA1*) and breast cancer gene 2 (*BRCA2*) with exacerbated pathogenic outcomes in breast cancer development. Notably, mutations occurring on exon 11 exhibited a heightened propensity for inducing mutation-mediated diseases. These mutations demonstrated a consistent correlation with an earlier age of onset, as evidenced by multiple studies[59]. A further study focused on germline mutations of *BRCA1* in breast and ovarian cancers further affirmed this correlation, linking the codon number of the gene mutation to the ratio of breast to ovarian cancer incidence[60]. In concert with these studies on mutation location with the *BRCA1* gene, additional correlations emerged concerning variations in the structural modeling of individual mutations on *BRCA1* and their consequent physiological outcomes[61]. Moreover, the present study unveiled molecular and pathological differences among mutations, underscoring the diverse physiological outcomes associated with each mutation.

Similar correlations have been identified in Kirsten rat sarcoma viral oncogene homolog (KRAS)-driven tumors. A study conducted by Hunter *et al.* indicated that assessing the structural and biochemical properties of KRAS mutations (genetic drivers in various cancers) can offer valuable insights into the pathogenicity and potential therapeutic approaches for the resultant tumors[62]. The discoveries elucidated in these cancer studies highlight the potential implications of advancing our understanding of genotype-phenotype interactions. Moreover, the complex intermediaries governing these relationships (including mutation location, resultant structure, and physicochemical and biochemical properties) emerge as critical components in fAD.

It is important to acknowledge the limited literature on clinical measures and phenotypes for certain mutations included in this study, attributed to their scarcity in reported cases. As a result, it became necessary to incorporate studies characterized by lower overall quality and smaller sample sizes, ensuring an adequate breadth of comparative phenotypic data. Phenotypic findings derived from case studies were also integrated where essential, particularly in cases where only a limited number of families (1 – 2 families) with a specific mutation had been identified and studied for academic inclusion. Given the rarity of certain APP mutation subtypes linked to fAD pathology, the availability of experimentally identified toxicity data for these specific AD mutation subtypes is notably constrained. These limitations hinder our capacity to concretely validate the accuracy of our modeled toxicity findings. Nevertheless, it is imperative to emphasize that all models underwent rigorous accuracy testing in accordance with the relevant parameters, as delineated in Section 3.

In addition to analyzing the impact of mutations on the overall physical and chemical properties of the entire APP, there exists an avenue for further research that delves into the potential phenotypic implications arising from substituted amino acid residues. Such an inquiry would involve a comprehensive exploration of the physicochemical properties associated with these pathogenic mutations. Undertaking further research in this realm holds the promise of improving our mechanistic understanding of fAD. A more robust evaluation of how the AD phenotype responds to different variants within potentially pathogenic gene sequences can significantly contribute to improving future diagnostics and therapeutics for AD.

5. Conclusion

Our investigation has unveiled a significant correlation between the location of genetic mutations within the protein sequence and specific physicochemical properties, as well as clinical presentations among different fAD subtypes. This insight underscores the intricate relationship between genetic variations and the resultant clinical heterogeneity within the fAD spectrum.

Notably, mutations that exhibited higher structural similarity when superimposed tended to manifest analogous physical and clinical characteristics. This observation highlights the relevance of shared structural features in predicting clinical outcomes across certain fAD subtypes. However, the converse is also true, as our analysis unveiled varying neuropathological findings that exhibited a stronger correlation with increasing epitope toxicity burden.

Remarkably, despite this correlation, epitope toxicity did not exert a substantial influence on clinical outcomes.

In essence, our findings underscore the significance of precise genetic mutation profiling within fAD subtypes. These insights have far-reaching implications for the development of tailored diagnostic and therapeutic strategies, allowing for a more nuanced approach to the clinical management of fAD. Our research forms a crucial stepping stone in the ongoing quest to decipher the complex interplay between genetics, physicochemical properties, and clinical presentations in neurodegenerative disorders like fAD.

Acknowledgments

None.

Funding

None.

Conflict of interest

The authors declare that they have no competing interests.

Author contributions

Conceptualization: Mourad Tayebi and Utpal K Adhikari
Formal analysis: All authors
Investigation: Mourad Tayebi and Utpal K Adhikari
Methodology: Georgia Uebergang
Writing – original draft: All authors
Writing – review and editing: Mourad Tayebi and Utpal K Adhikari

Ethics approval and consent to participate

Not applicable.

Consent for publication

Not applicable.

Availability of data

Detailed results of our analyses are included in this article and its additional files. The raw data supporting the conclusions of this article will be made available by the authors without undue reservation.

References

1. Alonso Vilatela ME, López-López M, Yescas-Gómez P, 2012, Genetics of Alzheimer's disease. *Arch Med Res*, 8: 622–631.

   https://doi.org/10.1016/j.arcmed.2012.10.017

2. Giri M, Zhang M, Lü Y, 2016, Genes associated with alzheimer's disease: An overview and current status. *Clin Interv Aging*, 11: 665–681.

   https://doi.org/10.2147/CIA.S105769

3. Dementia: Key Facts, 2022. Available from: https://www.who.int/news-room/fact-sheets/detail/dementia [Last accessed on 2022 Dec 30].

4. Selkoe DJ, 2011, Alzheimer's disease. *Cold Spring Harb Perspect Biol*, 3: a004457.

   https://doi.org/10.1101/cshperspect.a004457

5. Trambauer J, Fukumori A, Steiner H, 2020, Pathogenic Aβ generation in familial Alzheimer's disease: Novel mechanistic insights and therapeutic implications. *Curr Opin Neurobiol*, 61: 73–81.

   https://doi.org/10.1016/j.conb.2020.01.011

6. Marechal L, Campion D, Hannequin D, 2020, Familial forms of Alzheimer's disease. *Presse Med*, 32: 756–763.

7. Hoogmartens J, Cacace R, Van Broeckhoven C, 2021, Insight into the genetic etiology of Alzheimer's disease: A comprehensive review of the role of rare variants. *Alzheimers Dement* (*Amst*), 13: e12155.

   https://doi.org/10.1002/dad2.12155

8. Jayne T, Newman M, Verdile G, *et al.*, 2016, Evidence for and against a pathogenic role of reduced γ- secretase activity in familial Alzheimer's disease. *J Alzheimers Dis*, 52: 781–799.

   https://doi.org/10.3233/JAD-151186

9. Patterson C, Feightner JW, Garcia A, *et al.*, 2008, Diagnosis and treatment of dementia: 1. Risk assessment and primary prevention of Alzheimer disease. *CMAJ*, 178: 548–556.

   https://doi.org/10.1503/cmaj.070796

10. Li NM, Liu KF, Qiu YJ, *et al.*, 2019, Mutations of beta-amyloid precursor protein alter the consequence of Alzheimer's disease pathogenesis. *Neural Regen Res*, 14: 658–665.

    https://doi.org/10.4103/1673-5374.247469

11. Cai Y, An SSA, Kim S, 2015, Mutations in presenilin 2 and its implications in Alzheimer's disease and other dementia-associated disorders. *Clin Interv Aging*, 10: 1163–1172.

    https://doi.org/10.2147/CIA.S85808

12. Shea Y, Chu L, Chan A, *et al.*, 2016, A systematic review of familial Alzheimer's disease: Differences in presentation of clinical features among three mutated genes and potential ethnic differences. *J Formos Med Assoc*, 115: 67–75.

    https://doi.org/10.1016/j.jfma.2015.08.004

13. Kasuga K, Kikuchi M, Tokutake T, *et al.*, 2015, Systematic review and meta-analysis of Japanese familial Alzheimer's disease and ftdp-17. *J Hum Genet*, 60: 281–283.

    https://doi.org/10.1038/jhg.2015.15

14. Ryan N, Rossor M, 2010, Correlating familial Alzheimer's disease gene mutations with clinical phenotype. *Biomark Med*, 4: 99–112.

    https://doi.org/10.2217/bmm.09.92

15. Zou Z, Liu C, Che C, 2014, Clinical genetics of Alzheimer's

disease. *Biomed Res Int*, 2014: 291862.

16. Wu L, Rosa-Neto P, Hsiung GYR, *et al.,* 2014, Early-onset familial Alzheimer's disease (EOFAD). *Can J Neurol Sci*, 39: 436–445.

    https://doi.org/10.1017/s0317167100013949

17. Kutoku Y, Ohsawa Y, Kuwano R, *et al.*, 2015, A second pedigree with amyloid-less familial Alzheimer's disease harboring an identical mutation in the amyloid precursor protein gene (E693delta). *Intern Med*, 54: 205–208.

    https://doi.org/10.2169/internalmedicine.54.3021

18. Tomiyama T, Shimada H, 2020, APP Osaka mutation in familial Alzheimer's disease-its discovery, phenotypes, and mechanism of recessive inheritance. *Int J Mol Sci*, 21: 1413.

    https://doi.org/10.3390/ijms21041413

19. Kowalska A, 2004, Genetic counseling and testing for families with Alzheimer's disease. *Neurol Neurochir Pol*, 6: 495–501.

20. UniProt Consortium, 2021, Uniprot: The universal protein knowledgebase in 2021. *Nucleic Acids Res*, 49: D480–D489.

    https://doi.org/10.1093/nar/gkaa1100

21. Mutations: APP, 1996-2022, 2022. Available from: https://www.alzforum.org/mutations/app [Last accessed on 2023 Mar 30].

22. Duvaud S, Gabella C, Lisacek F, *et al.*, 2005, Protein identification and analysis tools on the expasy server. In: Walker JM, (ed). The Proteomics Protocols Handbook. United States: Humana Press, p571–607.

23. Roy A, Kucukural A, Zhang Y, 2010, I-TASSER: A unified platform for automated protein structure and function prediction. *Nat Protoc*, 5: 725–738.

    https://doi.org/10.1038/nprot.2010.5

24. Yang J, Yan R, Roy A, *et al.*, 2015, The I-TASSER suite: Protein structure and function prediction. *Nat Methods*, 12: 7–8.

    https://doi.org/10.1038/nmeth.3213

25. Zhang Y, 2008, I-TASSER server for protein 3D structure prediction. *BMC Bioinformtics*, 9: 40.

    https://doi.org/10.1186/1471-2105-9-40

26. Heo L, Park H, Seok C, 2013, Galaxyrefine: Protein structure refinement driven by side-chain repacking. *Nucleic Acids Res*, 41: W384–W388.

    https://doi.org/10.1093/nar/gkt458

27. Lee GR, Heo L, Seok C, 2016, Effective protein model structure refinement by loop modeling and overall relaxation. *Proteins*, 84: 294–301.

    https://doi.org/10.1002/prot.24858

28. Laskowski R, Chistyakov V, 2013, PDBsum. European Bioinformatics Institute. Available from: https://www.ebi.ac.uk/thornton-srv/databases/cgi-bin/pdbsum [Last accessed on 2022 Dec 30].

29. Bowie JU, Lüthy R, Eisenberg D, 1991, A method to identify protein sequences that fold into a known three-dimensional structure. *Science*, 253: 164–170.

    https://doi.org/10.1126/science.1853201

30. Lüthy R, Bowie JU, Eisenberg D, 1992, Assessment of protein models with three-dimensional profiles. *Nature*, 356: 83–85.

    https://doi.org/10.1038/356083a0

31. Colovos C, Yeates TO, 1993, Verification of protein structures: Patterns of nonbonded atomic interactions. *Protein Sci*, 2: 1511–1519.

    https://doi.org/10.1002/pro.5560020916

32. Sippl MJ, 1993, Recognition of errors in three-dimensional structures of proteins. (ProSA). *Proteins*, 17: 355–362.

    https://doi.org/10.1002/prot.340170404

33. Wiederstein M, Sippl MJ, 2007, ProSA-web: Interactive web service for the recognition of errors in three-dimensional structures of proteins. *Nucleic Acids Res*, 35: 407–410.

34. DeLano WL, 2002, Pymol: An open-source molecular graphics tool. *CCP4 Newsl Protein Crystallogr*, 40: 82–92.

35. Nielsen M, Lundegaard C, Worning P, *et al.,* 2003, Reliable prediction of T-cell epitopes using neural networks with novel sequence representations. *Protein Sci*, 12: 1007–1017.

    https://doi.org/10.1110/ps.0239403

36. Ponomarenko J, Bui H, Li W, *et al.*, 2008. Ellipro: A new structure-based tool for the prediction of antibody epitopes. *BMC Bioinformatics*, 9: 514.

    https://doi.org/10.1186/1471-2105-9-514

37. Vita R, Mahajan S, Overton J, *et al.*, 2018, The immune epitope database (IEDB): 2018 update. *Nucleic Acids Res*, 47: D339–D343.

    https://doi.org/10.1093/nar/gky1006

38. Jespersen MC, Peters B, Nielsen M, *et al.*, 2017, Bepipred-2.0: Improving sequence-based B-cell epitope prediction using conformational epitopes. *Nucleic Acids Res*, 45: W24–W29.

    https://doi.org/10.1093/nar/gkx346

39. Gupta S, Kapoor P, Chaudhary K, *et al.*, 2013, *In silico* approach for predicting toxicity of peptides and proteins. *PLoS One*, 8: e73957.

    https://doi.org/10.1371/journal.pone.0073957

40. Gupta S, Kapoor P, Chaudhary K, *et al.*, 2015, Peptide toxicity prediction. *Methods Mol Biol*, 1268: 143–157.

    https://doi.org/10.1007/978-1-4939-2285-7_7

41. Lanoiselée HM, Nicolas G, Wallon D, *et al.*, 2017, APP, PSEN1, and PSEN2 mutations in early-onset Alzheimer disease: A genetic screening study of familial and sporadic

cases. *PLoS Med*, 14: e1002270.

https://doi.org/10.1371/journal.pmed.1002270

42. Yoshikai S, Sasaki H, Doh-Ura K, *et al.*, 1990, Genomic organization of the human amyloid beta-protein precursor gene. *Gene*, 87: 257–263.

https://doi.org/10.1016/0378-1119(90)90310-n

43. Levy E, Carman MD, Fernandez-Madrid IJ, *et al.*, 1990, Mutation of the Alzheimer's disease amyloid gene in hereditary cerebral hemorrhage, Dutch type. *Science*, 248: 1124–1126.

https://doi.org/10.1126/science.2111584

44. Wisniewski T, Ghiso J, Frangione B, 1991, Peptides homologous to the amyloid protein of Alzheimer's disease containing a glutamine for glutamic acid substitution have accelerated amyloid fibril formation. *Biochem Biophys Res Commun*, 179: 1247–1254.

https://doi.org/10.1016/0006-291x(91)91706-i

45. Haass C, Hung AY, Selkoe DJ, *et al.*, 1994, Mutations associated with a locus for familial Alzheimer's disease result in alternative processing of amyloid beta-protein precursor. *J Biol Chem*, 269: 17741–17748.

46. Rocchi A, Pellegrini S, Siciliano G, *et al.*, 2003, Causative and susceptibility genes for Alzheimer's disease: A review. *Brain Res Bull*, 61: 1–24.

https://doi.org/10.1016/s0361-9230(03)00067-4

47. Kumar-Singh S, Cras P, Wang R, *et al.*, 2002, Dense-core senile plaques in the Flemish variant of Alzheimer's disease are vasocentric. *Am J Pathol*, 161: 507–520.

https://doi.org/10.1016/S0002-9440(10)64207-1

48. Castellani RJ, Honda K, Zhu X, *et al.*, 2004, Contribution of redox-active iron and copper to oxidative damage in Alzheimer disease. *Ageing Res Rev*, 3: 319–326.

https://doi.org/10.1016/j.arr.2004.01.002

49. Ryan NS, Biessels GJ, Kim L, *et al.*, 2015, Genetic determinants of white matter hyperintensities and amyloid angiopathy in familial Alzheimer's disease. *Neurobiol Aging*, 36: 3140–3151.

https://doi.org/10.1016/j.neurobiolaging.2015.08.026

50. Ryan NS, Nicholas JM, Weston PS, *et al.*, 2016, Clinical phenotype and genetic associations in autosomal dominant familial Alzheimer's disease: A case series. *Lancet Neurol*, 15: 1326–1335.

https://doi.org/10.1016/S1474-4422(16)30193-4

51. Żekanowski C, Styczyńska M, Pepłońska B, *et al.*, 2003, Mutations in presenilin 1, presenilin 2 and amyloid precursor protein genes in patients with early-onset Alzheimer's disease in Poland. *Exp Neurol*, 184: 991–996.

https://doi.org/10.1016/S0014-4886(03)00384-4

52. Lindquist SG, Nielsen JE, Stokholm J, *et al.*, 2008, Atypical early-onset Alzheimer's disease caused by the Iranian APP mutation. *J Neurol Sci*, 268: 124–130.

https://doi.org/10.1016/j.jns.2007.11.021

53. Edwards-Lee T, Ringman JM, Chung J, *et al.*, 2005, An African American family with early-onset Alzheimer disease and an APP (T714I) mutation. *Neurology*, 64: 377–379.

https://doi.org/10.1212/01.WNL.0000149761.70566.3E

54. Valerija D, Stefanova E, Jankovic M, *et al.*, 2012, Genetic testing in familial and young-onset Alzheimer's disease: Mutation spectrum in a serbian cohort. *Neurobiol Aging*, 33: 1481.e7–e12.

https://doi.org/10.1016/j.neurobiolaging.2011.12.007

55. Guerreiro RJ, Baquero M, Blesa R, *et al.*, 2010, Genetic screening of Alzheimer's disease genes in Iberian and African samples yields novel mutations in presenilins and APP. *Neurobiol Aging*, 31: 725–731.

https://doi.org/10.1016/j.neurobiolaging.2008.06.012

56. Wang Q, Jia J, Qin W, *et al.*, 2015, A novel AβPP M722K mutation affects amyloid-β secretion and Tau phosphorylation and may cause early-onset familial Alzheimer's disease in Chinese individuals. *J Alzheimers Dis*, 47: 157–165.

https://doi.org/10.3233/JAD-143231

57. Larner AJ, 2013, Presenilin-1 mutations in Alzheimer's disease: An update on genotype-phenotype relationships. *J Alzheimers Dis*, 47: 653–659.

https://doi.org/10.3233/JAD-130746

58. Canevelli M, Piscopo P, Talarico G, *et al.*, 2014, Familial Alzheimer's disease sustained by presenilin 2 mutations: Systematic review of literature and genotype-phenotype correlation. *Neurosci Behav Rev*, 42: 170–179.

https://doi.org/10.1016/j.neubiorev.2014.02.010

59. Mehrgou A, Akouchekian M, 2016, The importance of BRCA1 and BRCA2 genes mutations in breast cancer development. *Med J Islam Repub Iran*, 30: 369.

60. Gayther S, Warren W, Mazoyer S, *et al.*, 1995, Germline mutations of the BRCA1 gene in breast and ovarian cancer families provide evidence for a genotype-phenotype correlation. *Nat Genet*, 11: 428–433.

https://doi.org/10.1038/ng1295-428

61. Linger RJ, Kruk PA, 2010, BRCA1 16 years later: Risk-associated BRCA1 mutations and their functional implications. *FEBS J*, 277: 3086–3096.

https://doi.org/10.1111/j.1742-4658.2010.07735.x

62. Hunter JC, Manandhar A, Carrasco MA, *et al.*, 2015, Biochemical and structural analysis of common cancer-associated KRAS mutations. *Mol Cancer Res*, 13: 1325–1335.

https://doi.org/10.1158/1541-7786.MCR-15-0203

ACCSCIENCE PUBLISHING

Advanced Neurology

ORIGINAL RESEARCH ARTICLE

Fried-Breadstick sign: A novel marker for healthy vasculature in magnetic resonance angiography

Yannan Yu[1,2], Yu-Yuan Xu[1], Xue Man[1], Ming-Li Li[3], Bo Hou[3], Shan Gao[1], Feng Feng[3], David S Liebeskind[2], and Wei-Hai Xu[1]*

[1]Department of Neurology, State Key Laboratory of Complex Severe and Rare Disease, Peking Union Medical College Hospital, Chinese Academy of Medical Sciences and Peking Union Medical College, Beijing, China

[2]Neurovascular Imaging Research Core and UCLA Stroke Center, Los Angeles, California, USA

[3]Department of Radiology, Peking Union Medical College Hospital, Chinese Academy of Medical Sciences and Peking Union Medical College, Beijing, China

Abstract

The Fried-Breadstick sign is characterized as a continuous signal loss at the center of the intracranial internal carotid artery (ICA) on time-of-flight magnetic resonance angiography (TOF-MRA). In this study, we present a novel imaging marker on TOF-MRA and investigate its potential association with ICA-middle cerebral artery (ICA-MCA) atherosclerosis and ischemic stroke. Vessel wall magnetic resonance imaging data were obtained from patients with recent clinical stroke or asymptomatic patients with suspected middle cerebral artery (MCA) atherosclerosis, covering the period from January 2007 to August 2015. We conducted a comparative analysis of ICA stenosis, MCA atherosclerosis and stenosis degree, and the terminal ICA bifurcation angle between ICA-MCAs with and without the Fried-Breadstick sign, involving a total of 1,005 ICA-MCAs from 553 patients. The Fried-Breadstick sign exhibited a higher prevalence in non-to-mild stenotic ICAs (57.5% vs. 9.8% in severely stenotic ICA, $P < 0.001$) and plaque-free MCAs (53.2% vs. 26.6% in MCAs with plaque, $P < 0.001$). Factors independently associated with the presence of the Fried-Breadstick sign included MCA stenosis degree (odds ratio [OR]: 0.85/10% increase, 95% confidence interval [CI]: 0.80 – 0.90), ICA stenosis (compared to non-to-mild stenosis, moderate stenosis: OR: 0.39, 95% CI: 0.28 – 0.54, severe stenosis: OR: 0.10, 95% CI: 0.06 – 0.17), and terminal ICA bifurcation angle (OR: 0.86/10° increase, 95% CI: 0.79 – 0.93). In atherosclerotic MCAs without luminal narrowing, the Fried-Breadstick sign was also less frequently observed than in plaque-free MCAs (34.6% vs. 53.2%, $P = 0.012$). In conclusion, the presence of the Fried-Breadstick sign is associated with healthier ICA-MCAs devoid of stenosis or plaque. The Fried-Breadstick sign may signify healthy ICA-MCA hemodynamics, serving as a potential screening tool for intracranial atherosclerosis without incurring additional cost or risk.

Keywords: Intracranial atherosclerosis; Middle cerebral artery; Hemodynamics; Vessel wall magnetic resonance imaging; Magnetic resonance angiography

***Corresponding Author:**
Wei-Hai Xu
(xuwh@pumch.cn)

Citation: Yu Y, Li M, Gao S, *et al.*, 2023, Fried-Breadstick sign: A novel marker for healthy vasculature in magnetic resonance angiography. *Adv Neuro,* 2(4): 1238. https://doi.org/10.36922/an.1238

Received: July 4, 2023

Accepted: November 28, 2023

Published Online: December 21, 2023

1. Introduction

Intracranial atherosclerotic disease (ICAD) stands as a significant contributor to stroke globally, particularly among patients with Asian, Hispanic, and African ancestry[1]. Recent studies have underscored the pivotal role of hemodynamic characteristics, alongside systemic risk factors, in the pathophysiology of ICAD[2,3]. Within a regularly shaped, healthy artery, blood flow typically manifests as either parabolic laminar flow, with maximal flow velocity at the center[4], or spiral laminar flow, characterized by relatively low velocity at the rotational axis[5,6]. Plaque tends to develop in regions where laminar flow is disrupted, such as arterial bifurcations and curvatures[7-9].

Signal loss in the center of intracranial and extracranial internal carotid arteries on time-of-flight magnetic resonance angiography (TOF-MRA) is a common occurrence and is typically considered an artifact[10]. Bradley *et al.* have proposed that this signal loss is secondary to a centered high flow velocity producing a parabolic laminar flow beyond the maximum flow-related enhancement[11]. Alternative speculations include the possibility of a truncation artifact[10] or the presence of two streams of laminar flow[12]. This phenomenon has raised our interest in its prevalence and its potential association with ICAD and strokes. Therefore, our investigation aimed to determine the prevalence and associated factors of this phenomenon in both ICAD patients and a healthy population. We hypothesized that the central signal loss in the intracranial internal carotid artery (ICA) is indicative of a healthy intracranial vasculature. Descriptively, due to its resemblance to a traditional Chinese food item known as the Fried-Breadstick (FB, Figure 1A and B) on maximum intensity projection (MIP) images, we have termed it the FB sign.

2. Materials and methods

2.1. Patients

We conducted a comprehensive review of prospectively collected data from vessel wall magnetic resonance imaging (MRI) at our institution, spanning from January 2007 to August 2015. Individuals were eligible for inclusion in this study if they met one of the following criteria: (i) exhibited middle cerebral artery (MCA) atherosclerosis and experienced an acute first-ever stroke in the MCA territory, as confirmed by diffusion-weighted imaging (DWI); (ii) demonstrated MCA atherosclerosis without a history of clinical stroke or transient ischemic attacks (TIA); and (iii) displayed no MCA atherosclerosis and had no history of clinical stroke or TIA. Exclusion criteria encompassed evidence of cardioembolism, extracranial carotid atherosclerosis (>50% stenosis) assessed through carotid ultrasound, or non-atherosclerotic stenosis (moyamoya disease, radiation-induced vasculopathy, infection, dissection, or autoimmune disease). Each patient's bilateral MCAs were subject to analysis, with exclusion criteria applied in instances where MRI quality was inadequate for analysis, imaging data were unavailable, or the M1 segment was occluded.

2.2. Ethics approval and consent

The study protocol was approved by the ethics committee of the Peking Union Medical College Hospital (JS-3479D). Before participation, written consent was obtained from all patients or their families.

2.3. The protocol of MRI

The comprehensive vessel wall MRI imaging protocol, as previously described[13,14], was employed in this study. Patients were imaged using a 3-tesla (3T) magnetic resonance scanner (Signa VH/I, GE Medical Systems, USA, from January 2007 to June 2013; GE Discovery MR750, GE Medical Systems, USA, from June 2013 to August 2015) equipped with a standard 8-channel head coil. The imaging protocol comprised conventional 3-dimensional (3D) TOF-MRA, DWI, and T1- and T2-weighted vessel wall imaging of the MCA. From the period of January 2007 to June 2013, the parameters for 3D TOF-MRA were as follows: repetition time/echo time (TR/TE), 19 – 27 ms/2.7 – 3.3 ms; flip angle, 20°; field-of-view (FOV), 24 cm × 16 cm; matrix size, 320 × 256; slice thickness, 1.6 mm; slab thickness, 8.5 cm; 1 signal average; and scan time, 4 min. Subsequently, a 2D T2-weighted vessel wall MRI was acquired perpendicular to the long axis of the M1 segment of the MCA following 3D TOF-MRA. The parameters for this acquisition were TR/TE, 3000 ms/50 ms; FOV, 13 cm × 13 cm; matrix size, 256 × 256; slice thickness, 2 mm; and 4 signal averages. From June 2013 to August 2015, the 3D TOF-MRA was obtained with the following parameters: TR/TE, 16~22/2.1~2.7ms; flip angle, 20°; FOV, 20 cm × 18 cm; matrix size, 320 × 288; slice thickness, 1.2 mm; slab thickness 10 cm; 1 signal averages; and scan time 5 min. 2D T2-weighted vessel wall MRI was obtained using TR/TE, 4200/60 ms; FOV, 13 × 13 cm; matrix size, 256 × 256; slice thickness, 2 mm; and 4 signal averages. MIP images were reconstructed in axial and coronal planes with a rotation angle interval of 10° or 15°.

2.4. Imaging analysis

Imaging data were analyzed by two independent evaluators who were blinded to clinical information. To evaluate

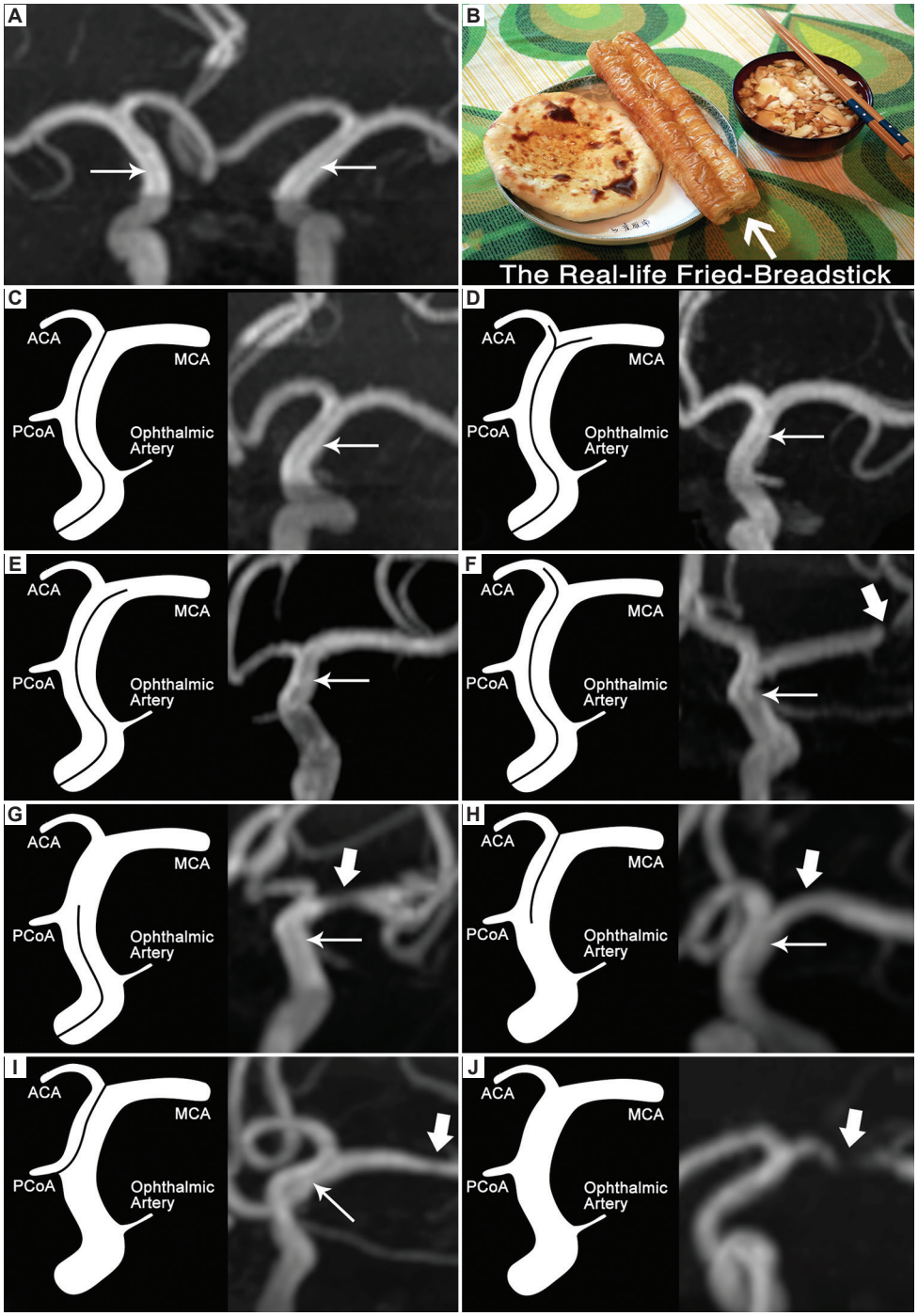

Figure 1. The examples of Fried-Breadstick signs. (A) The Fried-Breadstick sign (arrows) is shown on MIP images. (B) The real-life Fried-Breadstick. (C-E) Normal fried-breadstick signs: A continuous longitudinal line of signal loss at the center of the ICA lumen from C6 to C7 segments, which can extend to MCA. (F-I) Abnormal fried-breadstick signs: The signal loss extends to ACA (F) and only exists in the C6 segment (G) or C7 segment (H-I). (J) The absence of Fried-Breadstick sign: no signal loss at all. The black lines in the artery illustrations and the thin arrows on MIP images (C-I) indicate the signal loss in ICA. The thick arrows (F-J) indicate the MCA stenosis.
Abbreviations: ACA: Anterior cerebral artery; ICA: Internal carotid artery; MCA: Middle cerebral artery; MIP: Maximum intensity projection; PCoA: Posterior communicating artery.

intraobserver agreement, one of the readers repeated the image analysis 1 month after the first analysis. The inter-observer and intra-observer agreement of the FB sign was assessed using kappa (κ) statistics[15].

2.4.1. Fried-Breadstick sign

On MIP TOF-MRA images, the presence of the FB sign was defined as a continuous longitudinal line of signal loss[12,16] at the center of the intracranial ICA lumen, specifically from the C6 to C7 segments as per Bouthillier classification[17] (Figure 1C-E). An abnormal FB sign (Figure 1F-I) was identified when the signal loss was interrupted or only extended to the anterior cerebral artery (ACA). The absence of the FB sign was determined if there was no signal loss at the center of the ICA.

2.4.2. ICA stenosis

The ICA stenosis was classified as non-to-mild stenosis (≤50%), moderate stenosis (50 – 70%), and severe stenosis (≥70%) on the MIP MRA images, calculated as 100% × (1 - narrowest ICA segment diameter/reference ICA segment diameter). The degree of MCA stenosis was assessed at the site of maximal luminal narrowing with plaque presence on T2-weighted vessel wall images. Reference sites were the plaque-free sites proximal and distal to the site of maximal narrowing (with the average area used for analysis). In cases where plaque involved the entire M1 segment, the plaque-free counterpart of the contralateral artery served as the reference site[18]. The formula for MCA stenosis degree was expressed as 100% × (1 - luminal area at the maximal luminal narrowing site/reference luminal area).

2.4.3. Terminal ICA bifurcation

Anatomy factors, such as bifurcation angle, influence hemodynamics and the development of atherosclerosis[19,20]. In this study, the bifurcation angle was measured for each ICA bifurcation on MIP MRA images, excluding those without the origin of ACA. The plane where the initial segments of MCA and ACA overlap was first identified on MIP images. Subsequently, the image was rotated 90° to the MCA-ACA plane, and the bifurcation angle was manually measured (Figure 2).

2.4.4. MCA atherosclerosis

A plaque was identified as eccentric vessel wall thickening in which the thinnest wall thickness was <50% of the thickest wall thickness, as determined by visual inspection[21]. Each patient's MCAs were analyzed individually. MCAs were classified as atherosclerotic if the plague was observed in the M1 segment on vessel wall MRI or as plaque-free if no plaque was detected and there was no history of strokes or TIA.

Each MCA territory was further classified into 4 groups: asymptomatic (no history of stroke or TIA), small single subcortical infarct (SSI, a single regular-shaped infarct in the perforator territory of the MCA with a diameter ≤20 mm[22]), large SSI (a single regular-shaped infarct within the MCA perforator territory with a diameter >20 mm), and non-SSI (with ≥1 cortical or ≥2 subcortical stroke lesions[23]).

2.5. Statistical analysis

Inter-observer and intra-observer agreement were assessed using Cohen's κ coefficient and intraclass correlation coefficient. Continuous variables were analyzed with Student's *t*-test or Mann–Whitney *U*-test, while binary variables were assessed using the χ^2 test or Fisher's exact test. The Bonferroni method was applied to adjust the significance level in pairwise comparison among subgroups. Logistic regression was performed to identify independent factors for the presence of the FB sign and to provide an explanation for this phenomenon. Multinomial logistic regression was performed to determine if the FB sign is an independent factor for different stroke patterns. A 10% change in MCA stenosis degree and a 10° alteration in bifurcation angle were considered as one unit in the

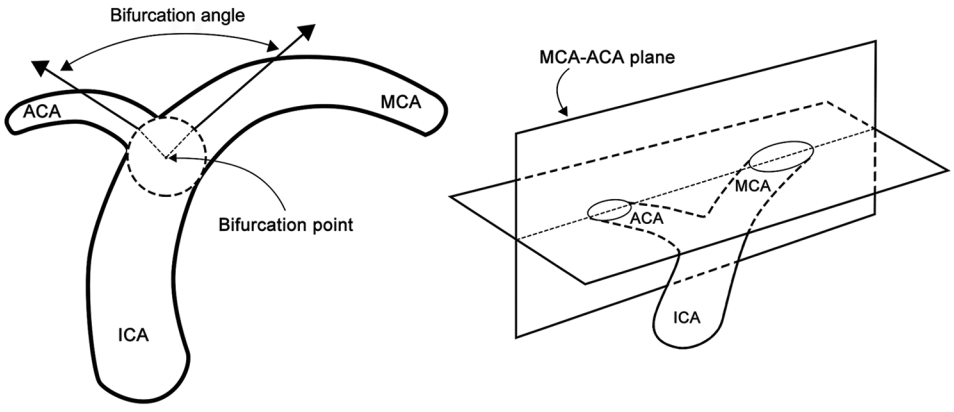

Figure 2. Bifurcation angle measurement. The bifurcation angle is measured on the MCA-ACA plane, as illustrated here. Abbreviations: ACA: Anterior cerebral artery; ICA: Internal carotid artery; MCA: Middle cerebral artery.

logistic regression analysis for OR evaluation. A $P < 0.05$ was considered statistically significant for all tests, and they were all two-sided.

3. Results

3.1. Demographic characteristics

Among 1538 patients in our database, 553 met the inclusion criteria, comprising 137 with a recent stroke in the MCA territory and 416 without a history of stroke or TIA (Table 1). The FB sign and ICA-MCAs were assessed bilaterally for each patient. We excluded 101 MCAs due to occlusions, poor image quality, or a lack of vessel wall images. Ultimately, 1005 ICA-MCAs were included in the analysis (Table 2).

3.2. Inter and intraobserver agreement

The interobserver and intraobserver agreements for identifying the FB sign were 0.692 (95% CI: 0.544 – 0.841) and 0.825 (95% CI: 0.699 – 0.951), respectively. Additionally, the agreements for measuring luminal area were 0.919 (95% CI: 0.845 – 0.958) and 0.933 (95% CI: 0.872 – 0.96).

Table 1. Demographic and clinical data of patients (subjects) with and without stroke

Demographic and clinical characteristic	Patients with stroke (*n*=137)	Patients without stroke (*n*=416)	*P*-value
Male (*n* [%])	104 (75.9)	249 (59.0)	0.001
Age (x±SD years)	57±15	58±15	0.833
Hypertension (*n* [%])	82 (59.9)	245 (58.9)	0.843
Dyslipidemia (*n* [%])	59 (43.1)	196 (47.1)	0.410
Diabetes (*n* [%])	32 (23.4)	74 (17.8)	0.151
Current smoker (*n* [%])	54 (39.4)	136 (32.6)	0.151
Coronary artery disease (*n* [%])	17 (12.5)	37 (8.9)	0.219

Table 2. Distribution of ICA stenosis and atherosclerotic MCA

ICA stenosis	Atherosclerotic MCA		*P*-value
	Plaque-free MCA (*n*=429)	Atherosclerotic MCA (*n*=576)	
Non-to-mild ICA stenosis (*n* [%])	259 (60.4)	197 (34.2)	<0.001
Moderate ICA stenosis (*n* [%])	118 (27.5)	186 (32.3)	N/A
Severe ICA stenosis (*n* [%])	52 (12.1)	193 (33.5)	N/A

Abbreviations: ICA: Internal carotid artery; MCA: Middle cerebral artery.

3.3. Relationship between the Fried-Breadstick sign and intracranial atherosclerosis

The FB sign occurred more frequently in non-to-mild stenotic ICAs (57.5% vs. 31.6% vs. 9.8%, $P < 0.001$) compared to moderately and severely stenotic ICAs. The prevalence of the FB sign decreased as the ICA-MCA stenosis degree increased (Figure 3). Moreover, the FB sign was more prevalent in plaque-free MCAs (53.2% vs. 26.6%, $P < 0.001$) than in atherosclerotic MCAs. The FB sign exhibited a sensitivity of 53% and a specificity of 73% for identifying plaque-free MCAs. Additionally, in atherosclerotic MCAs without narrowing lumen (with plaque detected on vessel wall MRI), the FB sign occurred less frequently than in plaque-free MCAs (34.6% vs. 53.2%, $P = 0.012$).

After adjustment for whether the new MRI protocol was used, factors independently associated with the presence of the FB sign included MCA stenosis degree (OR: 0.85/10% increase, 95% CI: 0.80 – 0.90), ICA stenosis (compared to non-to-mild stenosis, moderate stenosis: OR: 0.39, 95% CI: 0.28 – 0.54, severe stenosis: OR: 0.10, 95% CI: 0.06 – 0.17), and bifurcation angle (OR: 0.86/10° increase, 95% CI: 0.79 – 0.93) (Table 3). The probability of the FB sign at different ICA and MCA stenosis degrees is plotted in Figure S1. The results remain consistent with the analysis in separate patient groups scanned with the 2 MRA protocols in the study period (Table S1).

3.4. Relationship between stroke patterns and the Fried-Breadstick sign

The FB sign occurred most frequently in small SSI (43.6%) compared with large SSI (37.5%, $P = 0.6$), non-SSI (16.4%, $P = 0.003$), and asymptomatic MCAs (25.9%, $P = 0.017$) (Figure 3). The FB sign had a sensitivity of 44% and a specificity of 74% for identifying small SSI in symptomatic patients. ICA-MCAs with small SSI also showed a significantly lower MCA stenosis degree (23%, interquartile range [IQR]: 6 – 41%) compared with large SSI (37%, IQR: 22 – 65%, $P = 0.02$), non-SSI (62%, IQR: 45 – 79%, $P < 0.001$), and asymptomatic MCAs (35%, IQR: 18 – 55%, $P = 0.008$). After adjusting for MCA stenosis degree and ICA stenosis, the FB sign is independently associated with small SSI (relative risk ratio: 5.35, 95% CI: 1.48 – 19.33) but not large SSI (relative risk ratio: 2.36, 95% CI: 0.66 – 8.44) when compared to non-SSIs. The ICA stenosis was not significantly different among different infarct patterns.

4. Discussion

This study explored the prevalence of the FB sign in a large sample of patients with ICAD and healthy intracranial

Table 3. Univariate and multivariate analysis of the FB sign

Variable	Univariate analysis			Multivariate analysis	
	Presence of FB sign (*n*=381)	Absent or abnormal FB sign (*n*=624)	*P*-value	OR (95% CI)	*P*-value
Moderate ICA stenosis (*n* [%])	96 (25.1)	208 (33.4)	<0.001*	0.39 (0.28 – 0.54)	<0.001*
Severe ICA stenosis (*n* [%])	24 (6.3)	221 (35.5)		0.10 (0.06 – 0.17)	<0.001*
MCA Stenosis degree (median % [IQR])	0 (0, 23)	20 (0, 49)	0.010*	0.85 (0.80 – 0.90)	<0.001*
Bifurcation angle, (x±SD degree [°])	96±18	102±22	<0.001*	0.86 (0.79 – 0.93)	<0.001*

Note: *P<0.05. Abbreviations: CI: Confidence interval; FB: Fried-breadstick; ICA: Internal carotid artery; IQR: Interquartile range; MCA: Middle cerebral artery; OR: Odds ratio; SD: Standard deviation.

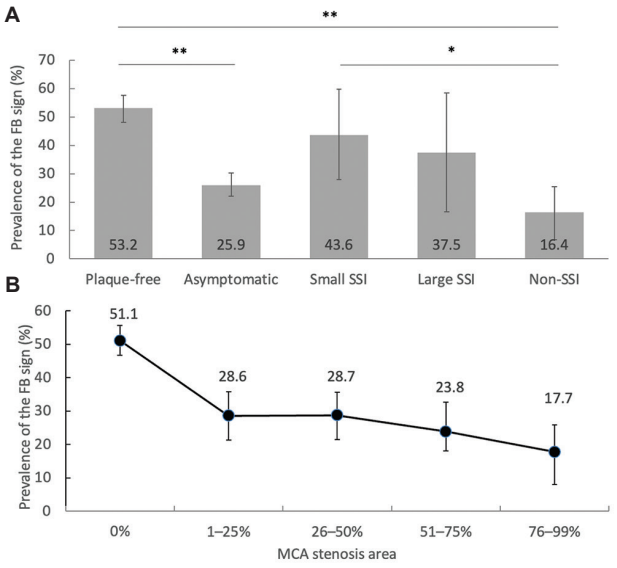

Figure 3. The prevalence of the Fried-Breadstick sign in different groups and MCA stenosis. (A) The FB sign is most frequently present in plaque-free MCAs and least frequently in MCAs with non-SSI. *P < 0.005, **P < 0.001. (B) The FB sign prevalence decreases as the MCA stenosis degree increases. To note, the MCA stenosis is measured in terms of area stenosis (refer to Figure S2) for the prevalence change of the Fried-Breadstick sign concerning MCA diameter stenosis. The error bar represents the 95% confidence interval.
Abbreviations: FB: Fried-breadstick; MCA: Middle cerebral artery; SSI: Single subcortical infarct.

vasculatures. Additionally, it investigated the relationship between the presence of the FB sign and ICAD. We observed that the FB sign is more frequently present in plaque-free MCAs or in cases of low-grade ICA-MCA stenosis compared to high-grade ICA-MCA stenosis. Even in atherosclerotic MCAs without luminal narrowing, the FB sign was less frequently presented than in plaque-free MCAs, suggesting the absent or abnormal FB sign is associated with atherosclerosis. These results support our hypothesis that the FB sign is associated with a relatively healthy ICA-MCA vasculature without severe atherosclerosis. Since the FB sign can be easily identified and assessed on routine TOF-MRA, it holds promise for stratifying stroke risk in patients with intracranial atherosclerosis in future trials, with no additional costs or risks.

The underlying mechanisms of the FB sign are intricate and remain unclear. TOF-MRA is a gradient echo sequence based on the flow-related enhancement theory[16]. The signal intensity of the intracranial arteries on TOF-MRA is associated with flow velocities in the vessel lumen. Both high velocity and low velocity of blood flow, or in-plane blood flow, could cause signal loss[24,25]. Saloner *et al.*[26] investigated central signal loss with computational fluid dynamics, phantom, and healthy volunteers. They simulated parabolic laminar flow and demonstrated that slow peripheral laminar flow formed a counter-rotating secondary flow when entering a curved vessel, leading to central intraluminal signal loss from saturation of the spin magnetization[26]. The study supported the idea that the combination of parabolic laminar flow and ICA curvature contributed to the signal loss, which matched our observation. Since other flow types were not simulated in the above-mentioned study, another possible explanation for the central signal loss is the spiral laminar flow. Spiral laminar flow demonstrates a relatively low velocity or in-plane blood flow in the rotational axis and high velocity around the rotational axis[5]. The spiral laminar flow is created by the rotational compressive pumping of the heart and maintained by the multi-planar tapered, curved, and branching arterial geometry[5,27]. Mostly seen in large arteries, including ICAs[6,28], the spiral flow contributes to the relatively uniform wall shear stress in the bifurcation region[29], flow stabilization, and the suppression of flow disturbance and stagnation[30]. The loss of spiral laminar flow has been reported to be associated with the presence and progression of atherosclerotic diseases[27]. Although turbulent flow was not simulated in curved vasculature in previous literature, it is unlikely for turbulent flow to manifest as a uniform central signal loss, given its complicated flow direction and speed. Turbulent flow can lead to dephasing artifacts in TOF-MRA[31,32], manifested as signal loss affecting both the central and peripheral of the vessel lumen.

Arterial bifurcations are the most frequent sites affected by atherosclerosis due to complex regional hemodynamics, a topic extensively studied in coronary and cervical carotid arteries but scarcely in intracranial arteries[19,33,34]. It is reasonable to speculate that intracranial arterial bifurcations, such as the terminal ICA bifurcation, share similar characteristics in hemodynamics and are prone to atherosclerosis, as evidenced by an autopsy study[35]. A smaller bifurcation angle is a geometric feature associated with less atherosclerotic burden[19,36] and positive effects on local hemodynamics[20]. This observation further supports the FB sign as a marker for healthy ICA-MCA vasculature, as its presence is independently associated with a smaller terminal ICA bifurcation angle.

TOF-MRA is a routine and non-invasive method for screening ICAD and guiding medical management, but it only detects secondary changes of atherosclerosis, such as luminal narrowing. Considering that the FB sign is more prevalent in plaque-free MCAs compared to atherosclerotic MCAs without luminal narrowing, the absence of the FB sign may provide additional value in identifying patients with early-stage atherosclerosis but without luminal narrowing. In such cases, further confirmation through vessel wall imaging or intervention with early prevention strategies may be warranted[37].

Diagnosing stroke etiology is critical for tailoring the treatment plan for stroke prevention. The FB sign exhibits a distinct distribution in stroke patterns, indicating its potential for distinguishing ICAD-related strokes from non-ICAD-related strokes. In strokes that are likely attributed to MCA atherosclerosis, the FB sign is more frequently observed in small SSI, typically associated with cerebral small vessels[38,39], and linked to fewer neurological deficits and lower recurrence rates[40,41]. The FB sign is least frequent in the non-SSI stroke pattern, often characterized by a territorial infarct, watershed infarct, and mixed infarct patterns. Non-SSI stroke patterns are considered associated with embolic mechanisms[23], involving disrupted laminar flow and the formation of turbulent flow in severely stenotic sites of atherosclerotic plaque, leading to subsequent plaque rupture[42]. The prevalence of the FB sign is intermediate for the large SSI stroke pattern, likely due to its mixed etiologies involving branch atheromatous disease[43], which is associated with large vessel atherosclerosis, and lipohyalinosis[44], which is indicative of small vessel disease. These findings contribute to a better understanding of the pathophysiology of stroke patterns and hemodynamic disruptions in ICAD patients.

Our study has several limitations that warrant consideration. Firstly, our study cohort was exclusively scanned with 3T GE scanners, and the findings may not be directly applicable to 1.5T scanners or those from other MRI manufacturers. Additionally, many patients included in the plaque-free group presented with multiple stroke risk factors, potentially leading to an underestimation of the FB sign's prevalence in the healthy population. The imaging modality used in this study did not visualize intracranial ICA plaque, and though we excluded extracranial carotid artery stenosis exceeding 50%, mild extracranial artery stenosis or other anatomical variation might have affected the blood flow in the ICA. Furthermore, we did not analyze the prevalence of the FB sign in other arteries or investigate the coexistence of other vascular abnormalities, such as ICA dolichoectasias or fenestrations. This study did not comprehensively analyze all possible geometric or plaque-related characteristics. Given the absence of *in vivo* data on intracranial hemodynamics related to the FB sign, our proposed mechanisms are speculative and based on previous theories. The classification of the FB sign may simplify the underlying continuous process. It is important to note that visualizing the FB sign requires good patient compliance during MRI scanning, and interpreting the FB sign in acute stroke patients should be approached with specific caution. Further investigations, ideally incorporating direct evidence from computational fluid dynamics, are warranted to verify our hypotheses.

5. Conclusion

The phenomenon of central signal loss in ICA is commonly considered an artifact observed on TOF-MRA images. However, this study delves into the association between central signal loss and intracranial atherosclerosis, revealing that central signal loss occurs more frequently in patients exhibiting healthy ICA-MCAs. Conversely, its occurrence is less frequent in patients with intracranial atherosclerosis, such as ICA or MCA stenosis. This preliminary investigation suggests that central signal loss in the ICA may serve as an imaging marker indicative of healthy ICA-MCA vasculature. To capture its visual resemblance to a traditional Chinese fried breadstick, we have aptly named this phenomenon the "Fried-Breadstick sign."

Acknowledgments

The authors thank all the participants who gave their time to the study.

Funding

This study is supported by the National Science Fund for Distinguished Young Scholars (82025013), the National Natural Science Foundation of China (81671370 and 81471207), and the National Key Technologies R&D Program of China (2017YFC1307902).

Conflict of Interest

The authors declare no conflict of interest.

Author contribution

Conceptualization: Yan-Nan Yu, Wei-Hai Xu
Data curation: Yu-Yuan Xu, Ming-Li Li, Bo Hou, Shan Gao, Feng Feng
Formal analysis: Xue Man, Yan-Nan Yu, Wei-Hai Xu
Investigation: Yan-Nan Yu, Wei-Hai Xu, Xue Man
Methodology: Yan-Nan Yu, Wei-Hai Xu
Writing – original draft: Yan-Nan Yu, Wei-Hai Xu
Writing – review & editing: Yan-Nan Yu, Wei-Hai Xu, David S Liebeskind

Ethics approval and consent to participate

The study protocol was approved by the ethics committee of the Peking Union Medical College Hospital (JS-3479D). Written consent was obtained from all patients or from the family members.

Consent for publication

Written consent was obtained from all patients or from the family members to publish their data.

Availability of data

Data used in this work is available from the corresponding author upon reasonable request.

References

1. Wong LK, 2006, Global burden of intracranial atherosclerosis. *Int J Stroke*, 1: 158–159.

   https://doi.org/10.1111/j.1747-4949.2006.00045.x

2. Wu C, Schnell S, Vakil P, *et al*., 2017, *In vivo* assessment of the impact of regional intracranial atherosclerotic lesions on brain arterial 3D hemodynamics. *AJNR Am J Neuroradiol*, 38: 515–522.

   https://doi.org/10.3174/ajnr.A5051

3. Pu Y, Lan L, Leng X, *et al*., 2017, Intracranial atherosclerosis: From anatomy to pathophysiology. *Int J Stroke*, 12: 236–245.

   https://doi.org/10.1177/1747493016685716

4. Chatzizisis YS, Coskun AU, Jonas M, *et al*., 2007, Role of endothelial shear stress in the natural history of coronary atherosclerosis and vascular remodeling: Molecular, cellular, and vascular behavior. *J Am Coll Cardiol*, 49: 2379–2393.

   https://doi.org/10.1016/j.jacc.2007.02.059

5. Kokkalis E, Aristokleous N, Houston JG, 2016, Haemodynamics and flow modification stents for peripheral arterial disease: A review. *Ann Biomed Eng*, 44: 466–476.

   https://doi.org/10.1007/s10439-015-1483-4

6. Stonebridge PA, Brophy CM, 1991, Spiral laminar flow in arteries? *Lancet*, 338: 1360–1361.

   https://doi.org/10.1016/0140-6736(91)92238-w

7. Van der Kolk AG, Zwanenburg JJ, Brundel M, *et al*, 2015, Distribution and natural course of intracranial vessel wall lesions in patients with ischemic stroke or TIA at 7.0 tesla MRI. *Eur Radiol*, 25: 1692–700.

   https://doi.org/10.1007/s00330-014-3564-4

8. Huang YN, Gao S, Li SW, *et al*., 1997, Vascular lesions in Chinese patients with transient ischemic attacks. *Neurology*, 48: 524–525.

   https://doi.org/10.1212/wnl.48.2.524

9. Yu YN, Li ML, Xu YY, *et al*., 2018, Middle cerebral artery geometric features are associated with plaque distribution and stroke. *Neurology*, 91: e1760–e1769.

   https://doi.org/10.1212/WNL.0000000000006468

10. Van Tyen R, Saloner D, Jou LD, *et al*., 1994, MR imaging of flow through tortuous vessels: A numerical simulation. *Magn Reson Med*, 31: 184–195.

    https://doi.org/10.1002/mrm.1910310212

11. Bradley WG Jr., Waluch V, 1985, Blood flow: Magnetic resonance imaging. *Radiology*, 154: 443–450.

    https://doi.org10.1148/radiology.154.2.3966131

12. Miraux S, Franconi JM, Thiaudiere E, 2006, Blood velocity assessment using 3D bright-blood time-resolved magnetic resonance angiography. *Magn Reson Med*, 56: 469–473.

    https://doi.org/10.1002/mrm.20990

13. Li ML, Xu WH, Song L, *et al*., 2009, Atherosclerosis of middle cerebral artery: Evaluation with high-resolution MR imaging at 3T. *Atherosclerosis*, 204: 447–452.

    https://doi.org/10.1016/j.atherosclerosis.2008.10.019

14. Xu WH, Li ML, Gao S, *et al*., 2010, *In vivo* high-resolution MR imaging of symptomatic and asymptomatic middle cerebral artery atherosclerotic stenosis. *Atherosclerosis*, 212: 507–511.

    https://doi.org/10.1016/j.atherosclerosis.2010.06.035

15. McHugh ML, 2012, Interrater reliability: The kappa statistic. *Biochem Med* (*Zagreb*), 22: 276–282.

16. Bradley WG Jr., Waluch V, Lai KS, *et al*., 1984, The appearance of rapidly flowing blood on magnetic resonance images. *AJR Am J Roentgenol*, 143: 1167–1174.

    https://doi.org/10.2214/ajr.143.6.1167

17. Bouthillier A, vanLoveren HR, Keller JT, 1996, Segments of the internal carotid artery: A new classification. *Neurosurgery*, 38: 425–432, discussion 432–433.

    https://doi.org/10.1097/00006123-199603000-00001

18. Xu YY, Li ML, Gao S, *et al*., 2016, Non-moyamoya vessel

network formation along steno-occlusive middle cerebral artery. *Neurology*, 86: 1957–1963.

https://doi.org/10.1212/WNL.0000000000002698

19. Phan TG, Beare RJ, Jolley D, *et al.*, 2012, Carotid artery anatomy and geometry as risk factors for carotid atherosclerotic disease. *Stroke*, 43: 1596–1601.

https://doi.org/10.1161/STROKEAHA.111.645499

20. Beier S, Ormiston J, Webster M, *et al.*, 2016, Impact of bifurcation angle and other anatomical characteristics on blood flow-a computational study of non-stented and stented coronary arteries. *J Biomech*, 49: 1570–1582.

https://doi.org/10.1016/j.jbiomech.2016.03.038

21. Xu WH, Li ML, Gao S, *et al.*, 2011, Plaque distribution of stenotic middle cerebral artery and its clinical relevance. *Stroke*, 42: 2957–2959.

22. Wardlaw JM, Smith EE, Biessels GJ, *et al.*, 2013, Neuroimaging standards for research into small vessel disease and its contribution to ageing and neurodegeneration. *Lancet Neurol*, 12: 822–838.

https://doi.org/10.1016/S1474-4422(13)70124-8

23. Wong KS, Gao S, Chan YL, *et al.*, 2002, Mechanisms of acute cerebral infarctions in patients with middle cerebral artery stenosis: A diffusion-weighted imaging and microemboli monitoring study. *Ann Neurol*, 52: 74–81.

https://doi.org/10.1002/ana.10250

24. Ozsarlak O, Van Goethem JW, Maes M, *et al.*, 2004, MR angiography of the intracranial vessels: Technical aspects and clinical applications. *Neuroradiology*, 46: 955–972.

https://doi.org/10.1007/s00234-004-1297-9

25. Kodama T, Watanabe K, 1997, Influence of imaging parameters, flow velocity, and pulsatile flow on three-dimensional time-of-flight MR angiography: Experimental studies. *Eur J Radiol*, 26: 83–91.

https://doi.org/10.1016/s0720-048x(96)01152-7

26. Saloner D, van Tyen R, Dillon WP, *et al.*, 1996, Central intraluminal saturation stripe on MR angiograms of curved vessels: Simulation, phantom, and clinical analysis. *Radiology*, 198: 733–739.

27. Stonebridge PA, 2011, Three-dimensional blood flow dynamics: Spiral/helical laminar flow. *Methodist Debakey Cardiovasc J*, 7: 21–26.

https://doi.org/10.14797/mdcj-7-1-21

28. Stonebridge PA, Suttie SA, Ross R, *et al.*, 2016, Spiral laminar flow: A survey of a three-dimensional arterial flow pattern in a group of volunteers. *Eur J Vasc Endovasc Surg*, 52: 674–680.

https://doi.org/10.1016/j.ejvs.2016.07.018

29. Gallo D, Steinman DA, Bijari PB, *et al.*, 2012, Helical flow in carotid bifurcation as surrogate marker of exposure to disturbed shear. *J Biomech*, 45: 2398–2404.

https://doi.org/10.1016/j.jbiomech.2012.07.007

30. Stonebridge PA, Buckley C, Thompson A, *et al.*, 2004, Non spiral and spiral (helical) flow patterns in stenoses. *In vitro* observations using spin and gradient echo magnetic resonance imaging (MRI) and computational fluid dynamic modeling. *Int Angiol*, 23: 276–283.

31. Mustert BR, Williams DM, Prince MR, 1998, *In vitro* model of arterial stenosis: Correlation of MR signal dephasing and trans-stenotic pressure gradients. *Magn Reson Imaging*, 16: 301–310.

https://doi.org/10.1016/s0730-725x(97)00304-4

32. Wilcock DJ, Jaspan T, Worthington BS, 1995, Problems and pitfalls of 3-D TOF magnetic resonance angiography of the intracranial circulation. *Clin Radiol.*, 50(8): 526–532.

https://doi.org/10.1016/s0009-9260(05)83186-1

33. Antoniadis AP, Giannopoulos AA, Wentzel JJ, *et al.*, 2015, Impact of local flow haemodynamics on atherosclerosis in coronary artery bifurcations. *EuroIntervention*, 11 Suppl V: V18–V22.

https://doi.org/10.4244/EIJV11SVA4

34. Giannoglou GD, Antoniadis AP, Koskinas KC, *et al.*, 2010, Flow and atherosclerosis in coronary bifurcations. *EuroIntervention*, 6 Suppl J: J16–J23.

https://doi.org/10.4244/EIJV6SUPJA4

35. Denswil NP, van der Wal AC, Ritz K, *et al.*, 2016, Atherosclerosis in the circle of Willis: Spatial differences in composition and in distribution of plaques. *Atherosclerosis*, 251: 78–84.

https://doi.org/10.1016/j.atherosclerosis.2016.05.047

36. Ziyrek M, Sertdemir AL, Duran M, 2020, Effect of coronary artery bifurcation angle on atherosclerotic lesion localization distance to the bifurcation site. *J Saudi Heart Assoc*, 32: 399–407.

https://doi.org/10.37616/2212-5043.1071

37. Turan TN, Kicielinski KP, 2021, Asymptomatic intracranial atherosclerotic stenosis: The risk above the carotids. *J Am Coll Cardiol*, 78: 572–574.

https://doi.org/10.1016/j.jacc.2021.05.042

38. Caplan LR, 2015, Lacunar infarction and small vessel disease: Pathology and pathophysiology. *J Stroke*, 17: 2–6.

https://doi.org/10.5853/jos.2015.17.1.2

39. Pasi M, Cordonnier C. 2020, Clinical relevance of cerebral small vessel diseases. *Stroke*, 51: 47–53.

https://doi.org/10.1161/STROKEAHA.119.024148

40. Kwon HM, Lynn MJ, Turan TN, *et al.*, 2016, Frequency, risk factors, and outcome of coexistent small vessel disease and

intracranial arterial stenosis: Results from the stenting and aggressive medical management for preventing recurrent stroke in intracranial stenosis (SAMMPRIS) trial. *JAMA Neurol*, 73: 36–42.

https://doi.org/10.1001/jamaneurol.2015.3145

41. Salgado AV, Ferro JM, Gouveia-Oliveira A, 1996, Long-term prognosis of first-ever lacunar strokes. A hospital-based study. *Stroke*, 27: 661–666.

https://doi.org/10.1161/01.str.27.4.661

42. Groen HC, Gijsen FJ, Van der Lugt A, *et al.*, 2007, Plaque rupture in the carotid artery is localized at the high shear stress region: A case report. *Stroke*, 38: 2379–2381.

https://doi.org/10.1161/STROKEAHA.107.484766

43. Donnan GA, Bladin PF, Berkovic SF, *et al.*, 1991, The stroke syndrome of striatocapsular infarction. *Brain*, 114: 51–70.

44. Decavel P, Vuillier F, Moulin T, 2012, Lenticulostriate infarction. *Front Neurol Neurosci*, 30: 115–119.

https://doi.org/10.1159/000333606

ACCSCIENCE PUBLISHING

Advanced Neurology

SHORT COMMUNICATION

Sexual behavior and risk of diagnosis with multiple sclerosis: A retrospective case–control study

Matthew Kennis*, Katherine Thompson, and Elijah W. Hale

School of Medicine, University of Colorado, Anschutz Medical Campus, Aurora, Colorado, United States of America

Abstract

Adolescence is a critical window during which psychosocial factors have significant effects on the lifetime risk of multiple sclerosis (MS). Sexual behavior is relevant early in adulthood and has not been described in its relationship to MS. Using a retrospective secondary analysis of cross-sectional data in the TriNetX database, we investigated the connection between orientation of sexual behavior and MS risk. We identified 13,595 males and 9,589 females with same-sex behavior and 64,409 males and 137,450 females with opposite-sex behavior. Cohorts were balanced on age, race, and ethnicity. Males engaging in same-sex behavior had a 2.80-fold higher risk of MS diagnosis (95% confidence interval [CI]: 1.66 – 4.73), and females engaging in same-sex behavior had a 2.30-fold higher risk of MS diagnosis (95% CI: 1.65 – 3.20). Our findings thus advance the understanding of MS risk in the context of social determinants of health.

Keywords: Multiple sclerosis; Sexual behavior; Adverse childhood experiences; Adolescence

***Corresponding author:**
Matthew Kennis
(matthew.kennis@cuanschutz.edu)

Citation: Kennis M, Thompson K, Hale EW, 2023, Sexual behavior and risk of diagnosis with multiple sclerosis: A retrospective case–control study. *Adv Neuro,* 2(4): 1383.
https://doi.org/10.36922/an.1383

Received: July 27, 2023

Accepted: November 28, 2023

Published Online: December 12, 2023

1. Introduction

Multiple sclerosis (MS) is a demyelinating disease of the central nervous system with heterogenous symptomatology due to variably affected neuronal tracts[1]. While some factors such as Epstein–Barr virus (EBV) infection are well established as being associated with an increased risk of MS, certain factors such as adolescent obesity and sunlight exposure have been identified recently, reinforcing the importance of continued research into MS risk factors[2]. Many studies have recently focused on adolescence, as it has been identified as a particular time window during which lifestyle and environmental factors seem to have the greatest effect on the lifetime risk of MS[3].

Adolescence and young adulthood are also associated with the development of patterns of sexual behavior and identity formation[4]. While personal identities such as gay, lesbian, bisexual, or queer may arise later in life, sexual behavior with individuals of the same sex often initially occurs in adolescence[5]. Despite the known impact of same-sex behavior on other neurologic conditions, such as amyotrophic lateral sclerosis and dementia[6,7], research into the intersection between MS and sexual behavior has been limited[8].

Individuals who engage in same-sex sexual behavior are a unique subset of the general population, with known health disparities relating to stigma and discrimination[9,10]. In addition, they also have unique healthcare needs that may impact MS care, such as use of pre-exposure prophylaxis medications in men who have sex with men[11]. Other unique factors, such as monkeypox vaccination, are also greatly increased in this population[12]. Research into the current gap of knowledge regarding the ways in which MS differs in this unique subpopulation could hold potential implications for future treatment. As a first step, we sought to investigate the association between orientation of sexual behavior and MS risk.

2. Methods

We collected aggregate, de-identified data from the TriNetX research database. TriNetX is a health information database with over 85 million unique patient records. We obtained data from the past 20 years ranging from April 3, 2002, to April 3, 2022, at 58 large health-care organizations. Subject inclusion and exclusion criteria were defined using International Classification of Diseases (ICD) codes. We created an investigative cohort defined by the presence of same-sex high-risk sexual behavior (ICD-10: Z72.52) and/or bisexual high-risk sexual behavior (ICD10: Z72.53) and the absence of opposite-sex high-risk sexual behavior (ICD-10: Z72.51)[13]. A comparator cohort was created, defined by the presence of opposite-sex high-risk sexual behavior (ICD-10: Z72.51) and the absence of same-sex high-risk sexual behavior (ICD-10: Z72.52, Z72.53). Finally, a third control cohort was created from patients who participated in any virtual visit encounter in the TrinetX database and lacked any previous history of high-risk sexual behavior (ICD-10: Z72.5). All patients were 18 years or older. The data were extracted from TriNetX on April 3, 2022.

The two investigative cohorts were stratified by sex; males with exclusively same-sex behavior were compared to males with opposite-sex behavior. We balanced cohorts based on age, sex, race, ethnicity, infectious mononucleosis, and EBV seropositivity using the TriNetX software, which uses nearest-neighbor matching with a difference between propensity scores less than or equal to 0.1. After matching, we investigated the outcome of lifetime diagnosis of MS (ICD-10: G35). Rates of diagnosis were used to calculate risk ratio and odds ratio [OR]. Significance for this study was set at $P < 0.05$. This study only utilized aggregated, deidentified patient data and thus was exempted from review by the Colorado Multiple Institutional Review Board (COMIRB).

3. Results

We identified 234,022 adults with high-risk sexual behavior. Of these patients, we identified 13,595 males and 9,589 females with same-sex behavior and 64,409 males and 137,450 females with opposite-sex behavior. Our control cohort consisted of 711,077 adults without documented high-risk sexual behavior. Full characteristics for the cohorts, including age, race, ethnicity, other diagnoses such as infectious mononucleosis, and laboratory values for EBV antibody, are tabulated in Table 1.

The risk of MS was significantly higher for individuals engaging in same-sex behavior compared to individuals engaging in opposite-sex behavior. Males engaging in same-sex behavior had a 2.80-fold higher risk of MS diagnosis (95% confidence interval [CI]: 1.66 – 4.73) and females engaging in same-sex behavior had a 2.30-fold higher risk (95% CI: 1.65 – 3.20) of MS diagnosis (Figure 1). There was no significant risk difference between adults engaging in any form of high-risk sexual behavior compared to adults not engaging in high-risk sexual behavior ($P = 0.41$). Table 2 contains information on cohort size and number of patients with the outcome of interest.

4. Discussion

Our study found a significant association between same-sex sexual behavior and the lifetime risk of MS. The association was prominent in both male and female patients, indicating a need for targeted research in this understudied area. Importantly, the lifetime risk of MS in this population was found to be over twice that of individuals engaging only in opposite-sex sexual encounters. The risk for males was nearly 3 times higher (OR: 2.80, 95% CI: 1.66 – 4.73) whereas the risk for females was 2.3 times higher (OR: 2.30, 95% CI: 1.65 – 3.20). These ratios were calculated after adjusting for age, sex, race, and ethnicity, in addition to the recently identified risk factor of EBV seropositivity, which had a notably low prevalence in our study population. This allowed the impact of sexual behavior on MS to be isolated as much as possible. This finding invokes the need for further inquiry into MS in this unique population.

One theory for this increased risk could lie in an increased level of stress experienced by these individuals, notably during their adolescent years. Youths engaging in same-sex behavior but identifying as heterosexual experience higher rates of bullying and suicidality[14], which are types of adverse childhood experiences[15]. Adverse childhood experiences are known to be linked to increased neuroinflammation, increased autoimmune diseases, and earlier age of MS diagnosis, which could be a contributing factor to the large association we found[16]. Youths who engage in same-sex behavior and identify as LGBTQ+ also experience higher rates of adverse childhood experiences[17]. Future research could investigate the

Table 1. Comparison of characteristics between (a) adults engaging in all forms of high-risk sexual behavior versus adults not engaging in high-risk sexual behavior; (b) males engaging in high-risk homosexual and/or bisexual behavior versus males engaging in high-risk heterosexual behavior; (c) females engaging in high-risk homosexual and/or bisexual behavior versus females engaging in high-risk heterosexual behavior

Cohort demographics before matching for age, sex, race, ethnicity, infectious mononucleosis, and EBV seropositivity						
Variable	**Adults engaging in high-risk behavior**	**Adults not engaging in high-risk sexual behavior**	**Males engaging in same-sex high-risk behavior**	**Males engaging in opposite-sex high-risk behavior**	**Females engaging in same-sex high-risk behavior**	**Females engaging in opposite-sex high-risk behavior**
N	234,022	711,077	13,595	64,409	9,589	137,450
Current age, mean (±SD)	35.4 (14.2)	49.2 (20)	46.5 (19.4)	36.1 (13.6)	56.8 (20.7)	32.3 (11.3)
Sex (male, female)	37%, 63%	41%, 59%	100%, 0	100%, 0	0, 100%	0, 100%
Race						
White (n)	50% (117,194)	75% (529,825)	71% (9,645)	49% (32,157)	80% (7,632)	46% (63,497)
Black or African American (n)	31% (66,890)	9% (67,016)	12% (1,663)	30% (20,040)	12% (1,148)	35% (47,151)
Ethnicity						
Hispanic or Latino (n)	14% (31,494)	53% (374,785)	13% (1,781)	13% (8,876)	6% (600)	14% (19,170)
Other diagnoses						
Mood disorders	25% (57,895)	14% (101,370)	30% (4,038)	16% (10,818)	48% (4,618)	27% (36,654)
Anxiety disorders	21% (49,874)	19% (133,785)	28% (3,804)	14% (9,285)	46% (4,441)	23% (30,728)
Infectious mononucleosis	0.7% (1,711)	0.4% (3,074)	0.3% (43)	0.7% (456)	0.4% (35)	0.8% (1,141)
Laboratory value						
Presence of EBV nuclear IgG antibody	0.02% (50)	0% (0)	0.08% (10)	0.02% (13)	0.1% (10)	0.02% (32)
Cohort demographics after matching for age, sex, race, ethnicity, infectious mononucleosis, and EBV seropositivity						
N	220,969	220,969	12,383	12,383	7,128	7,128
Current age, mean (±SD)	35.8 (14.5)	35.3 (14.8)	43.0 (16.7)	43.0 (16.6)	48.8 (17.5)	48.9 (17.7)
Sex (male, female)	37%, 63%	39%, 61%	100%, 0	100%, 0	0, 100%	0, 100%
Race						
White (n)	53% (116,277)	56% (123,983)	68% (8,434)	68% (8,436)	74% (5,237)	73% (5,203)
Black or African American (n)	29% (64,086)	17% (36,572)	13% (1,633)	18% (2,173)	16% (1,117)	17% (1,183)
Ethnicity						
Hispanic or Latino (n)	14% (31,494)	14% (31,485)	14% (1,770)	15% (1,906)	8% (584)	9% (617)
Other diagnoses						
Mood disorders	25% (55,850)	16% (36,172)	29% (3,584)	20% (2,466)	49% (3,459)	36% (2,553)
Anxiety disorders	22% (48,261)	19% (43,042)	27% (3,334)	17% (2,094)	46% (3,305)	31% (2,207)
Infectious mononucleosis	0.8% (1,649)	0.8% (1,662)	0.3% (43)	0.3% (32)	0.5% (32)	0.4% (28)
Laboratories						
Presence of EBV nuclear IgG antibody	0.02% (47)	0% (0)	0.08% (10)	0.08% (10)	0.08% (10)	0.08% (10)

Abbreviations: EBV: Epstein–Barr virus, SD: Standard deviation, CI: Confidence interval.

impact of self-identity on MS; however, as sexual behavior can be more easily divided into clear categories, it is more appropriate than sexual identity for this initial step into sexuality-focused MS research.

Given our findings, the lack of clinical studies characterizing MS disease course and pharmacologic treatment response in individuals engaging in same-sex behavior is a glaring oversight, as other subgroups have been shown to have important clinical differences. African American patients are known to experience a more aggressive MS disease course, with more frequent relapses, worse post-relapse recovery, and faster transition to secondary progressive MS[12]. Increased severity of MS progression has similarly been demonstrated in Hispanic

Table 2. Outcome of diagnosis with multiple sclerosis (G35) between (a) adults engaging in all forms of high-risk sexual behavior versus adults not engaging in high-risk sexual behavior; (b) males engaging in high-risk homosexual and/or bisexual behavior versus males engaging in high-risk heterosexual behavior; (c) females engaging in high-risk homosexual and/or bisexual behavior versus females engaging in high-risk heterosexual behavior; cohorts are matched for age, race, and ethnicity

Cohort	N	Patients with outcome of multiple sclerosis	Risk	Risk ratio	Odds ratio (95% CI)	*P*-value
High-risk sexual behavior versus absence of high-risk sexual behavior						
Adults engaging in high-risk sexual behavior	220,969	742	0.336%	0.959 (0.867, 1.060)	0.959 (0.867, 1.060)	0.4103
Adults not engaging in high-risk sexual behavior	220,969	774	0.350%			
Male same-sex high-risk behavior versus male opposite-sex high-risk behavior						
Males engaging in same-sex high-risk behavior	12,593	53	0.428%	2.789 (1.653, 4.708)	2.797 (1.655, 4.727)	<0.0001
Males engaging in opposite-sex high-risk behavior	12,593	19	0.153%			
Female same-sex high-risk behavior versus female opposite-sex high-risk behavior						
Females engaging in same-sex high-risk behavior	7,128	116	1.627%	2.275 (1.639, 3.156)	2.296 (1.649, 3.196)	<0.0001
Females engaging in opposite-sex high-risk behavior	7,128	51	0.715%			

Abbreviation: EBV: Epstein–Barr virus.

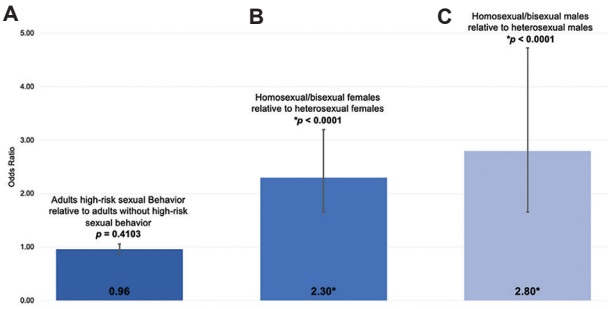

Figure 1. Odds ratio (OR) of multiple sclerosis diagnosis between (A) adults engaging in all forms of high-risk sexual behavior versus adults not engaging in high-risk sexual behavior (OR: 0.96; $P = 0.4103$); (B) females engaging in high-risk homosexual and/or bisexual behavior versus females engaging in high-risk heterosexual behavior (OR: 2.30*; *$P < 0.0001$); (C) males engaging in high-risk homosexual and/or bisexual behavior versus males engaging in high-risk heterosexual behavior (OR: 2.80*; *$P < 0.0001$) – all cohorts are matched for age, race, ethnicity, infectious mononucleosis, and Epstein–Barr virus seropositivity.

Americans[13]. Our results generate further questioning around whether negative MS outcomes may analogously apply to this sexual minority population. Regarding pharmacologic treatment, recent research has shown that men who have sex with men are far more likely than the general population to use pre-exposure prophylaxis medications or to have been immunized with the recent monkeypox vaccine, which may interact in unforeseen ways with common therapies for MS[11,12]. The gap in research for individuals engaging in same-sex behavior may be hindering the development of adequate treatment and identification strategies for this patient population already known to be at risk for negative health outcomes due to societal and health-care inequalities[8-10].

Our findings may be useful for a range of providers interested in comprehensive patient care, not only those who focus on the LGBTQ+ population. Patients present for care with a wide variety of concerns, and sexual health is an important aspect of overall wellness[4]. The strong association noted in our study could help identify individuals in the prodromal stage of MS development. The prodrome may be useful for successful intervention in slowing or stopping MS progression, but a prerequisite is successful identification[18]. As all patients in our study disclosed their patterns of sexual behavior to a health-care provider, our data are reflective of individuals who may have shown prodromal symptoms and have a known personal factor that may increase a provider's index of suspicion for MS.

As with all retrospective database studies, our study was limited by the de-identified, aggregate nature of the data which prevented us from longitudinally investigating specific characteristics or obtaining detailed socioeconomic status information, which could be a confounding factor. It is also worthwhile to note that patients engaging in exclusively same-sex or opposite-sex behavior may not identify with any specific sexual identity. Up to 11% of individuals identifying as heterosexual may have same-

sex behaviors, and up to 30% of individuals engaging in same-sex behaviors may identify as heterosexual[19]. The ICD-10 codes utilized may also underestimate the true risk, as codes are entered manually by providers and may be neglected in some cases.

Our findings advance the understanding of MS risk in a unique patient population known to be at risk for negative health outcomes[15,19]. Early identification is a crucial factor in the evolution of MS and can enable patients to experience a longer time without debilitating symptoms[20]. It is our hope that these findings could enable health-care providers to suspect and diagnose MS earlier in patients who might otherwise go unnoticed. Future study should seek to rectify the absence of sexuality-focused research in the field of MS, with an eye toward ensuring better patient outcomes and promoting health-care equity.

5. Conclusion

In conclusion, our study uncovered a novel correlation between same-sex sexual behavior and an elevated risk of MS, underscoring the importance of exploring this association further. Both male and female individuals engaging in same-sex behavior demonstrated a notably higher likelihood of MS diagnosis compared to those with opposite-sex behavior, emphasizing the need for targeted research in this understudied area.

However, it is crucial to acknowledge the limitations of our study. The use of de-identified, aggregate data restricted the detailed exploration of individual characteristics and socioeconomic factors, potentially influencing the observed results. Additionally, the complexity of sexual behavior and identity suggests that the ICD-10 codes used may not fully capture the nuanced experiences of individuals.

Moving forward, future investigations should delve deeper into the impact of adverse childhood experiences related to same-sex behavior, shedding light on potential stress-related mechanisms underlying the increased MS risk. Moreover, there is a pressing need for research focusing on disease progression and treatment responses in individuals engaging in same-sex behavior, ensuring that health-care providers can tailor interventions effectively. Addressing these gaps will not only enhance our understanding of MS in this specific population but also pave the way for more inclusive and equitable health-care practices.

Acknowledgments

The authors would like to acknowledge Jessica Solomon Sanders, M.D (University of Colorado Anschutz Medical Campus) for her guidance in the preparation of this manuscript.

Funding

None.

Conflict of interest

The authors have no conflicts of interest to disclose.

Author contributions

Conceptualization: Matthew Kennis, Elijah W. Hale
Data curation: All authors
Formal analysis: All authors
Investigation: All authors
Writing – original draft: All authors
Writing – review & editing: All authors

Ethics approval and consent to participate

This study only utilized aggregated, deidentified patient data and thus was exempted from review by the COMIRB.

Consent for publication

Not applicable.

Availability of data

The original contributions presented in the study are included in the article; further inquiries can be directed to the corresponding author.

Further disclosure

The abstract of this paper has previously been presented at the 2023 American Academy of Neurology Annual Meeting in Boston, Massachusetts on April 27, 2023.

References

1. Owens B, 2016, Multiple sclerosis. *Nature*, 540: S1.

   https://doi.org/10.1038/540s1a

2. Abdollahpour I, Nedjat S, Mansournia MA, *et al*., 2018, Lifestyle factors and multiple sclerosis: A population-based incident case-control study. *Mult Scler Relat Disord*, 22: 128–133.

   https://doi.org/10.1016/j.msard.2018.03.022

3. Abdollahpour I, Sormani MP, Nedjat S, *et al*., 2021, The role of nutritional factors during adolescence in multiple sclerosis onset: A population-based incident case-control study. *Nutr Neurosci*, 24: 500–507.

   https://doi.org/10.1080/1028415X.2019.1647689

4. Kågesten A, van Reeuwijk M, 2021, Healthy sexuality development in adolescence: Proposing a competency-based framework to inform programmes and research. *Sex Reprod Health Matters*, 29: 1996116.

   https://doi.org/10.1080/26410397.2021.1996116

5. Brewster KL, Tillman KH, Holway GV, 2021, Timing of first sexual experience with a same-sex partner: A life course approach. *Arch Sex Behav*, 50: 3587–3599.

   https://doi.org/10.1007/S10508-021-02043-3

6. Poletti B, Carelli L, Solca F, *et al.*, 2019, Sexuality and intimacy in ALS: Systematic literature review and future perspectives. *J Neurol Neurosurg Psychiatry*, 90: 712–719.

   https://doi.org/10.1136/jnnp-2018-319684

7. Perales-Puchalt J, Gauthreaux K, Flatt J, *et al.*, 2019, Risk of dementia and mild cognitive impairment among older adults in same-sex relationships. *Int J Geriatr Psychiatry*, 34: 828–835.

   https://doi.org/10.1002/gps.5092

8. Anderson A, Dierkhising J, Rush G, *et al.*, 2021, Experiences of sexual and gender minority people living with multiple sclerosis in Northern California: An exploratory study. *Mult Scler Relat Disord*, 55: 103214.

   https://doi.org/10.1016/j.msard.2021.103214

9. Gonzales G, Blewett LA, 2014, National and state-specific health insurance disparities for adults in same-sex relationships. *Am J Public Health*, 104: e95–e104.

   https://doi.org/10.2105/ajph.2013.301577

10. Hsieh N, Shuster SM, 2021, Health and health care of sexual and gender minorities. *J Health Soc Behav*, 62: 318–333.

    https://doi.org/10.1177/00221465211016436

11. Hamilton K, Hasney L, Cohn T, *et al.*, 2022, PrEP demographics and disparity: The race, ethnicity, gender identity, sex assigned at birth, sexual orientation and age of current PrEP use. *J Community Health Nurs*, 39: 213–226.

    https://doi.org/10.1080/07370016.2022.2073791

12. Goyal L, Ajmera K, Pandit R, *et al.*, 2022, Prevention and treatment of monkeypox: A step-by-step guide for healthcare professionals and general population. *Cureus*, 14: e28230.

    https://doi.org/10.7759/cureus.28230

13. ICD-10: International Statistical Classification of Diseases and Related Health Problems: Tenth Revision. Available from: https://apps.who.int/iris/handle/10665/42980 [Last accessed on 2022 Aug 29].

14. Montoro R, Thombs B, Igartua KJ, 2015, The association of bullying with suicide ideation, plan, and attempt among adolescents with GLB or unsure sexual identity, heterosexual identity with same-sex attraction or behavior, or heterosexual identity without same-sex attraction or behavior. *Sante Ment Que*, 40: 55–75.

    https://doi.org/10.7202/1034911ar

15. Andersen JP, Blosnich J, 2013, Disparities in adverse childhood experiences among sexual minority and heterosexual adults: Results from a multi-state probability-based sample. *PLoS One*, 8: e54691.

    https://doi.org/10.1371/journal.pone.0054691

16. Shaw MT, Pawlak NO, Frontario A, *et al.*, 2017, Adverse childhood experiences are linked to age of onset and reading recognition in multiple sclerosis. *Front Neurol*, 8: 242.

    https://doi.org/10.3389/fneur.2017.00242

17. Tran NM, Henkhaus LE, Gonzales G, 2022, Adverse childhood experiences and mental distress among US adults by sexual orientation. *JAMA Psychiatry*, 79: 377–379.

    https://doi.org/10.1001/jamapsychiatry.2022.0001

18. Marrie RA, Allegretta M, Barcellos LF, *et al.*, 2022, From the prodromal stage of multiple sclerosis to disease prevention. *Nat Rev Neurol*, 18: 559–572.

    https://doi.org/10.1038/S41582-022-00686-x

19. Geary RS, Tanton C, Erens B, *et al.*, 2018, Sexual identity, attraction and behaviour in Britain: The implications of using different dimensions of sexual orientation to estimate the size of sexual minority populations and inform public health interventions. *PLoS One*, 13: e0189607.

    https://doi.org/10.1371/journal.pone.0189607

20. Makhani N, Tremlett H, 2021, The multiple sclerosis prodrome. *Nat Rev Neurol*, 17: 515–521.

    https://doi.org/10.1038/S41582-021-00519-3

ACCSCIENCE PUBLISHING

Advanced Neurology

CASE REPORT

Expanding the spectrum of gene-associated reflex seizures: A case report of a "bidet-induced" reflex epilepsy

Tommaso Lo Barco[1,2]*, Jacopo Proietti[2,3], Luna Fontanelli[4], Ilaria Campari[4], Benedetta Piccolo[5], Francesca Ormitti[6], and Emanuela Claudia Turco[5]

[1]Child Neuropsychiatry Unit, Epilepsy Center, "C. Poma Hospital", Mantova, Italy

[2]Center for Research on Epilepsies in Pediatric Age (CREP), Verona, Italy

[3]Child Neuropsychiatry Unit, Department of Surgical Sciences, Dentistry, Gynaecology and Pediatrics, University of Verona, Full Member of European Reference Network EpiCARE, Verona, Italy

[4]Child Neuropsychiatry Unit, Department of Mental Health and Pathological Addictions, Azienda USL di Parma, Parma, Italy

[5]Child Neurology and Psychiatry Unit, University Hospital of Parma, Parma, Italy

[6]Neuroradiology Unit, University Hospital of Parma, Parma, Italy

Abstract

In this case report, we present the case of a 20-month-old girl who manifested paroxysmal "bidet-induced" episodes characterized by impaired awareness, pallor, and hypotonia, with a duration of less than a minute. Initial neurological examination yielded unremarkable results, prompting further investigation. A video-electroencephalogram recording documented the epileptic nature of these episodes, revealing an ictal discharge originating from the right central-temporal region. A brain magnetic resonance imaging exhibited a sulcal/gyral asymmetry within the central sulci, along with the presence of the "power button sign" within the right central sulcus. These findings were indicative of a focal cortical dysplasia type-2. Subsequent genetic analysis through a gene panel identified the presence of an *NPRL2* variant. Mutations affecting this particular gene are known to disrupt the normal functioning of the GATOR1 complex, potentially causing focal cortical dysplasia and various forms of epilepsy, including familial focal epilepsy with variable foci. On the diagnosis, the patient received levetiracetam, and the ictal episodes promptly ceased. At the most recent follow-up (at 4 years old), the patient remained free of seizures without the need for any treatment, and her neurodevelopment so far had exhibited no abnormalities. Considering the landscape of epilepsy-related *GATOR1* variants, it is conceivable that this gene family may play a significant role in the pathogenesis of benign forms of focal reflex seizures, including bathing epilepsy.

Keywords: NPRL2; GATOR1; mTOR; Reflex seizures; Focal cortical dysplasia; Focal epilepsy with variable foci

***Corresponding author:**
Tommaso Lo Barco
(tommaso.lobarco@gmail.com)

Citation: Lo Barco T, Proietti J, Fontanelli L, *et al*., 2023, Expanding the spectrum of gene-associated reflex seizures: A case report of a "bidet-induced" reflex epilepsy. *Adv Neuro,* 2(4): 1379. https://doi.org/10.36922/an.1379

Received: July 26, 2023

Accepted: October 12, 2023

Published Online: November 20, 2023

1. Background

A reflex seizure is characterized by its consistent or nearly consistent elicitation by a specific stimulus or trigger[1]. These seizures encompass a diverse range and are usually

classified based on the nature of the triggering stimuli: sensory, motor, or cognitive; simple or complex. However, patients experiencing seizures triggered by the same stimulus can exhibit significant disparities in electroclinical features, etiologies, and prognosis[1].

Given this considerable variability, accurately classifying a patient with reflex seizures as their first manifestation into a specific syndrome and etiological category can be challenging.

Reflex seizures that manifest during the early years of life often raise concerns, as they can be indicative of serious diseases, such as structural epilepsies or developmental and epileptic encephalopathies[2-4]. Even when initial brain magnetic resonance imaging (MRI) results appear unremarkable, the presence of normal neurodevelopment and a negative electroencephalogram (EEG) at the onset does not completely exclude the possibilities of severe underlying conditions. Recent advancements in neurogenetic diagnostic techniques have expedited the identification of potential genetic variants responsible for seizures. However, interpreting these findings can be complicated.

Recently, there have been reports in the literature of genetic variants associated with reflex seizures in children who exhibit neither development and cognitive impairment nor structural lesions[5,6].

In this report, we present the case of a young girl who experienced "bidet-induced" reflex seizures in her 2nd year of life and was found to carry a variant of the *NPRL2* gene.

2. Case presentation

A 20-month-old girl presented with paroxysmal "bidet-induced" episodes characterized by impaired awareness, pallor, perioral cyanosis, buccal automatisms, and hypotonia. These episodes lasted for less than a minute and spontaneously resolved. They were triggered by pouring cold or warm water over genitalia. However, they did not occur in response to cleaning with wipes, tactile stimulation of the perineum, or during a complete bathing. At the age of 16 months, she had experienced a febrile seizure. Her neurodevelopmental milestones were within the expected normal range, and there were no remarkable familial medical history factors.

Polygraphic video-EEG recording demonstrated a normal background activity with no interictal abnormalities. During the recording, an attempt was made to trigger an episode by scrubbing the perineum with lukewarm water. The EEG revealed a high-voltage polymorphic ictal activity originating from the right central-temporal region, with secondary diffusion to the contralateral hemisphere. These clinical manifestations included cyanosis, hypotonia, and impaired awareness, with a duration of nearly 1 min (Figure 1).

Brain MRI findings revealed a focal sulcal/gyral asymmetry in the perirolandic regions. This asymmetry was attributed to the deeper section of the ascending branch of the right central sulcus, resembling the characteristic "power button sign" (Figure 2). This central sulcus variant is highly suggestive of a focal cortical dysplasia type 2, which involves the interposition of a precentral sulcal segment between the central sulcus and a hook-shaped anterior ascending branch[7].

Blood screening, neurometabolic investigations, and microarray-based comparative genomic hybridization (array-CGH) yielded normal results. A next-generation sequencing (NGS) panel comprising 222 epilepsy-related genes revealed the presence of an *NPRL2* variant (c.180G>A p.[Met60Ile]), which had been inherited by her asymptomatic mother.

As part of her treatment, she received levetiracetam as an antiseizure medication, which promptly led to the cessation of ictal episodes. After 18 months of being free from seizures, her treatment was gradually tapered.

During the most recent follow-up, conducted when the patient was 4 years old, she remained free from seizures, and her EEG displayed no abnormalities. A neurodevelopment assessment was performed using the Griffiths Mental Developmental Scales, revealing a normal progression in motor, social, and cognitive skills, albeit with a mild impairment in expressive language.

3. Discussion

In this case report, we present the case of a young girl who began experiencing "bidet-induced" reflex seizures during the first months of life. This case exhibits a favorable seizure outcome and normal neurodevelopment.

In medical literature, there have been cases of reflex seizures induced by "diaper-changing" or "perineal stimulation" with onset in the 1st year of life. In most of these cases, such seizures are associated with an unfavorable prognosis, mainly in the context of conditions like Dravet syndrome or other conditions characterized by drug-resistant seizures and cognitive impairment.[3,4,8] Although the follow-up period for our patient is relatively short, the neurodevelopmental trajectory observed at the age of 4 years suggests the absence of developmental encephalopathy.

Bathing epilepsy (BE) is a condition characterized by the recurrence of seizures triggered by bathing in water heated to body temperature, primarily affecting children

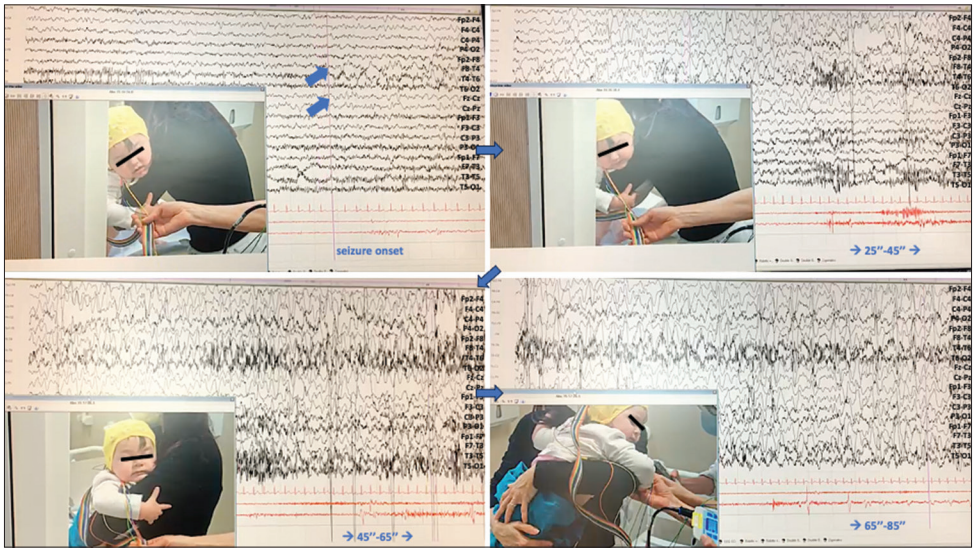

Figure 1. A few minutes after water was poured over the genitalia, an ictal discharge originated in the right central-temporal region, diffusing to the frontal area and subsequently to the left hemisphere. The patient experienced an impairment of awareness and exhibited cyanosis and hypotonia for a duration of 1 min.

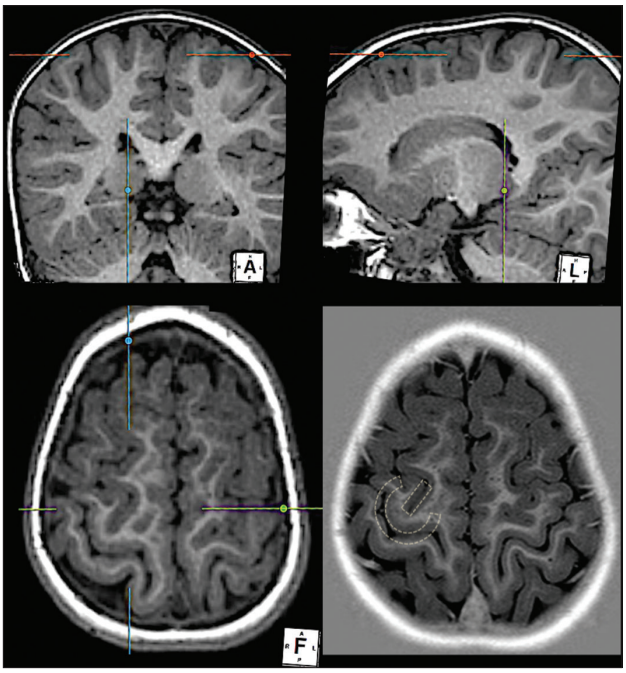

Figure 2. A brain magnetic resource imaging was performed when the patient was 20 months old. It is worth noting the presence of asymmetry in the perirolandic regions and the configuration of the ascending branch of the right central sulcus, which imparts the appearance commonly referred to as the "power button sign."

up to 3 years old who display normal neurodevelopment. Some patients exhibit a distinct sensitivity to the pouring of water on specific somatic areas, a phenomenon that has been described as a unique trigger in some of these patients[9]. For example, Franzoni *et al.* reported the case of a 4-month-old girl who developed seizures when lukewarm water was poured over her genitalia[10]. These seizures typically manifest with vegetative symptoms, including cyanosis, staring into space, limpness, and loss of alertness, and they are readily controlled with antifocal seizure medications. In the majority of patients, interictal EEG results are negative, though occasional focal slow waves may be observed during sleep recordings[9]. While isolated cases of non-provoked seizures have been reported, patients generally remain seizure-free and maintain normal neurodevelopment[9].

Given these features, the clinical presentation of our patient is consistent with the description of BE. However, we identified a variant of the *NPRL2* gene. *NPRL2* (NPR2-like, GATOR1 complex subunit) is located on chromosome 3p21.31. This gene plays a crucial role in the regulation of the mechanistic target of the rapamycin (mTOR) signaling pathway, which is essential for neuronal development, function, and plasticity. Mutations in the *NPRL2* gene disrupt the normal functioning of the GATOR1 complex, leading to mTOR pathway dysregulation and increased neuronal excitability, thereby contributing to the development of epilepsy[11].

Seizures associated with *NPRL2* variants are most frequently encompassed within the spectrum of what is termed the "GATOR1 phenotype,"[12] mainly involving familial focal epilepsy with variable foci (FFEVF), lateral temporal lobe epilepsy, and autosomal dominant sleep-related hypermotor epilepsy[12,13]. Cortical malformations are a common occurrence, often arising

due to a second-hit mechanism (germinal mutation + somatic mutation), and they may exhibit subtlety in the cases of FFEVF[12,14].

In our case, the *NPRL2* variant was inherited from the asymptomatic mother. It is well-established that epilepsies associated with GATOR-pathway-related genes often exhibit variable penetrance, with individuals carrying the same mutation displaying different types of epilepsies or remaining asymptomatic[14]. Therefore, it is worth considering the potential causative role of the *NPRL2* variant in the emergence of BE in our patient. In particular, while the brain MRI did not reveal a distinct cortical malformation — probably because the myelination process masks focal cortical dysplasias in some stages of maturation – the observed asymmetry in the perirolandic regions and the presence of the "power button sign" within the right central sulcus strongly suggest focal cortical dysplasia type 2[7]. A second-hit mechanism, involving a somatic mutation causing a cortical dysplasia in the sensorimotor cortex, and the inherited *NPRL2* variant, may be responsible for this reflex epilepsy.

Small lesions or epileptogenic zones within the perirolandic areas are observed in patients whose seizures are triggered by prolonged cutaneous contact, rubbing, or tapping of specific areas. Typically, seizures in such cases commence with ascending somatosensory sensations followed by focal clonic movements, all while awareness is maintained[15,16]. In contrast, our patient exhibited a different seizure semiology, and it is noteworthy that attempting to induce a seizure by rubbing the ictogenic area without the presence of water failed to evoke the seizure.

In "classic" cases of BE, it is reported that brain MRI results are typically negative. However, due to the benign course of the condition, repeat MRI examinations are seldom conducted after the onset[10,11,17,18]. These patients are often suspected of having a genetic etiology, but as of now, no gene that is distinctive to BE has been identified. Recently, the *SYN1* gene has been associated with seizures triggered by diverse stimuli, including bathing. However, the onset of such seizures within the first 2 – 3 years of life is uncommon, cognitive impairment is frequent among affected individuals, and the condition predominantly affects males[5,19].

4. Conclusion

We reported a case of an unusual manifestation of BE, characterized by seizures triggered by the act of pouring water over genitalia. This patient carries a variant of the *NPRL2* gene, which could potentially be linked to the development of focal cortical dysplasia or FFEVF. When considering the landscape of epilepsy-related *GATOR1* variants, it becomes apparent that this gene family may play a role in benign forms of focal reflex seizures, including BE.

Acknowledgments

None.

Funding

None.

Conflict of interest

The authors declare that they have no competing interests.

Author contributions

Conceptualization: Tommaso Lo Barco
Investigation: Luna Fontanelli, Ilaria Campari, Benedetta Piccolo, Francesca Ormitti, Emanuela Claudia Turco
Writing – original draft: Tommaso Lo Barco
Writing – review and editing: Jacopo Proietti, Emanuela Claudia Turco

Ethics approval and consent to participate

The patient's caregiver gave verbal consent to participate in the study.

Consent for publication

A verbal consent was obtained from patient's caregiver for publication.

Availability of data

All data underlying the results are available as part of the article.

References

1. Riney K, Bogacz A, Somerville E, *et al.*, 2022, International League against Epilepsy classification and definition of epilepsy syndromes with onset at a variable age: Position statement by the ILAE Task Force on Nosology and Definitions. *Epilepsia*, 63: 1443–1474.

   https://doi.org/10.1111/epi.17240

2. Palmini A, Halasz P, Scheffer IE, *et al.*, 2005, Reflex seizures in patients with malformations of cortical development and refractory epilepsy. *Epilepsia*, 46: 1224–1234.

   https://doi.org/10.1111/j.1528-1167.2005.52904.x

3. Solazzi R, Fiorini E, Parrini E, *et al.*, 2018, Diaper changing-induced reflex seizures in CDKL5-related epilepsy. *Epileptic Disord*, 20: 428–433.

   https://doi.org/10.1684/epd.2018.0999

4. Jain P, Gulati P, Alsowat D, *et al.*, 2018, Perineal stimulation triggering seizures in a child with Dravet syndrome. *Seizure*,

62: 106–107.

https://doi.org/10.1016/j.seizure.2018.10.001

5. Parenti I, Leitão E, Kuechler A, *et al*., 2022, The different clinical facets of SYN1-related neurodevelopmental disorders. *Front Cell Dev Biol*, 10: 1019715.

https://doi.org/10.3389/fcell.2022.1019715

6. Michelucci R, Pulitano P, Di Bonaventura C, *et al*., 2017, The clinical phenotype of autosomal dominant lateral temporal lobe epilepsy related to reelin mutations. *Epilepsy Behav*, 68: 103–107.

https://doi.org/10.1016/j.yebeh.2016.12.003

7. Mellerio C, Roca P, Chassoux F, *et al*., 2014, The power button sign: A newly described central sulcal pattern on surface rendering MR images of type 2 focal cortical dysplasia. *Radiology*, 274: 500–507.

https://doi.org/10.1148/radiol.14140773

8. Feyissa AM, Patterson MC, Wong-Kisiel LC, 2016, Too old for a diaper! A child with diaper changing-induced seizures. *Pediatr Neurol*, 54: 91–92.

https://doi.org/10.1016/j.pediatrneurol.2015.09.007

9. Mosquera-Gorostidi A, Azcona-Ganuza G, Yoldi-Petri ME, *et al*., 2019, Ictal video-electroencephalography findings in bathing seizures: Two new cases and review of the literature. *Pediatr Neurol*, 99: 76–81.

https://doi.org/10.1016/j.pediatrneurol.2019.04.017

10. Franzoni E, Gentile V, Grosso S, *et al*., 2010, Bathing epilepsy: Report of two Caucasian cases. *Epileptic Disord*, 12: 88–90.

https://doi.org/10.1684/epd.2010.0295

11. Sun Y, Wan L, Yan H, *et al*., 2021, Phenotypic and genotypic characterization of NPRL2-related epilepsy: Two case reports and literature review. *Front Neurol*, 12: 780799.

https://doi.org/10.3389/fneur.2021.780799

12. Baldassari S, Picard F, Verbeek NE, *et al*., 2019, The landscape of epilepsy-related GATOR1 variants. *Genet Med*, 21: 398–408.

https://doi.org/10.1038/s41436-018-0060-2

13. Debopam S, 2022, DEPDC5-related epilepsy: A comprehensive review. *Epilepsy Behav*, 130: 108678.

https://doi.org/10.1016/j.yebeh.2022.108678

14. Baulac S, Ishida S, Marsan E, *et al*., 2015, Familial focal epilepsy with focal cortical dysplasia due to DEPDC5 mutations. *Ann Neurol*, 77: 675–683.

https://doi.org/10.1002/ana.24368

15. Sala-Padró J, Toledo M, Sarria S, *et al*., 2015, Reflex seizures triggered by cutaneous stimuli. *Seizure*, 33: 72–75.

https://doi.org/10.1016/j.seizure.2015.10.013

16. Kanemoto K, Watanabe Y, Tsuji T, *et al*., 2001, Rub epilepsy: A somatosensory evoked reflex epilepsy induced by prolonged cutaneous stimulation. *J Neurol Neurosurg Psychiatry*, 70: 541–543.

https://doi.org/10.1136/jnnp.70.4.541

17. Kravljanac R, Djuric M, Milovanovic M, *et al*., 2012, Epileptic seizures provoked by bathing with water at room temperature. *Epileptic Disord*, 14: 321–324.

https://doi.org/10.1684/epd.2012.0520

18. Cappellari AM, Bulgaro C, Bruschi G, *et al*., 2021, Bathing epilepsy: A video case report. *Epileptic Disord*, 23: 639–642.

https://doi.org/10.1684/epd.2021.1295

19. Nguyen DK, Rouleau I, Sénéchal G, *et al*., 2015, X-linked focal epilepsy with reflex bathing seizures: Characterization of a distinct epileptic syndrome. *Epilepsia*, 56: 1098–1108.

https://doi.org/10.1111/epi.13042

ACCSCIENCE PUBLISHING

Advanced Neurology

CASE REPORT

The coexistence of narcolepsy and multiple sclerosis: A case report

Jinglong Hu[1], Minkai Zhang[2], Linjie Yu[1], and Meijuan Zhang[1]*

[1]Department of Neurology, Drum Tower Hospital, Medical School and The State Key Laboratory of Pharmaceutical Biotechnology, Institute of Brain Science, Nanjing University, Nanjing, Jiangsu Province, China

[2]Department of Neurology, Fourth People' Hospital of Zhenjiang, Zhenjiang, Jiangsu Province, China

Abstract

Multiple sclerosis (MS) is a chronic inflammatory demyelinating disorder of the central nervous system, characterized by myelin degeneration. Aside from general symptoms such as visual impairment, muscle weakness, and sensory abnormalities, sleep disorders are sometimes experienced by MS patients. Here, we report a rare case of a 21-year-old young male patient presenting with both MS and narcolepsy. Moreover, we also reviewed the potential pathophysiological mechanisms that linked these two diseases, including the involvement of the immune system and neuronal damage. This case report emphasized the significance of further research into the relationship between MS and narcolepsy and provided a valuable theoretical basis that MS might be a key cause of narcolepsy. In addition, therapeutic strategies for MS, such as ofatumumab, might help alleviate narcolepsy.

Keywords: Multiple sclerosis; Narcolepsy; Sleep disorders

***Corresponding author:**
Meijuan Zhang
(juanzi1986126@163.com)

Citation: Hu J, Zhang M, Yu L, *et al*., 2023, The coexistence of narcolepsy and multiple sclerosis: A case report. *Adv Neuro,* 2(4): 1913.
https://doi.org/10.36922/an.1913

Received: September 25, 2023

Accepted: November 28, 2023

Published Online: December 14, 2023

1. Background

Multiple sclerosis (MS) is a chronic autoimmune disease of the central nervous system (CNS) mainly characterized by immune-mediated inflammation and multifocal demyelinating lesions in the brain and spinal cord, which can cause various neurological symptoms, including visual impairment, muscle weakness, sensory abnormalities, coordination disorders, and cognitive impairment[1]. Furthermore, approximately 20%–50% of MS patients present with sleep disorders, which can be attributed to multiple factors, such as nerve damage, pathophysiological processes, therapies, and mental health issues. Although sleep disorders are commonly disregarded by most clinicians, they have a significant impact on the overall health of patients as well as the clinical course of MS[2]. Narcolepsy is a globally recognized rare disease characterized by excessive daytime sleepiness, cataplexy, and nocturnal sleep disorder. According to the current classification, narcolepsy can be categorized, based on the presence of cataplexy, into type 1 (narcolepsy with cataplexy) and type 2 (narcolepsy without cataplexy). The etiology may be strongly linked to HINI influenza virus infection and the immune response to the influenza vaccine. In addition, genetic factors and changes in neurological function may also be associated with the pathogenesis of narcolepsy. Here, we report the case of a patient with MS and narcolepsy type 1, highlighting the complexity of MS

disorders and offering insights, for clinicians, into treating this rare comorbidity.

2. Case presentation

In April 2023, a 21-year-old male who experienced a notable increase in sleep duration over the past 5 years, accompanied by the urge to fall asleep, nightmares, and sleep paralysis during waking hours, reached out to seek medical consultation in our clinic. These symptoms were unpredictable and seemingly not correlated with changes in the body position or other discernible triggers. He has no history of chronic diseases or relevant familial inherited diseases. A series of evaluations regarding his condition were conducted.

Nocturnal polysomnography (nPSG) (Figure 1A-E) results revealed a marked reduction in the patient's average sleep onset latency to just 1.75 min. In multiple sleep latency test, we found that the patient consistently entered rapid eye movement (REM) sleep prematurely with latencies documented at 1.5 min, 7.5 min, and 14.5 min, respectively. The extended duration of the patient's non-REM stage 1 (NREM1) sleep was also recorded, constituting 47.3% of the entire sleep duration. Conversely, durations for NREM2 and NREM3 stages were found to be reduced, accounting for 35.3% and 9.6%, respectively. It is noteworthy that the orexin A level in the patient's cerebrospinal fluid was significantly reduced, measuring only at 8.49 pg/mL (normal range >200 pg/mL). Furthermore, testing of genes associated with narcolepsy susceptibility revealed that the patient is homozygous for *HLA-DQB1*06:02* and *TCRA* rs1154155, and heterozygous for *P2RY11* rs2305795. These genetic markers, combined with the diminished orexin A levels, present a comprehensive overview of the patient's predisposition. Upon integrating these findings, the patient was provisionally diagnosed with narcolepsy type 1 according to the International Classification of Sleep Disorders, 3rd edition (ICSD-3) criteria[3].

In July 2023, the patient experienced numbness in both lower limbs, and the condition deteriorated while he walked with his shoes on. He had no accompanying symptoms, such as dizziness, headache, blurred vision, slurred speech, or impaired speech comprehension. Neurological examination revealed horizontal nystagmus in both eyes from right to left, an abnormal sensation resembling the feeling of wearing boots on both lower limbs, hyperactive tendon reflexes in all limbs, positive bilateral Chaddock

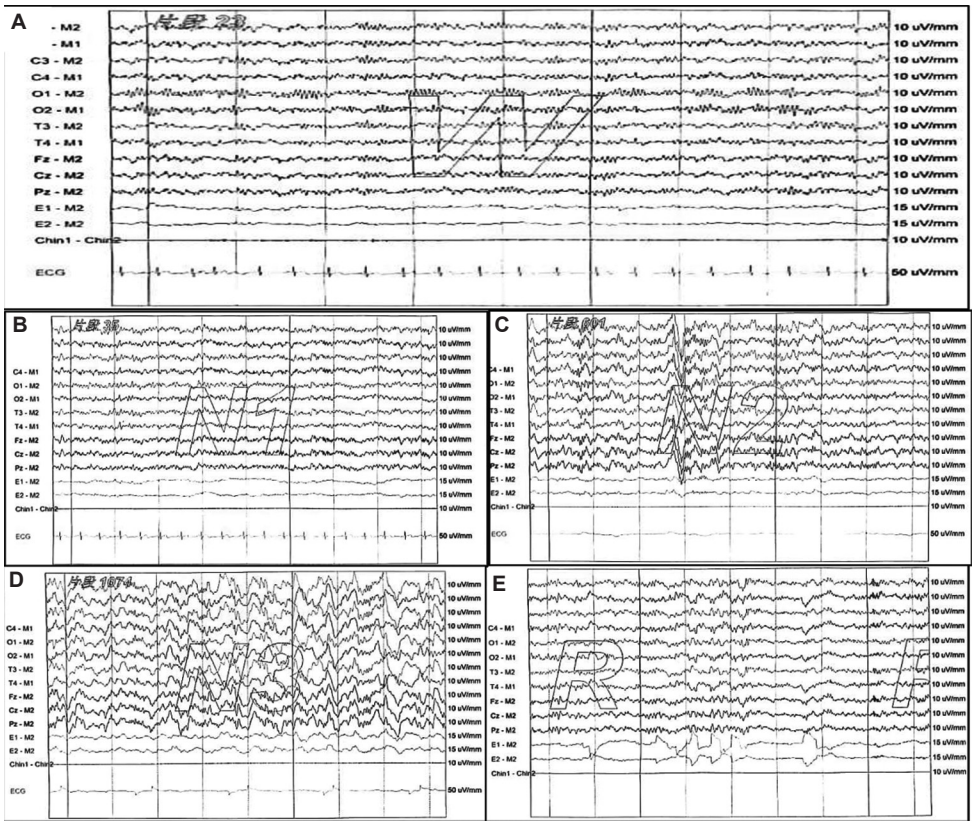

Figure 1. (A-E) Typical images of nocturnal polysomnography reports in awake (A), non-REM stage 1 (NREM1) (B), NREM2 (C), NREM3 (D), and rapid eye movement (E) stages.

and Hoffman signs, a positive Babinski sign on the right, a positive Romberg sign, and an ataxic gait.

As revealed by brain magnetic resonance imaging (MRI), multiple lesions with high T2 or FLAIR signals were present in the deep cerebral white matter surrounding the two lateral ventricles (Figure 2A-C). No abnormalities were observed in magnetic resonance angiography (Figure 2D). In addition, whole spine MRI showed multiple small punctate hyperintense signal shadows within the medulla oblongata and spinal cord on T2-weighted images (Figure 2E). Data on visual evoked potentials indicated less-than-satisfactory differentiation of bilateral P100 and prolonged latency. Results from cerebrospinal fluid puncture demonstrated a slight elevation in white blood cells, lgG level, and protein level, along with the presence of a positive oligoclonal band. To establish a clearer distinction from other demyelinating disorders affecting the nervous system, the patient underwent supplementary examinations to detect MOG and AQP-4 antibodies, which turned out to be negative. In accordance with McDonald's diagnostic criteria, these clinical and ancillary diagnostic findings supported a definitive diagnosis of MS in this case[4].

At the beginning, the patient received a course of shock therapy consisting of 1.0 g methylprednisolone administered daily for a consecutive 3 days. The dosage was then gradually tapered to 500 mg, 250 mg, and 120 mg, each lasting 3 days. Altogether, the entire treatment course accounted for 12 days. Subsequently, the patient was discharged with 60 mg oral prednisone and received subcutaneous administration of ofatumumab. In addition, various symptomatic management measures were implemented, including gastric protection, potassium supplementation, prevention of osteoporosis, and improvement of limb numbness. After synergistic therapy with methylprednisolone and ofatumumab, the patient's symptoms of limb numbness, unsteady gait, and daytime sleepiness improved significantly. On the manifestation of symptoms, the patient's expanded disability status scale (EDSS) score was recorded as 2 points. Follow-up was done 1 month after the initial treatment, during which the patient achieved improvement in EDSS score, which reduced to 1 point. In addition, there was an improvement in daytime sleepiness symptoms and in nighttime sleep disorders compared to before the treatment.

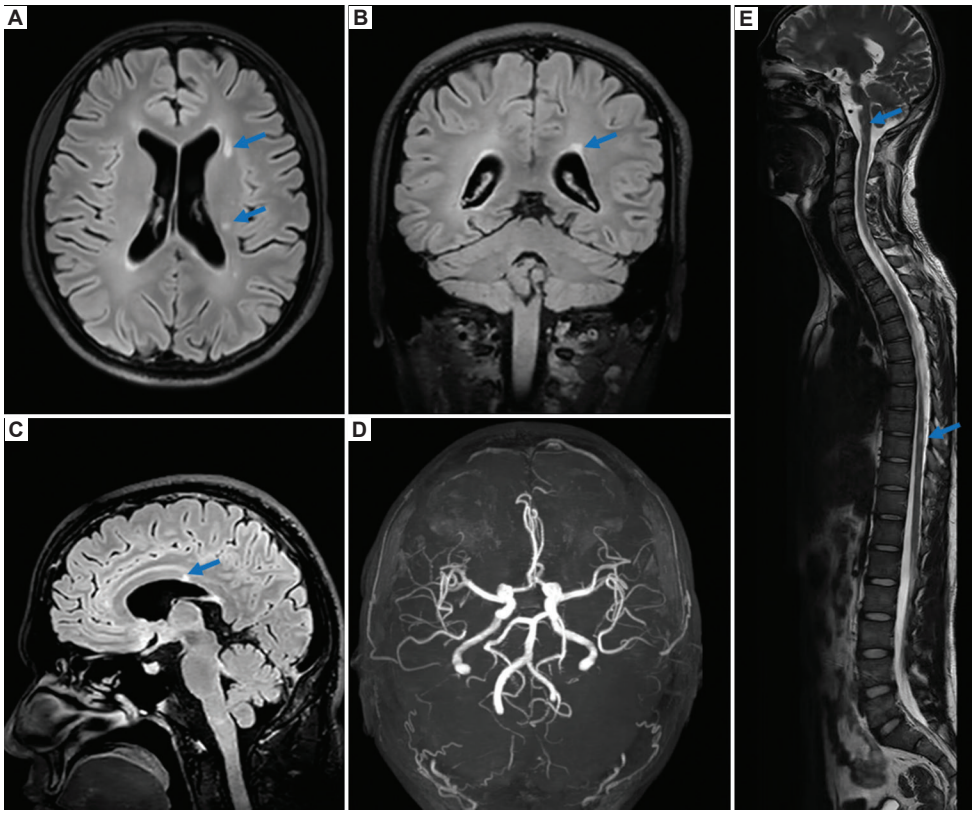

Figure 2. Magnetic resonance imaging (MRI) on July 14, 2023. (A-C) Axial T2-FLAIR sequences of cranial MRI show multiple hyperintense periventricular lesions around the lateral ventricles, as indicated by arrows. (D) Magnetic resonance angiography reveals no significant abnormalities. (E) T2-weighted sequences of whole spine MRI demonstrate multiple hyperintense lesions within the medulla oblongata and spinal cord, as indicated by arrows.

3. Discussion

We report a rare case of MS coexistence with narcolepsy. Previous limited studies have demonstrated a genetic association between narcolepsy and MS. However, their interaction and mutual influence still require an in-depth exploration. This special case of MS complicated by narcolepsy has prompted many thought-provoking explorations.

Narcolepsy is a chronic neurological disease accompanied by several defining clinical symptoms, including daytime drowsiness, hypnotic hallucinations, and sleep paralysis. Narcolepsy usually starts in adolescence and persists throughout an individual's life cycle, exerting a significant impact on daily functions[5]. It is estimated that the incidence of narcolepsy in the general population is about 0.047%[6]. However, studies on the incidence of narcolepsy in MS patients are very scarce. It is well known that the symptoms of narcolepsy are not uncommon in patients with MS. Approximately 12% of narcoleptic cases can be attributed to MS, and a study on the secondary causes of narcolepsy has revealed that MS is the fourth most significant risk factor after genetic diseases, CNS tumors, and brain damage. The *HLA-DR2/DQ6* is the most frequently associated HLA haplotype in MS. However, it is noteworthy that a considerable percentage of individuals diagnosed with narcolepsy also harbor the *DR2* gene[7]. This observation implies the possibility of a shared molecular genetic mechanism or potential overlap between the pathogenesis of these two disorders, providing valuable information for further research on their common pathophysiological basis.

Hypocretins, also known as orexins, belong a newly identified class of excitatory neuropeptides that are primarily synthesized by neurons in the posterolateral hypothalamus[8]. However, individuals diagnosed with narcolepsy suffer from a significant reduction of these pivotal neurons and therefore a decline in the concentration of hypocretin-1 in the cerebrospinal fluid[7]. Previous research has evidenced that individuals diagnosed with MS may develop demyelinating lesions in the hypothalamus, which result in a reduction of hypocretin-1 levels in the cerebrospinal fluid[9]. This condition possibly triggers the development of symptomatic hypersomnia or narcolepsy with cataplexy. In our case, demyelination-like changes in the hypothalamus were not captured by MRI. Nevertheless, other possibilities cannot be excluded. According to pertinent research, the decline in hypocretin-1 levels may be linked to inflammation in the CNS, rather than being exclusively ascribed to demyelination[10]. Therefore, in our case, despite the absence of evident hypothalamic demyelination on MRI scans, it is imperative to consider alternative neuropathophysiological mechanisms that may impact hypocretin-1 levels.

When MS coexists with narcolepsy, the complexity of its treatment strategies deepens. Disease-modifying therapy (DMT) is an intervention to improve the condition of MS and reduce the relapse rate by regulating the body's immune function. At present, the common DMTs for MS include siponimod, fingolimod, teriflunomide, dimethyl fumarate, and ofatumumab[11]. Existing studies have reported that immune regulation does not affect the sleep quality of MS patients and may even result in sleep disorders[12]. Several studies have also shown that some DMT treatments, such as natalizumab, have the potential to alleviate daytime drowsiness in patients with narcolepsy[13]. However, in this case, the MS symptoms were alleviated while the narcoleptic condition was significantly improved after ofatumumab treatment, although the efficacy of other DMTs in treating the coexistence of MS and narcolepsy still needs to be further explored. The continuous progress in medical technology, coupled with extensive research, will likely promote the emergence of novel DMTs. It is incumbent upon us to remain abreast of these developments and thoroughly investigate their potential value. This endeavor will not only enhance patient outcomes but also establish a more robust groundwork for forthcoming medical research and clinical practice.

4. Conclusion

The coexistence of MS and sleep disorders is common in clinical practice and will adversely affect the patient's health and quality of life. This case report sheds light on how to approach this comorbidity. In the future, we should delve into the exploration of the pathophysiological mechanisms shared by these two diseases and seek more effective therapeutic strategies. It is necessary to further explore comprehensive treatment methods to alleviate the symptoms and improve the quality of life of patients with this comorbidity.

Acknowledgments

None.

Funding

None.

Conflict of interest

The authors declare they have no competing interests.

Author contributions

Conceptualization: Meijuan Zhang
Data curation: Minkai Zhang, Linjie Yu

Formal analysis: Minkai Zhang, Linjie Yu
Writing–original draft: Jinglong Hu
Writing–review & editing: Meijuan Zhang

Ethics approval and consent to participate

Ethics approval was not needed, and the patient had given consent prior to participation.

Consent for publication

Consent for publication was obtained from the patient.

Availability of data

Data used in this case report is available from the corresponding author upon reasonable request.

References

1. Trapp BD, Peterson J, Ransohoff RM, *et al*., 1998, Axonal transection in the lesions of multiple sclerosis. *N Engl J Med*, 338: 278–285.

   https://doi.org/10.1056/nejm199801293380502

2. Barun B, 2013, Pathophysiological background and clinical characteristics of sleep disorders in multiple sclerosis. *Clin Neurol Neurosurg*, 115 Suppl 1: S82–S85.

   https://doi.org/10.1016/j.clineuro.2013.09.028

3. Golden EC, Lipford MC, 2018, Narcolepsy: Diagnosis and management. *Cleve Clin J Med*, 85: 959–969.

   https://doi.org/10.3949/ccjm.85a.17086

4. Thompson AJ, Banwell BL, Barkhof F, *et al*., 2018, Diagnosis of multiple sclerosis: 2017 revisions of the McDonald criteria. *Lancet Neurol*, 17: 162–173.

   https://doi.org/10.1016/s1474-4422(17)30470-2

5. Zawilska JB, Woldan-Tambor A, Płocka A, *et al*., 2012, Narcolepsy: Etiology, clinical features, diagnosis and treatment. *Postepy Hig Med Dosw*, 66: 771–786.

   https://doi.org/10.5604/17322693.1015529

6. Ohayon MM, Priest RG, Zulley J, *et al*., 2002, Prevalence of narcolepsy symptomatology and diagnosis in the European general population. *Neurology*, 58: 1826–1833.

   https://doi.org/10.1212/wnl.58.12.1826

7. Nishino S, Kanbayashi T, 2005, Symptomatic narcolepsy, cataplexy and hypersomnia, and their implications in the hypothalamic hypocretin/orexin system. *Sleep Med Rev*, 9: 269–310.

   https://doi.org/10.1016/j.smrv.2005.03.004

8. de Lecea L, Kilduff TS, Peyron C, *et al*., 1998, The hypocretins: Hypothalamus-specific peptides with neuroexcitatory activity. *Proc Natl Acad Sci U S A*, 95: 322–327.

   https://doi.org/10.1073/pnas.95.1.322

9. Kanbayashi T, Shimohata T, Nakashima I, *et al*., 2009, Symptomatic narcolepsy in patients with neuromyelitis optica and multiple sclerosis: New neurochemical and immunological implications. *Arch Neurol*, 66: 1563–1566.

   https://doi.org/10.1001/archneurol.2009.264

10. Kallweit U, Bassetti CLA, Oberholzer M, *et al*., 2018, Coexisting narcolepsy (with and without cataplexy) and multiple sclerosis: Six new cases and a literature review. *J Neurol*, 265: 2071–2078.

    https://doi.org/10.1007/s00415-018-8949-x

11. Orthmann-Murphy JL, Calabresi PA, 2017, Therapeutic application of monoclonal antibodies in multiple sclerosis. *Clin Pharmacol Ther*, 101: 52–64.

    https://doi.org/10.1002/cpt.547

12. Leonavicius R, Adomaitiene V, 2014, Features of sleep disturbances in multiple sclerosis patients. *Psychiatr Danub*, 26: 249–255.

13. Scammell TE, Luo G, Borker P, *et al*., 2020, Treatment of narcolepsy with natalizumab. *Sleep*, 43: zsaa050.

    https://doi.org/10.1093/sleep/zsaa050

Our Journals

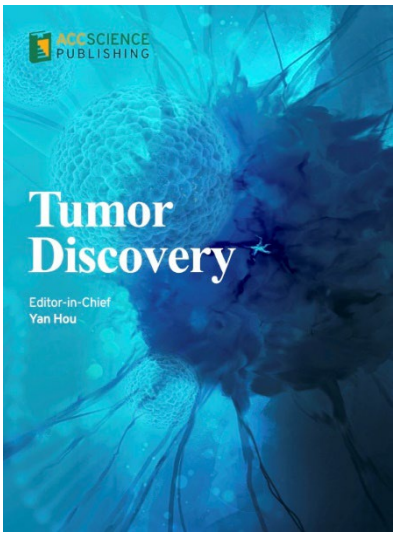

Tumor Discovery is a peer-reviewed and open-access journal that aims to present new cancer research with strong emphasis on fundamental and translational studies. *Tumor Discovery* covers topics, including but not limited to the following:

- Etiology and pathogenesis of cancer
- Mechanisms and molecular pathways underlying cancer initiation and progression
- Tumor metastasis
- Tumor evolution and heterogeneity
- Tumor microenvironment and tumor-host interactions
- Cancer genetics and genomics
- Cancer characterization using omics approaches
- Discovery and validation of cancer biomarker
- Discovery of new therapeutic targets
- New approaches of diagnostic and treatment modalities
- Statistical methods in cancer research

Global Translational Medicine is a quarterly journal that focuses on medicine, biological sciences, and biomaterials engineering. The goal of *Global Translational Medicine* is to provide a platform to researchers for showcasing their latest research works in translational medicine so as to advance the field towards the betterment of human health. Despite the advancement of omics and new technologies, the process of transforming these technologies and scientific research results into effective therapies and putting them into clinical use still has a long way to go. *Global Translational Medicine* provides a platform to fill the gaps in preclinical and inter-disciplinary research, to promote clinical translation of scientific research results, and to contribute to the conception of new and improved preventive measures as well as diagnostic and therapeutic techniques of diseases.

Global Translational Medicine covers the following themes: cardiovascular disease, metabolism/diabetes/obesity, neuroscience/neurology, cancer, biomaterials and their applications in medicine, proteomics/metabolomics, pharmacogenomics, biomarkers, bioinformatics and data mining, animal and clinical research, and medical methods arising from interdisciplinary crossover.

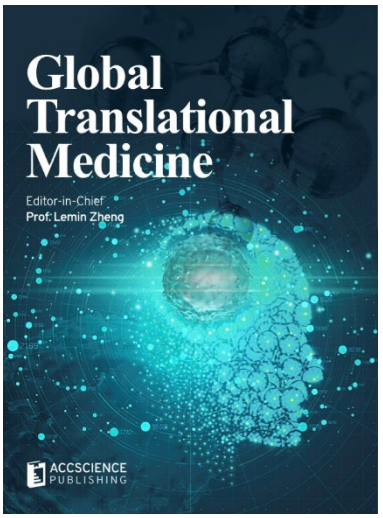

Start a new journal

Write to us via email if you are interested to start a new journal with AccScience Publishing. Please attach your CV, professional profile page and a brief pitch proposal in your email. We shall inform you of our decision whether we are interested to collaborate in starting a new journal.

Contact: info@accscience.com

https://accscience.com/journal/AN

Contact

www.accscience.com

8 Burn Road, #15-03 Trivex, Singapore 369977

Email: editorial@accscience.com
Phone: +65 8182 1586